USING MAST CELLS TO PROBE REGULATION OF PLASMA MEMBRANE HETEROGENEITY, MEMBRANE TRAFFICKING AND HOST-PATHOGEN INTERACTIONS

A Dissertation

Presented to the Faculty of the Graduate School

of Cornell University

in Partial Fulfillment of the Requirements for the Degree of

Doctor of Philosophy

By

Norah Lesley Smith

January 2012

USING MAST CELLS TO PROBE THE REGULATION OF PLASMA MEMBRANE HETEROGENEITY, MEMBRANE TRAFFICKING, AND HOST-PATHOGEN INTERACTIONS

Norah Lesley Smith, Ph.D.

Cornell University 2012

Cells of the immune system have many unique functions, but underlying similarities in signaling mechanisms and pathways make a well-defined model system useful. We utilize RBL mast cells to probe a variety of questions pertinent to immune cell function and infection. Mast cells serve as innate immune responders as well as the mediators of allergic disease. A major signaling cascade in mast cells is initiated by multivalent antigen crosslinking of immunoglobulin E (IgE)-FcεRI receptor complexes. Membrane reorganization and signal transduction involving multiple players leads to Ca^{2+} mobilization and protein kinase C activation that ultimately triggers the release of preformed mediators from secretory lysosomes and, additionally, to outward trafficking of recycling endosomes (RE). The first study investigates the dynamic lipid environment surrounding crosslinked IgE-FcεRI complexes. By isolating detergent-resistant membranes and performing detailed mass spectrometry analysis, cytoskeletal interactions are found to be important for regulating membrane lipid reorganization resulting from antigen stimulation. Next, we characterized the molecular basis of sphingosine inhibition of cell function. We find that sphingosine derivatives electrostatically interfere with phosphoinositide-dependent membrane processes, including both Ca^{2+} mobilization and exocytic processes such as degranulation and RE outward trafficking. The function and regulation of RE trafficking in immune cells,

especially as it pertains to cytokine secretion, is of great interest. We provide evidence, by immunofluorescence microscopy and cytokine secretion assays, that mast cells secrete both IL-4 and TNFα in a manner that is consistent with a role for RE in their secretion. The dynamic trafficking of RE in RBL mast cells makes them likely candidates in many processes, including interactions with pathogens. We provide strong evidence for a role for RE in the formation of the parasitophorous vacuole (PV) of the obligate intracellular parasite, *Toxoplasma gondii*. In addition, we find that *Toxoplasma gondii* infection of mast cells results in suppression of IgE-FcεRI signaling by interfering with the activation of phospholipase Cγ. Colllectively, these studies show RBL mast cells as a versatile model of cellular immune function in both health and disease.

BIOGRAPHICAL SKETCH

Norah was born May 1, 1980 to Ruth and Craig Smith in Saranac Lake, New York. She spent her formative years running, largely shoe-less, unkempt and happy, through the wilds of the Adirondack Park. When not tormenting her older sister, as only a younger sibling can, she enjoyed all sorts of academic, artistic and athletic pursuits. An extensive family of scientists and engineers encouraged her interests in science. In high school she had the unique opportunity to explore the wonders of the immune system with Dr. Karen Aguirre at the Trudeau Institute. In 1998, Norah arrived at Ithaca's Cornell University and started a Bachelor's degree in Chemical Engineering, but still interested in the immune system, began working in the laboratory of Barbara Baird and David Holowka exploring the allergic response. After four years Norah, with degree in hand, decided to become a non-practicing engineer and continued to pursue her interest in immunology. Barbara and Dave- thankfully- were happy to keep her on, first as a technician and then, also, as a graduate student. She is not certain where she will end up next, but if it is anything like the thirteen years she has been in Ithaca it will be both different and more wonderful than she expects.

For my family:

Mom, Dad, Molly and Brad, thank you for being the best of friends.

ACKNOWLEDGEMENTS

When you have been any place as long as I have been at Cornell, you owe a lot of people thanks. First and foremost, I must thank David Holowka and Barbara Baird for taking me into their lab as undergraduate research student so very long ago. They have been nothing but supportive since the day I arrived. The welcoming environment of their lab and their combined mentoring power encouraged me to pursue a graduate degree through the Employee Degree Program. They helped me learn critical thinking skills without losing sight of the big picture. Their lab has been a home to me for over a decade, and I would not be where I am today with out them, so thank you.

Thanks also to Cynthia Leifer for providing insightful guidance throughout my graduate career as a member of my committee. For generously agreeing to serve as my external committee member, I thank William Brown.

The nature of scientific research is collaborative, and I am indebted to the many people who I have worked with over the years. Collaborative projects with the McLafferty, Abruña, Ober, Clark and Appleton labs have been fruitful and interesting. Thanks in particular to Mei, Michele, Liz, Yelena and Lisa. I especially need to thank Eric Denkers and members of his lab: Barbara, Charlotte, Delbert and Sara. Thanks for allowing me to make your lab a second home here at Cornell for the past two years.

Thanks to all past and present members of the Baird-Holowka Lab. There have been so many of you! It has been my pleasure to work with all of you. In the early years Cheryl was helpful in guiding me, and Jon and Ryan were great friends. Stephanie,

Ethan and Sarah were my partners in crime for many years. In addition to providing excellent molecular biology assistance, Alice has been a firm and constant friend. The current members of team Balowka: Jinmin, Deepti, Kirsten, Josh, Sarah, Kate, Amit, Kari, Devin and Lily make my daily life at Cornell a great deal of fun.

Finally, thanks to my friends and family. There are far too many to name, but without your collective love, friendship and support, the road I've traveled would have been rough and uncomfortable. Instead it has been a nice adventure, and one I hope to continue with all of you in the future. Thanks so much for everything.

TABLE OF CONTENTS

LIST OF FIGURES

LIST OF TABLES

LIST OF ABBREVIATIONS

APC	antigen presenting cell
BCR	B cell receptor
BIM	bisindolyl malemide
BMDC	bone marrow dendritic cells
BMMF	bone marrow macrophage
BSS	buffered saline solution
Ca^{2+}	soluble calcium ion
CTxB	Cholera toxin, B subunit
D-spg	D-sphingosine
DAG	diacylglycerol
DC	dendritic cell
DMS	N.N'-dimethylsphingosine
DRM	detergent resistant membrane
ELISA	enzyme-linked immunosorbant assay
ER	endoplasmic reticulum
ESI/MS	electrospray ionization mass spectrometry
FTMS	Fourier transform mass spectrometry
GPI	glycophosphosphatidylinositol
IFNγ	interferon gamma
IgE	immunoglobulin E
IL	interleukin
IP_3	inositol-1,4,5-bisphosphate
ITAM	immune tyrosine activation motif
LAT	linker for the activation of T cells

LPS	lipopolysaccharide
L_D	liquid disordered
L_O	liquid ordered
MARCKS ED	myristolated, alanine-rich PKC substrate effector domain
MF	macrophage
MHC I	major histocompatability complex I
MIRR	multi-chain immune recognition receptor
P/S+M	ratio of poly unsaturated to saturated plus monounsaturated
PAMP	pathogen-associated molecular pattern
$PI(4,5)P_2$	phosphotidylinositol-4,5-bisphosphate
PKC	protein kinase C
PL	phospholipid
PLCγ	phospholipase C-gamma
PM	plasma membrane
PV	parisitophorous vacuole
PVM	parisitophorous vacuole membrane
Rab11-FIP	Rab11- family interacting protein
rBMMC	rat bone marrow mast cells
RE	recycling endosomes
SOC	store operated calcium
SOCE	store operated calcium entry
TCR	T cell receptor
TfR	transferrin receptor
TLR	Toll -like Receptor
TMS	N, N', N''-trimethylsphingosine
TNFα	tumor necrosis factor alpha

CHAPTER ONE

Introduction

1. The Immune System

Living organisms do not live in a sterile environment. Interacting with the world around them results in constant exposure to agents that range from innocuous to life threatening. As a result, all organisms have evolved mechanisms to mitigate detrimental effects due to contact with harmful agents. At the same time, these systems must also be tolerant to self-antigens or benign foreign materials. Higher eukaryotes, such as mice and man, have complex and finely regulated immune systems comprised of multiple components working in concert to keep the host healthy. These factors make for a robust system capable of fighting a large spectrum of insults, but they also increase the likelihood of aberrant or harmful responses.

An exhaustive review of immunology is well beyond the scope of this thesis, but a brief introduction is worthwhile. I will discuss some of the cell types of hematopoietic origin, and while most of these cells some have unique roles in generating effective immune responses, it is also important to appreciate the level of redundancy existing in the system. Multiple cell types can perform analogous functions, and signal transduction within immune cells share important common signaling modules. This dissertation reports on the use of mast cells to probe an assortment of questions that are not only important to their function, but also generally informative to important topics in immune signaling and biological function.

Medically, immunity is defined as an organism's resistance to pathogens or disease. Without pathogens, an immune system has limited utility. It is difficult to think about immunity without also thinking about pathogens or disease; after all, the two co-evolved. As a result much of what we know of the immune system is derived from the study of specific diseases.

Cells that Contribute to Immunity

To some extent, every cell in the body of an organism contributes to immune function. Skin and mucosal membranes serve as important physical barriers and play important roles in innate immunity. In a non-specific manner, these tissues serve as a first line of defense and block the vast majority of harmful agents. Similarly, nearly every nucleated cell expresses major histocompatibility complex I (MHC I) on its surface. This MHC I presents endogenous antigen to effector cells which, in turn, make important contributions to the type of adaptive response generated.

That being said, many of key players in both innate and adaptive immune functions are derived from hematopoietic stem cells. Hematopoietic stem cells differentiate into either myeloid or lymphoid progenitors. B and T lymphocytes are the primary cells derived from the lymphoid lineage. They both recognize antigen in a clonal manner and are critical for the generation of adaptive immunity. B cells are responsible for the production of antibodies, or immunoglobulins, the major component of humoral immunity. B cells also play a major role in antigen presentation. T cells further differentiate into helper $CD4^+$ (Th1 and Th2) and cytotoxic $CD8^+$ T cells. Helper T cells

are important in directing the quality of an immune response: Th1 cells induce an environment favoring cell-mediated immunity by cytotoxic T cells, whereas Th2 cells contribute primarily to humoral immunity. These effects are largely mediated by specific cytokine secretion profiles.

Cells of myeloid lineage are major contributors to innate immunity, and they include macrophages and monocytes, dendritic cells (DC), neutrophils, eosinophils, basophils and mast cells. Most cells of myeloid lineage express toll-like receptors (TLRs) that use pathogen-associated molecular patterns (PAMPs) to recognize potential threats. Cell signaling through TLRs is a major trigger for the innate immune response, as it generates chemokines and cytokines that recruit additional effector cells. Macrophages and dendritic cells both act as professional antigen presenting cells (APCs), presenting peptide antigen to T cells. Neutrophils, eosinophils, basophils and mast cells are all granulocytes that have preformed mediators stored in granules that can be rapidly released in response to activation. Many of these cells have phagocytic capabilities and can ingest whole organisms or large pieces of cellular debris. Ingested material is then degraded by the phago-lysosomal system. Additionally, activation of these cells can upregulate the secretion of cytokines important for additional effector cells of both the innate and adaptive systems.

Cytokine Secretion

Cytokines are essential for directing the traffic of immune effector cells to sites of infection, inflammation or damage. They also play important roles in determining what

type of immune response is generated in response to various insults. Secretion of IFNγ and IL-12 induce pro-inflammatory responses that are a hallmark of Th1 mediated responses. In contrast, IL-4, IL-5 and IL-13 are linked to Th2 mediated immunity. In response to ligand binding, immuno-receptors such as TLRs and cytokine receptors trigger transcription and translation of cytokines. The mechanisms of cytokine secretion have lately generated interest, and it is suggested that various cells may have different means of regulating cytokine release [1].

Mast Cells

Paul Ehrlich first identified mast cells in 1878. Mast cells were seen to be uniquely stained granule rich cells that were mistakenly thought to provide nourishment to surrounding tissues [2]. They were later correctly identified as cells of the immune system, being derived of myeloid lineage. Basophils and mast cells have similar function, but basophils circulate while mast cells are tissue-resident cells [3]. Mast cells circulate as an immature phenotype, and they mature at their destination, developing either a mucosal or a connective tissue phenotype [4]. Our studies primarily use RBL mast cells, which have a mucosal phenotype [5].

Mast cells are most commonly associated with type I hypersensitivity allergic responses. Mast cell-mediated allergic diseases are an important health concern, particularly in developed countries. In the United States, more than 50 million people annually are afflicted with allergic symptoms [6], ranging from a runny nose and watery eyes to life-threatening anaphylaxis. In allergic responses, immunoglobulin E (IgE)-

mediated reactions to antigen (allergen) result in the secretion of cell products, such as histamine, that contribute to disease manifestation.

Mast cells are not only mediators of allergic disease, but show diversity of function (Figure 1.1). As such, they play important protective roles in host defense through multiple immune mechanisms [7]. Increased serum levels of IgE and mast cell activity are also associated with combating parasitic helminth infections [8]. Helminth infection is a major concern in developing nations [9] and the agricultural industry [10]. As tissue resident cells, mast cells can act as primary mediators in responses to infection [4]. They can express MHC II and serve as APCs to T cells [11], and also act as phagocytes [12]. In addition to FcεRI expression, mast cells express other immune recognition receptors including Toll-like receptors (TLRs) and IgG receptors, FcγRIIb and FcγRI [7]. For example, in mast cells, recognition of LPS (lipopolysaccharide) is TLR4 dependent [13]. Mast cells can secrete multiple cytokines including IL-3, IL-4, IL-6 tumor necrosis factor α (TNFα), and IL-10. In human peripheral mast cells, preformed TNFα is secreted during degranulation [14, 15]; however, in RBL mast cells TNFα is not a preformed mediator in granules [16]. Rat peritoneal mast cells produce cytokines in response to LPS in a degranulation-independent manner [17]. Recent research shows that mast cell-derived IL-10 is important for limiting inflammation in contact hypersensitivity reactions [18].

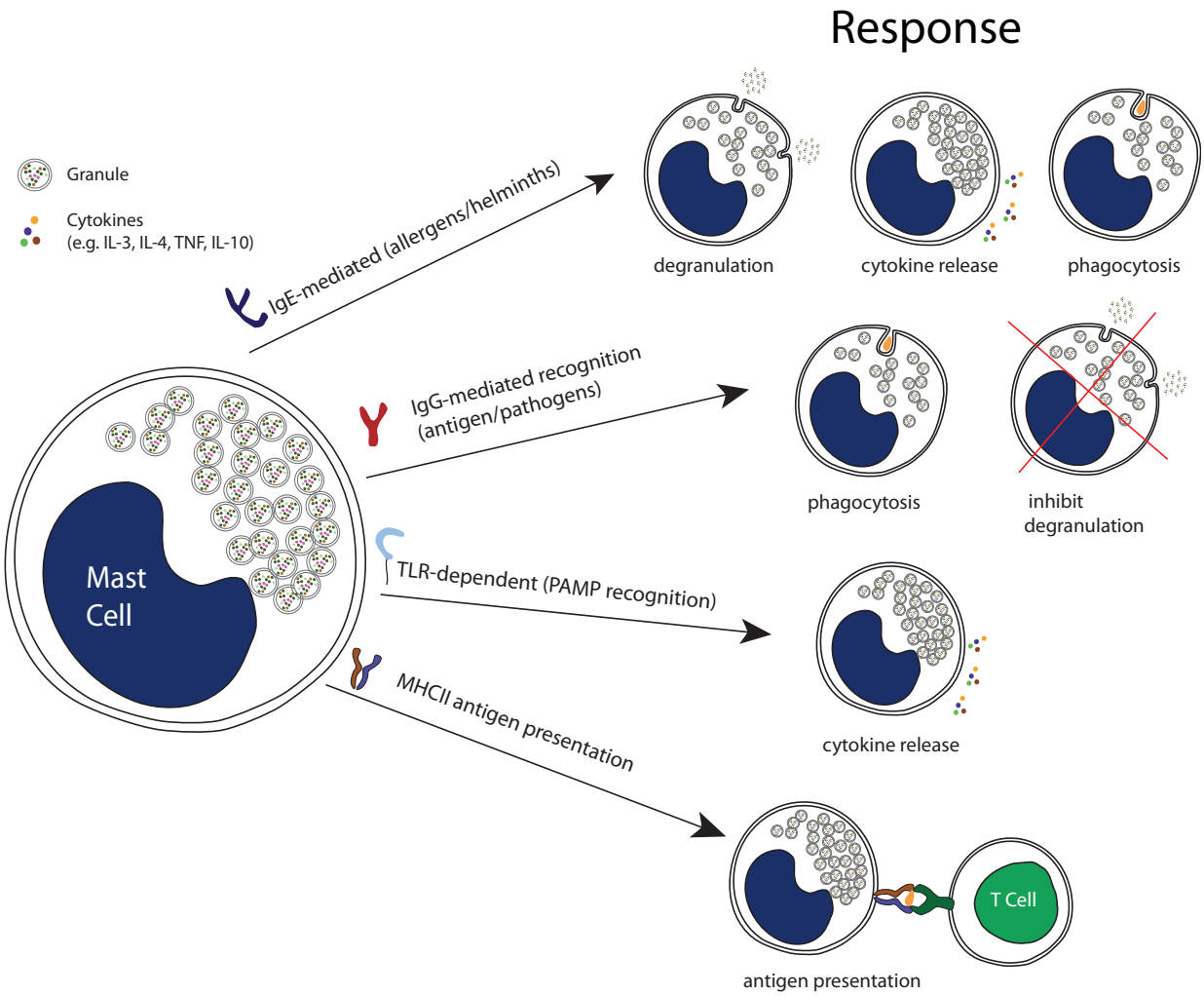

Figure 1.1. Mast Cells have multiple immune effector functions.

2. Signaling in Mast Cells

FcεRI

IgE-mediated signaling in mast cells occurs through activation of the high affinity receptor for IgE, FcεRI. FcεRI is a member of the multi-chain immune recognition receptor (MIRR) family, which includes T-cell receptors (TCR), B-cell receptors (BCR) and FcγRs [19]. For MIRR family members, antigen recognition (or antibody binding) and signal transduction are mediated by separate subunits. FcεRI on mast cells, and basophils, is a tetramer composed of an α, a β and two γ chains ($\alpha\beta\gamma_2$). The α subunit has an extracellular domain that binds IgE with high affinity and serves as the immune recognition site [20]. The two γ chains each have an immune tyrosine activation motif (ITAM) that act as signaling moieties. The β subunit also contains an ITAM that acts as a signal amplifier by binding Lyn kinase. In human antigen presenting cells, such as monocytes and dendritic cells, FcεRI is a trimer composed of $\alpha\gamma_2$ [21].

IgE/FcεRI-Mediated Signal Transduction

IgE is one of the five classes of antibodies secreted by B cells. In a primary response, mature B cells bind antigen in an epitope specific, clonal manner via the BCR. In the context of Th2 cytokines such as IL-4 and IL-13, these B cells differentiate into plasma cells that class switch to secrete large amounts of IgE with the specificity of the BCR [22]. This secreted antibody enters circulation where it can be bound by any cell expressing FcεRI, including mast cells. Upon secondary exposure to the antigen, IgE/FcεRI are crosslinked, and this event results in the redistribution of aggregated

receptor into ordered-lipid microdomains, often termed lipid rafts [23]. This redistribution allows for the phosphorylation of tyrosine residues within the ITAMs of FcεRI by Lyn kinase. The tyrosine kinase Syk is in turn recruited to the phosphorylated γ chains by its tandem SH2 domains. Activated Syk phosphorylates important downstream signaling molecules including the adaptor protein linker for the activation of T cells (LAT) and phospholipase Cγ (PLCγ). The recruitment of PLCγ results in the hydrolysis of phosphotidylinositol-4,5-bisphosphate ($PI(4,5)P_2$) at the plasma membrane to yield inositol-1,4,5-trisphosphate (IP_3) and diacylglycerol (DAG). IP_3 binds to IP_3 receptors on the ER membrane, and this results in release of Ca^{2+} from these stores. Ca^{2+} release promotes interactions between the calcium sensor Stim1 in the ER membrane and the store-operated calcium (SOC) channel at the PM, Orai1, triggering additional Ca^{2+} influx [24, 25]. Concurrent with Ca^{2+} mobilization, DAG activates protein kinase C (PKC). Together, these events trigger the degranulation of secretory lysosomes containing preformed mediators such as histamine, serine proteases, and serotonin. The signaling described above is depicted in Figure 1.2. In addition to degranulation, FcεRI signaling also triggers the production secondary lipid mediators, including prostaglandins and leukotrienes. Cytokines are also produced and contribute to the recruitment of many immune effector cells that carry out late-phase allergic responses. These include long-term inflammation and extensive tissue remodeling at the site of the allergic response.

Membrane Heterogeneity

In 1972, Singer and Nicholson developed the well-known fluid mosaic model that postulated that membrane lipids mainly acted as a support structure for the various

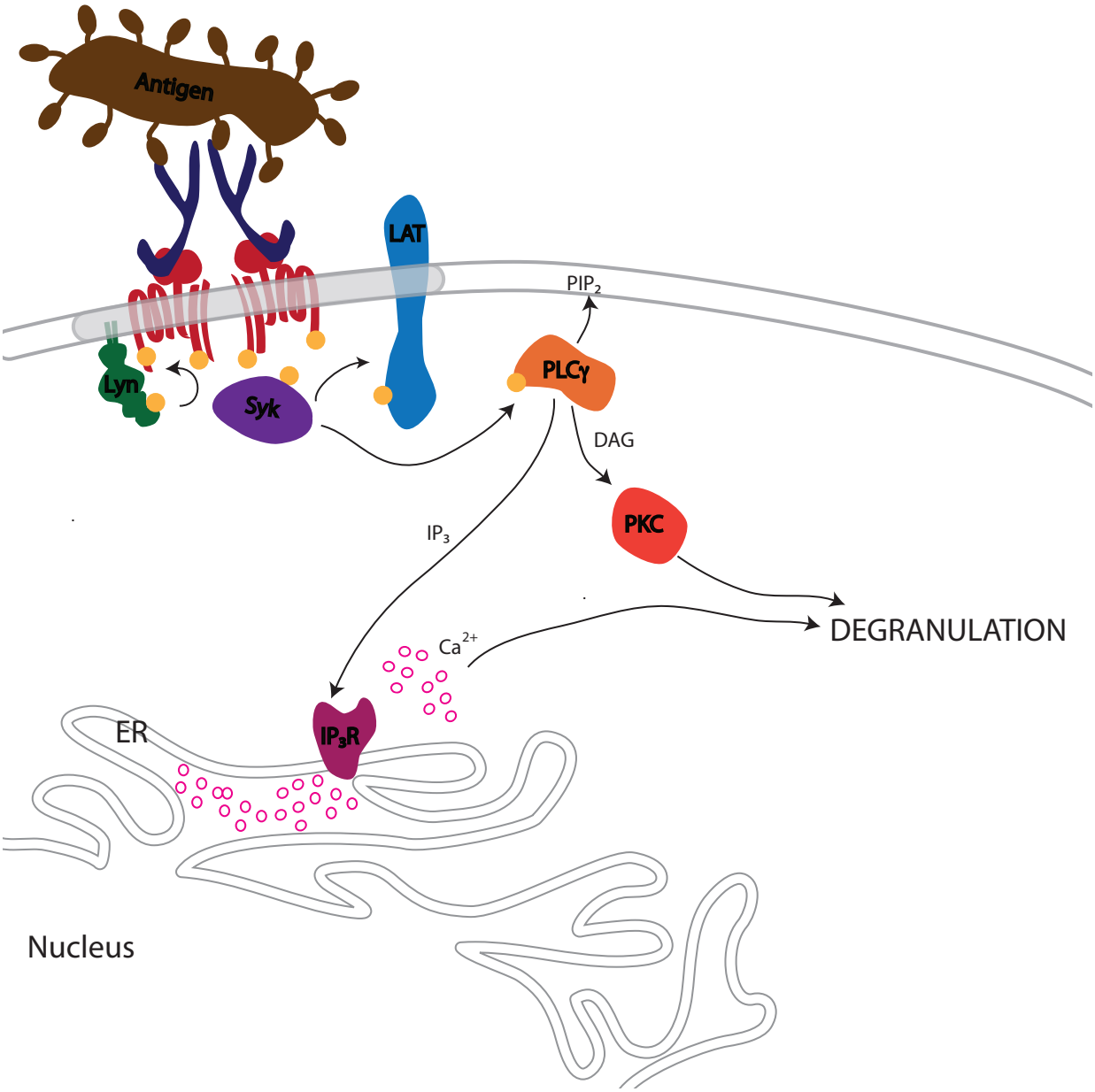

Figure 1.2. Schematic of the signal transduction that occurs through FcεRI. Crosslinking of FcεRI-IgE complexes by multivalent antigen leads to phosphorylation of receptor by Lyn kinase and the subsequent recruitment and activation of Syk which can then phosphorylate the adaptor protein LAT and other substrates. Consequent activation of PLCγ produces DAG and IP_3, and IP_3 activates IP_3 receptors on the endoplasmic reticulum (ER), causing calcium release from ER stores. Calcium mobilization and activation of PKC by DAG are necessary for maximal degranulation of secretory lysosomes.

signaling proteins that freely diffuse in the plasma membrane [26]. Work in model membranes demonstrated that two lipid phases, liquid ordered (L_O) and a liquid disordered (L_D), could coexist under physiologic conditions [27]. It wasn't until the 1990s that it was proposed that lipid micro-domains could affect signaling events at the plasma membrane [23, 28, 29]. From these early works, the concept of lipid rafts was born. Lipid rafts were shown to be enriched in phospholipids with saturated acyl chains, cholesterol and sphingolipids. Insolubility in cold non-ionic detergents (e.g. Triton-X 100) was a defining feature of lipid rafts for many years [30]. While the term lipid raft invokes a long-lived stable structure, it is now appreciated that membrane heterogeneity in living cells is highly dynamic and exists on submicron length scales [31].

In resting RBL cells, IgE/FcεRI is localized primarily in an L_D environment. It is only after crosslinking with multivalent antigen that it clusters in lipid rafts [32]. This regulated translocation is an important step, as it exposes ligated receptors to active Lyn kinase that is protected from inactivation due to its localization in lipid rafts [33, 34]. Reducing cholesterol by treatment with methyl β–cyclodextrin perturbs membrane heterogeneity such that normal receptor signaling is disrupted [35].

3. Recycling Endosomes

Many cellular functions rely on intracellular membrane trafficking. Recycling endosomes (RE) are now appreciated to be important participants in these processes. They were first identified by Hopkins and Trowbridge in 1983 as being involved in transferrin (TfR) receptor trafficking [36]. Yamishiro et al. further described RE as a

mildly acidic tubulovesicular organelle, distinct from the phagolysosomal system, and involved in the recycling of membrane proteins [37] (Figure 1.3). RE serve as a large internal reservoir of membrane lipids and other plasma membrane components. Our laboratory established that the ganglioside GM_1, as labeled by Cholera Toxin B (CTxB), populates the recycling endosome with a perinuclear localization in RBL mast cells [38]. More recently, there is accumulating evidence that RE are a heterogeneous population, such that CTxB-labeled RE are distinct from TfR-containing RE [39].

Biological Function of Recycling Endosomes

Though initially described as an organelle whose major function is recycling of internalized transmembrane proteins, it is now appreciated that RE are a highly dynamic organelle that can serve diverse functions in many cells types. In addition to their role as plasma membrane recycling compartments, RE have established roles in membrane intensive processes that require directed trafficking, such as in cytokinesis [40], phagocytosis in macrophages [41], and migration [42]. RE trafficking also actively participates in the maintainence of epithelial cell polarity via directed trafficking of basolateral proteins [43, 44], and export and secretion of cytokines in macrophages [41, 45] and NK cells [46]. In plasmacytoid dendritic cells (pDCs), storage of MHC I in RE may play important roles in cross-presentation of antigen [47]. In our laboratory, we established that IgE/FcεRI-mediated signaling triggers an outward trafficking response of CTxB-labeled RE [38], and that these RE are trafficked to sites of receptor ligation by immobilized antigen-patterned surfaces [48].

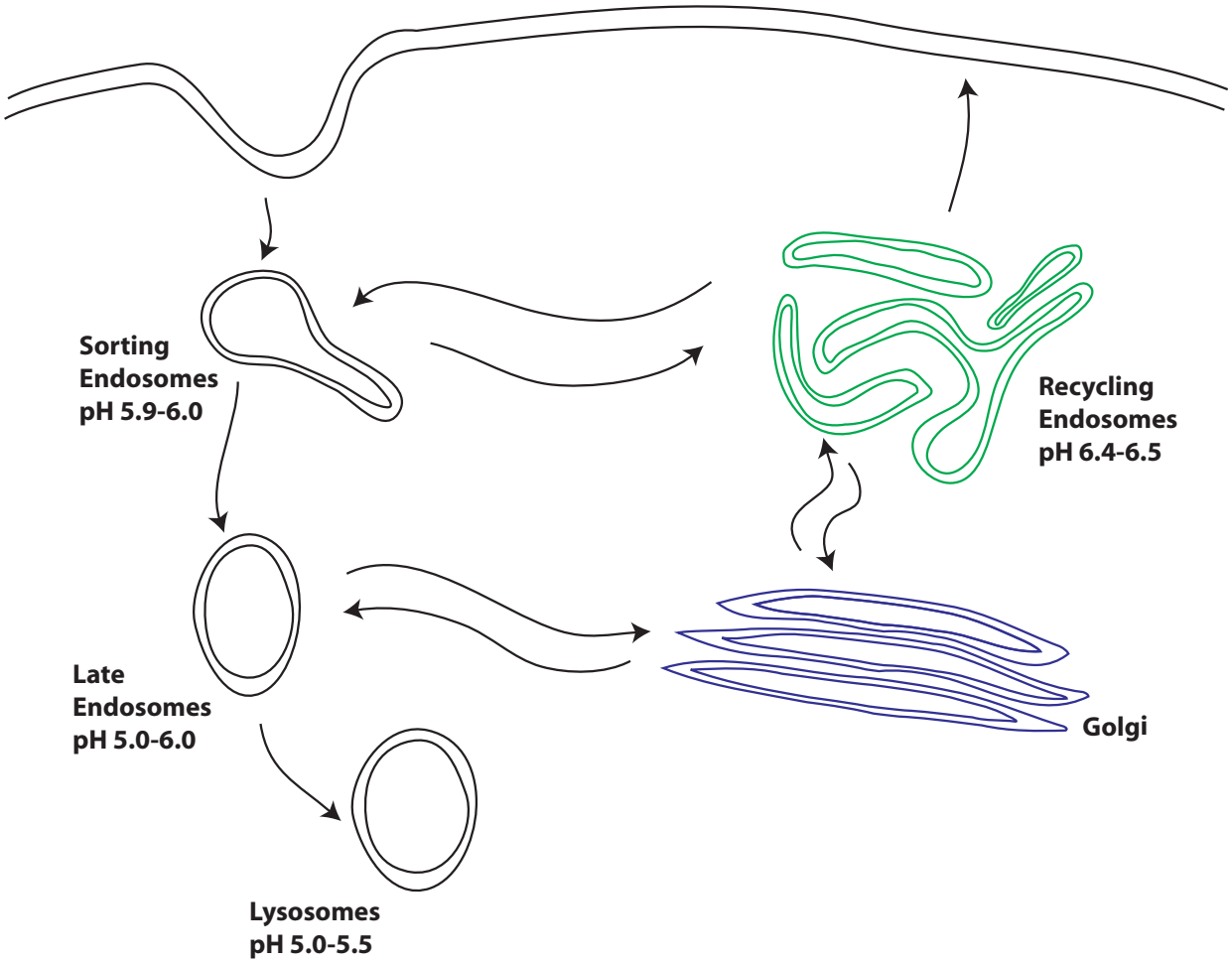

Figure 1.3. Recycling endosomes and the endo-lysosomal system. RE are a mildly acidic tubulovesicular organelle that is spatially and functionally separate from canonical lysosomal maturation. Figure adapted from Mukherjee et al. [87].

RE not only participate in normal cellular function, they also have important roles in host-pathogen interactions and disease states. RE contribute to enhancement of HIV particle release [49]. RE interactions with *Salmonella* vacuoles are important for vacuolar maturation [50]. Furthermore, reduction or absence of presenillin/γ-secretase activity, associated with the neurodegeneration seen in Alzheimer's disease, impairs RE trafficking [51]. RE-associated Rab11-overexpression can rescue neurodegenerative defects caused by Huntington's disease [52].

Regulators of RE Trafficking

Regulation of organelle function is intrinsically linked to membrane identity. Rabs and Arfs are large families of small GTPases whose members have differing organelle specificity and, due to this distribution, function to mediate and regulate membrane traffic between organelles. Rab11 and Rab4 show RE localization [53], and over-expression of dominant negative Rab11 results in delayed RE trafficking in multiple contexts [54]. Arf6 is also directly linked to RE to plasma membrane trafficking [55]. Furthermore, Balasubramanian and colleagues demonstrated that Arf6 selectively controls exocytosis and GM_1-CTxB labeled RE membranes [39], lending credence to the concept of RE as a heterogeneous pool that can be differentially regulated.

Rab11-family interacting proteins (Rab11-FIPs) are genetically diverse but share a common Rab11 binding domain (RBD) [56]. They are further broken down into two subclasses: Class I Rab11-FIPs are implicated in the recycling functions of RE [57] and Rab11-FIP2 interacts directly with the molecular motor protein myosin Vb [58]. Class II

Rab11-FIPs are important for RE function in cytokinesis [59, 60]. Moreover, Rab11-FIP3 also contributes to the structural identity of RE [61].

Vesicular fusion is a process regulated by soluble NSF attachment protein receptor (SNARE) proteins. Like the small GTPases, SNAREs also display specific subcellular localization. This ensures that vesicular fusion occurs at the appropriate place. VAMP3 is the SNARE primarily associated with RE trafficking. Murray et al, determined that VAMP3 co-localizes with TfR and TNFα in the RE of macrophages [41].

4. Toxoplasma gondii

T. gondii is an obligate intracellular, apicomplexan parasite. It can infect virtually any warm-blooded animal. In humans, infection rates vary widely according to geographic locations. In United States and the United Kingdom, somewhere between 16-40% of the populations are infected [62]. There are three main clonal lineages of *T. gondii*, types I, II and III [63], however recently a fourth lineage has been described [64]. Infection by type I parasites results in a lethal infection in mice while types II and III are less virulent [65]. The molecular bases for virulence differences between lineages are an active area of study.

Toxoplasma is an incredibly successful parasite, and infections generally result in latent infection that persists for the life of the host. For most immunocompetent individuals, infection is asymptomatic. However, in immunocompromised individuals, such as those with Acquired Immune Deficiency Syndrome (AIDS), severe encephalitis can occur as a result of parasite reactivation [66]. Acute toxoplasmosis in pregnant

women may be detrimental to fetal development, leading to auditory or visual impairment or mental retardation [67].

Life Cycle and Invasion

As is true of many parasites, *Toxoplasma* has a complex life cycle. There are three infective stages of the parasite: sporozoites, bradyzoites and tachyzoites. The sexual reproduction of *T. gondii* occurs in the gut of the definitive host, members of the family Felidae, most notably the domestic cat (*Felis catus*) [68, 69]. Oocysts containing sporozoites are shed in cat feces. Oocysts are incredibly durable structures that can withstand harsh environmental conditions [70], such that contamination of food or water is a general mechanism of parasite transmission. Another major mechanism of transmission is the consumption of tissues containing encysted bradyzoites. In intermediate hosts, it is generally the ingestion of either oocyts or tissue cysts that triggers disease. Sporozoites and bradyziotes convert to tachyziotes that can invade nearly any nucleated cell and divide rapidly to disseminate throughout the host.

Tachyziotes infect through a process of active invasion that is parasite-mediated, as depicted in Figure 1.4. This is in contrast to a host-mediated phagocytic process [71]. Upon initiation of invasion, the parasite secretes proteins from two specialized organelles, micronemes and rhoptries (Figure 1.4). These proteins facilitate the formation of a structure termed the moving junction [72] that aids in the invasion process (reviewed in [73]). The parasite acquires a vacuolar membrane during the invasion process. This parasitophorous vacuole (PV) is composed of host membrane that is

Figure 1.4. *T. gondii* infects cells via a rapid, active invasion process. Initial attachment (1) is followed by apical attachment (2) and release of microneme proteins. Subsequently, a moving junction is set up that involves both microneme and rhoptry proteins (RONs) (3). Additional rhoptry proteins (ROPs) are secreted into the target cell. As invasion progresses the moving junction moves towards the posterior of the parasite (4). This process forms the nascent PV. Following invasion the PV closes (5) and undergoes fission completing the invasion process. Figure adapted from Carruthers and Boothroyd [73].

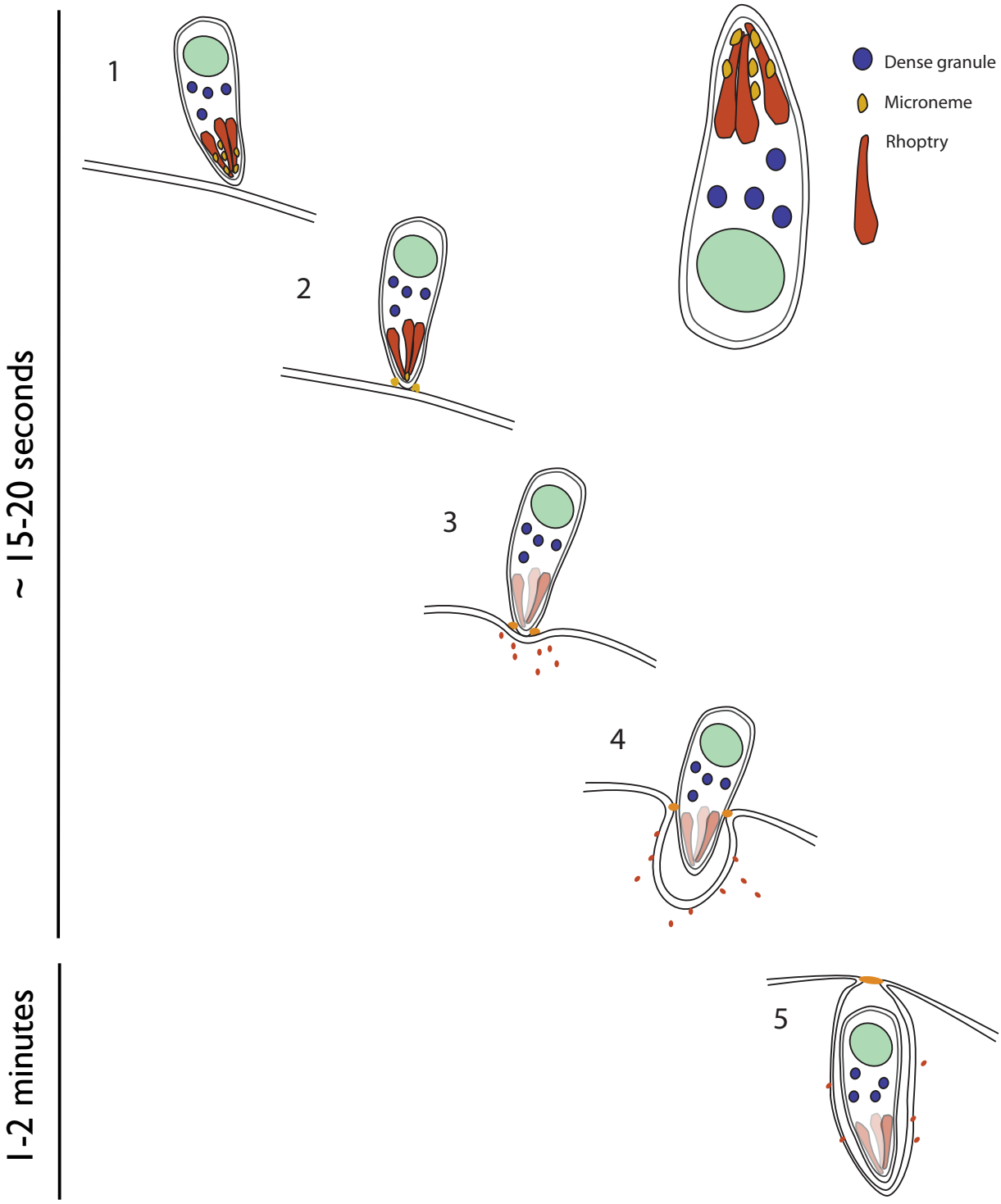
~ 15-20 seconds
1-2 minutes
1
2
3
4
5
Dense granule
Microneme
Rhoptry

largely devoid of plasma membrane proteins [74, 75]. Throughout replication, tachyzoites remain in the PV, but retain access to necessary host metabolites [76] and cholesterol [77]. After initial infection and replication, tachyziotes convert to the slower growing bradyziote that establish cysts, particularly in muscle and brain tissue. These long-lived cysts represent an avenue for parasite dissemination as many intermediate hosts serve as food sources.

Immune Modulation by T. gondii

The long-term survival and successful transmission associated with cyst formation requires that *T. gondii* spread throughout the body of the host while limiting immunopathology associated with large scale infections. To this end, *Toxoplasma* has developed multiple mechanisms to subvert the normal immune response to suit its needs [78, 79]. Parasites preferentially infect cells of the immune system, such as macrophages and dendritic cells [80, 81], possibly because these cells can efficiently move the tachyziotes around the body [82]. Infecting immune cells may seem counterproductive, but in infected cells apoptotic death signals are actively dowregulated [83], and production of the anti-inflammatory cytokine IL-10 is upregulated [84]. Furthermore, while parasite infection results in the generation of IL-12 that promotes the induction of IFNγ-secreting Th1 T lymphocytes, infected cells are not responsive to signaling mediated by IFNγ [79]. Dissecting the molecular mechanisms that *T. gondii* utilizes is an area of active study. New evidence suggests that parasite-secreted proteins, particularly those secreted by parasite rhoptries, modulate signaling by interference with kinase-mediated signaling pathways within the host [85, 86].

6. Current Studies

Mast cells are the common denominator of this dissertation. Mast cells play central roles in both host defense and detrimental allergic responses. To this end, fully understanding how signaling is regulated or can be exogenously modulated is vital to the control of both helminth infections and allergic disease. Furthermore, the work presented here demonstrates that mast cells are useful tools that provide information to expand our knowledge in areas as diverse as membrane heterogeneity and host-pathogen interactions.

Chapter 2 investigates how mast cell signaling by antigen alters the lipid composition of membrane domains that contain the IgE/FcεRI signaling platform, allowing for the retention of more polyunsaturated phospholipid species. We show similar lipid changes can be induced by destablilizing the actin cytoskeleton, whereas its stabilization prevents the antigen-stimulated changes. These insights provide evidence that cytoskeletal components play crucial roles in regulating membrane heterogeneity at the plasma membrane. Chapter 3 characterizes the molecular basis of sphingosine-mediated inhibition of mast cell signaling, highlighting the contribution that plasma membrane polyphosphoinositides play in both granule and recycling endosomal exocytic events. Chapter 4 documents our further investigations of RE, most notably the possible role they play in the secretion of cytokines in mast cells. Our interest in the diverse functions of recycling endosomes, aided by the discrete morphological distribution of RE in RBL cells, led us to investigate their possible contribution to the establishment of the PVM of *Toxoplasma gondii* in newly invaded cells. Chapter 5

shows compelling evidence that RE does, in fact, contribute to the PVM. Finally, in Chapter 6, we establish that *T. gondii* rapidly modulates IgE/FcεRI-mediated signaling that results in reduced degranulation responses. Further, we provide evidence that this inhibition is mediated by imparing PLCγ_1 activation. We postulate that this inhibitory function may be relevant to infection of other immune cells.

REFERENCES

1. Stow, J.L., et al., *Cytokine secretion in macrophages and other cells: pathways and mediators.* Immunobiology, 2009. **214**(7): p. 601-12.

2. Vyas, H. and G. Krishnaswamy, *Paul Ehrlich's "Mastzellen"--from aniline dyes to DNA chip arrays: a historical review of developments in mast cell research.* Methods Mol Biol, 2006. **315**: p. 3-11.

3. Prussin, C. and D.D. Metcalfe, *5. IgE, mast cells, basophils, and eosinophils.* J Allergy Clin Immunol, 2006. **117**(2 Suppl Mini-Primer): p. S450-6.

4. Metcalfe, D.D., D. Baram, and Y.A. Mekori, *Mast cells.* Physiol Rev, 1997. **77**(4): p. 1033-79.

5. Seldin, D.C., et al., *Homology of the rat basophilic leukemia cell and the rat mucosal mast cell.* Proc Natl Acad Sci U S A, 1985. **82**(11): p. 3871-5.

6. *Airborne allergens: Something in the air*, in *NIH Publication* N.I.o.A.a.I. Disease, Editor. 2003.

7. Marshall, J.S., *Mast-cell responses to pathogens.* Nat Rev Immunol, 2004. **4**(10): p. 787-99.

8. Ierna, M.X., et al., *Mast cell production of IL-4 and TNF may be required for protective and pathological responses in gastrointestinal helminth infection.* Mucosal Immunol, 2008. **1**(2): p. 147-55.

9. Brooker, S., A.C. Clements, and D.A. Bundy, *Global epidemiology, ecology and control of soil-transmitted helminth infections.* Adv Parasitol, 2006. **62**: p. 221-61.

10. Hoste, H., S. Sotiraki, and J.F. de Jesus Torres-Acosta, *Control of endoparasitic nematode infections in goats.* Vet Clin North Am Food Anim Pract, 2011. **27**(1): p. 163-73.

11. Baram, D., Y.A. Mekori, and R. Sagi-Eisenberg, *Synaptotagmin regulates mast cell functions.* Immunol Rev, 2001. **179**: p. 25-34.

12. Pierini, L., D. Holowka, and B. Baird, *Fc epsilon RI-mediated association of 6-micron beads with RBL-2H3 mast cells results in exclusion of signaling proteins from the forming phagosome and abrogation of normal downstream signaling.* J Cell Biol, 1996. **134**(6): p. 1427-39.

13. McCurdy, J.D., T.J. Lin, and J.S. Marshall, *Toll-like receptor 4-mediated activation of murine mast cells.* J Leukoc Biol, 2001. **70**(6): p. 977-84.

14. Steffen, M., et al., *Presence of tumour necrosis factor or a related factor in human basophil/mast cells.* Immunology, 1989. **66**(3): p. 445-50.

15. Gordon, J.R. and S.J. Galli, *Mast cells as a source of both preformed and immunologically inducible TNF-alpha/cachectin.* Nature, 1990. **346**(6281): p. 274-6.

16. Baumgartner, R.A., et al., *Secretion of TNF from a rat mast cell line is a brefeldin A-sensitive and a calcium/protein kinase C-regulated process.* J Immunol, 1994. **153**(6): p. 2609-17.

17. Leal-Berumen, I., P. Conlon, and J.S. Marshall, *IL-6 production by rat peritoneal mast cells is not necessarily preceded by histamine release and can be induced by bacterial lipopolysaccharide.* J Immunol, 1994. **152**(11): p. 5468-76.

18. Grimbaldeston, M.A., et al., *Mast cell-derived interleukin 10 limits skin pathology in contact dermatitis and chronic irradiation with ultraviolet B.* Nat Immunol, 2007. **8**(10): p. 1095-104.

19. Cambier, J.C., *Antigen and Fc receptor signaling. The awesome power of the immunoreceptor tyrosine-based activation motif (ITAM).* J Immunol, 1995. **155**(7): p. 3281-5.

20. Hakimi, J., et al., *The alpha subunit of the human IgE receptor (FcERI) is sufficient for high affinity IgE binding.* J Biol Chem, 1990. **265**(36): p. 22079-81.

21. Kinet, J.P., *The high-affinity IgE receptor (Fc epsilon RI): from physiology to pathology.* Annu Rev Immunol, 1999. **17**: p. 931-72.

22. Geha, R.S., H.H. Jabara, and S.R. Brodeur, *The regulation of immunoglobulin E class-switch recombination.* Nat Rev Immunol, 2003. **3**(9): p. 721-32.

23. Field, K.A., D. Holowka, and B. Baird, *Fc epsilon RI-mediated recruitment of p53/56lyn to detergent-resistant membrane domains accompanies cellular signaling.* Proc Natl Acad Sci U S A, 1995. **92**(20): p. 9201-5.

24. Calloway, N., D. Holowka, and B. Baird, *A basic sequence in STIM1 promotes Ca2+ influx by interacting with the C-terminal acidic coiled coil of Orai1.* Biochemistry, 2010. **49**(6): p. 1067-71.

25. Calloway, N., et al., *Molecular clustering of STIM1 with Orai1/CRACM1 at the plasma membrane depends dynamically on depletion of Ca2+ stores and on electrostatic interactions.* Mol Biol Cell, 2009. **20**(1): p. 389-99.

26. Singer, S.J. and G.L. Nicolson, *The fluid mosaic model of the structure of cell membranes.* Science, 1972. **175**(23): p. 720-31.

27. Maxfield, F.R., *Plasma membrane microdomains.* Curr Opin Cell Biol, 2002. **14**(4): p. 483-7.

28. Brown, D.A. and J.K. Rose, *Sorting of GPI-anchored proteins to glycolipid-enriched membrane subdomains during transport to the apical cell surface.* Cell, 1992. **68**(3): p. 533-44.

29. Simons, K. and E. Ikonen, *Functional rafts in cell membranes.* Nature, 1997. **387**(6633): p. 569-72.

30. Brown, D.A. and E. London, *Functions of lipid rafts in biological membranes.* Annu Rev Cell Dev Biol, 1998. **14**: p. 111-36.

31. Veatch, S.L., et al., *Critical fluctuations in plasma membrane vesicles.* ACS Chem Biol, 2008. **3**(5): p. 287-93.

32. Field, K.A., D. Holowka, and B. Baird, *Compartmentalized activation of the high affinity immunoglobulin E receptor with membrane domains.* J Biol Chem, 1997. **272**(7): p. 4276-80.

33. Young, R.M., D. Holowka, and B. Baird, *A lipid raft environment enhances Lyn kinase activity by protecting the active site tyrosine from dephosphorylation.* J Biol Chem, 2003. **278**(23): p. 20746-52.

34. Young, R.M., et al., *Reconstitution of regulated phosphorylation of FcepsilonRI by a lipid raft-excluded protein-tyrosine phosphatase.* J Biol Chem, 2005. **280**(2): p. 1230-5.

35. Sheets, E.D., D. Holowka, and B. Baird, *Critical role for cholesterol in Lyn-mediated tyrosine phosphorylation of FcepsilonRI and their association with detergent-resistant membranes.* J Cell Biol, 1999. **145**(4): p. 877-87.

36. Hopkins, C.R. and I.S. Trowbridge, *Internalization and processing of transferrin and the transferrin receptor in human carcinoma A431 cells.* J Cell Biol, 1983. **97**(2): p. 508-21.

37. Yamashiro, D.J., et al., *Segregation of transferrin to a mildly acidic (pH 6.5) para-Golgi compartment in the recycling pathway.* Cell, 1984. **37**(3): p. 789-800.

38. Naal, R.M., et al., *Antigen-stimulated trafficking from the recycling compartment to the plasma membrane in RBL mast cells.* Traffic, 2003. **4**(3): p. 190-200.

39. Balasubramanian, N., et al., *Arf6 and microtubules in adhesion-dependent trafficking of lipid rafts.* Nat Cell Biol, 2007. **9**(12): p. 1381-91.

40. Dyer, N., et al., *Spermatocyte cytokinesis requires rapid membrane addition mediated by ARF6 on central spindle recycling endosomes.* Development, 2007. **134**(24): p. 4437-47.

41. Murray, R.Z., et al., *A role for the phagosome in cytokine secretion.* Science, 2005. **310**(5753): p. 1492-5.

42. Veale, K.J., et al., *Recycling endosome membrane incorporation into the leading edge regulates lamellipodia formation and macrophage migration.* Traffic, 2010. **11**(10): p. 1370-9.

43. Ang, A.L., et al., *Recycling endosomes can serve as intermediates during transport from the Golgi to the plasma membrane of MDCK cells.* J Cell Biol, 2004. **167**(3): p. 531-43.

44. Lock, J.G. and J.L. Stow, *Rab11 in recycling endosomes regulates the sorting and basolateral transport of E-cadherin.* Mol Biol Cell, 2005. **16**(4): p. 1744-55.

45. Manderson, A.P., et al., *Subcompartments of the macrophage recycling endosome direct the differential secretion of IL-6 and TNFalpha.* J Cell Biol, 2007. **178**(1): p. 57-69.

46. Reefman, E., et al., *Cytokine secretion is distinct from secretion of cytotoxic granules in NK cells.* J Immunol, 2010. **184**(9): p. 4852-62.

47. Di Pucchio, T., et al., *Direct proteasome-independent cross-presentation of viral antigen by plasmacytoid dendritic cells on major histocompatibility complex class I.* Nat Immunol, 2008. **9**(5): p. 551-7.

48. Wu, M., et al., *Differential targeting of secretory lysosomes and recycling endosomes in mast cells revealed by patterned antigen arrays.* J Cell Sci, 2007. **120**(Pt 17): p. 3147-54.

49. Varthakavi, V., et al., *The pericentriolar recycling endosome plays a key role in Vpu-mediated enhancement of HIV-1 particle release.* Traffic, 2006. **7**(3): p. 298-307.

50. Smith, A.C., et al., *Interaction of the Salmonella-containing vacuole with the endocytic recycling system.* J Biol Chem, 2005. **280**(26): p. 24634-41.

51. Zhang, M., et al., *Presenilin/gamma-secretase activity regulates protein clearance from the endocytic recycling compartment.* Faseb J, 2006. **20**(8): p. 1176-8.

52. Richards, P., et al., *Dendritic spine loss and neurodegeneration is rescued by Rab11 in models of Huntington's disease.* Cell Death Differ, 2011. **18**(2): p. 191-200.

53. Sonnichsen, B., et al., *Distinct membrane domains on endosomes in the recycling pathway visualized by multicolor imaging of Rab4, Rab5, and Rab11.* J Cell Biol, 2000. **149**(4): p. 901-14.

54. Ullrich, O., et al., *Rab11 regulates recycling through the pericentriolar recycling endosome.* J Cell Biol, 1996. **135**(4): p. 913-24.

55. D'Souza-Schorey, C., et al., *ARF6 targets recycling vesicles to the plasma membrane: insights from an ultrastructural investigation.* J Cell Biol, 1998. **140**(3): p. 603-16.

56. Horgan, C.P. and M.W. McCaffrey, *The dynamic Rab11-FIPs.* Biochem Soc Trans, 2009. **37**(Pt 5): p. 1032-6.

57. Lindsay, A.J. and M.W. McCaffrey, *Rab11-FIP2 functions in transferrin recycling and associates with endosomal membranes via its COOH-terminal domain.* J Biol Chem, 2002. **277**(30): p. 27193-9.

58. Hales, C.M., J.P. Vaerman, and J.R. Goldenring, *Rab11 family interacting protein 2 associates with Myosin Vb and regulates plasma membrane recycling.* J Biol Chem, 2002. **277**(52): p. 50415-21.

59. Wilson, G.M., et al., *The FIP3-Rab11 protein complex regulates recycling endosome targeting to the cleavage furrow during late cytokinesis.* Mol Biol Cell, 2005. **16**(2): p. 849-60.

60. Fielding, A.B., et al., *Rab11-FIP3 and FIP4 interact with Arf6 and the exocyst to control membrane traffic in cytokinesis.* EMBO J, 2005. **24**(19): p. 3389-99.

61. Horgan, C.P., et al., *Rab11-FIP3 is critical for the structural integrity of the endosomal recycling compartment.* Traffic, 2007. **8**(4): p. 414-30.

62. Hill, D. and J.P. Dubey, *Toxoplasma gondii: transmission, diagnosis and prevention.* Clin Microbiol Infect, 2002. **8**(10): p. 634-40.

63. Howe, D.K. and L.D. Sibley, *Toxoplasma gondii comprises three clonal lineages: correlation of parasite genotype with human disease.* J Infect Dis, 1995. **172**(6): p. 1561-6.

64. Khan, A., et al., *Genetic analyses of atypical Toxoplasma gondii strains reveal a fourth clonal lineage in North America.* Int J Parasitol, 2011. **41**(6): p. 645-55.

65. Sibley, L.D. and J.C. Boothroyd, *Virulent strains of Toxoplasma gondii comprise a single clonal lineage.* Nature, 1992. **359**(6390): p. 82-5.

66. Dubey, J.P., *Advances in the life cycle of Toxoplasma gondii.* Int J Parasitol, 1998. **28**(7): p. 1019-24.

67. Montoya, J.G. and J.S. Remington, *Management of Toxoplasma gondii infection during pregnancy.* Clin Infect Dis, 2008. **47**(4): p. 554-66.

68. Dubey, J.P., N.L. Miller, and J.K. Frenkel, *The Toxoplasma gondii oocyst from cat feces.* J Exp Med, 1970. **132**(4): p. 636-62.

69. Frenkel, J.K., J.P. Dubey, and N.L. Miller, *Toxoplasma gondii in cats: fecal stages identified as coccidian oocysts.* Science, 1970. **167**(3919): p. 893-6.

70. Dubey, J.P., *Toxoplasmosis - a waterborne zoonosis.* Vet Parasitol, 2004. **126**(1-2): p. 57-72.

71. Lingelbach, K. and K.A. Joiner, *The parasitophorous vacuole membrane surrounding Plasmodium and Toxoplasma: an unusual compartment in infected cells.* J Cell Sci, 1998. **111 (Pt 11)**: p. 1467-75.

72. Besteiro, S., J.F. Dubremetz, and M. Lebrun, *The moving junction of apicomplexan parasites: a key structure for invasion.* Cell Microbiol, 2011. **13**(6): p. 797-805.

73. Carruthers, V. and J.C. Boothroyd, *Pulling together: an integrated model of Toxoplasma cell invasion.* Curr Opin Microbiol, 2007. **10**(1): p. 83-9.

74. Mordue, D.G., et al., *Invasion by Toxoplasma gondii establishes a moving junction that selectively excludes host cell plasma membrane proteins on the basis of their membrane anchoring.* J Exp Med, 1999. **190**(12): p. 1783-92.

75. Mordue, D.G., et al., *Toxoplasma gondii resides in a vacuole that avoids fusion with host cell endocytic and exocytic vesicular trafficking pathways.* Exp Parasitol, 1999. **92**(2): p. 87-99.

76. Sinai, A.P. and K.A. Joiner, *Safe haven: the cell biology of nonfusogenic pathogen vacuoles.* Annu Rev Microbiol, 1997. **51**: p. 415-62.

77. Coppens, I., A.P. Sinai, and K.A. Joiner, *Toxoplasma gondii exploits host low-density lipoprotein receptor-mediated endocytosis for cholesterol acquisition.* J Cell Biol, 2000. **149**(1): p. 167-80.

78. Laliberte, J. and V.B. Carruthers, *Host cell manipulation by the human pathogen Toxoplasma gondii.* Cell Mol Life Sci, 2008. **65**(12): p. 1900-15.

79. Leng, J., B.A. Butcher, and E.Y. Denkers, *Dysregulation of macrophage signal transduction by Toxoplasma gondii: past progress and recent advances.* Parasite Immunol, 2009. **31**(12): p. 717-28.

80. Bierly, A.L., et al., *Dendritic cells expressing plasmacytoid marker PDCA-1 are Trojan horses during Toxoplasma gondii infection.* J Immunol, 2008. **181**(12): p. 8485-91.

81. Denkers, E.Y. and B.A. Butcher, *Sabotage and exploitation in macrophages parasitized by intracellular protozoans.* Trends Parasitol, 2005. **21**(1): p. 35-41.

82. Lambert, H. and A. Barragan, *Modelling parasite dissemination: host cell subversion and immune evasion by Toxoplasma gondii.* Cell Microbiol, 2010. **12**(3): p. 292-300.

83. Sinai, A.P., et al., *Mechanisms underlying the manipulation of host apoptotic pathways by Toxoplasma gondii.* Int J Parasitol, 2004. **34**(3): p. 381-91.

84. Khan, I.A., T. Matsuura, and L.H. Kasper, *IL-10 mediates immunosuppression following primary infection with Toxoplasma gondii in mice.* Parasite Immunol, 1995. **17**(4): p. 185-95.

85. Saeij, J.P., et al., *Polymorphic secreted kinases are key virulence factors in toxoplasmosis.* Science, 2006. **314**(5806): p. 1780-3.

86. Taylor, S., et al., *A secreted serine-threonine kinase determines virulence in the eukaryotic pathogen Toxoplasma gondii.* Science, 2006. **314**(5806): p. 1776-80.

87. Mukherjee, S., R.N. Ghosh, and F.R. Maxfield, *Endocytosis.* Physiol Rev, 1997. **77**(3): p. 759-803.

CHAPTER TWO

IgE Receptor-Mediated Alteration of Membrane-Cytoskeletal Interactions Revealed by Mass Spectrometric Analysis of Detergent-Resistant Membranes[1]

SUMMARY

We use electrospray ionization mass spectrometry to quantify >100 phospholipid (PL) components in detergent-resistant membrane (DRM) domains that are related to ordered membrane compartments commonly known as lipid rafts. We previously compared PL compositions of DRMs with plasma membrane vesicles and whole cell lipid extracts from RBL mast cells, and we made the initial observation that antigen stimulation of IgE receptors (FcεRI) causes a significant change in the PL composition of DRMs [Fridriksson, E. K., et al. (1999) *Biochemistry 38*, 8056-8063]. We now characterize the signaling requirements and time course for this change, which is manifested as an increase in the recovery of polyunsaturated PL in DRM, particularly in phosphatidylinositol species. We find that this change is largely independent of tyrosine phosphorylation, stimulated by engagement of FcεRI, and can be activated by Ca^{2+} ionophore independent of antigen stimulation. Unexpectedly, we found that inhibitors of actin polymerization (cytochalasin D, latrunculin A) cause a similar, but more rapid, change in the PL composition of DRMs in the absence of FcεRI activation, indicating that perturbations in the actin cytoskeleton affect the organization of plasma membrane

---

[1] Published as X. Han*, N. L. Smith*, D. Sil, D. A. Holowka, F. W. McLafferty and B. A. Baird. *IgE Receptor-Mediated Alteration of Membrane-Cytoskeletal Interactions Revealed by Mass Spectrometric Analysis of Detergent-Resistant Membranes*. Biochemistry, 2009. **48**(27): p6540-50. Reprinted with permission.

domains. Consistent with this interpretation, a membrane-permeable stabilizer of F-actin, jasplakinolide, prevents antigen-stimulated changes in DRM PL composition. These results are confirmed by a detailed analysis of multiple experiments, showing that receptor and cytochalasin D-stimulated changes in DRM lipid composition follow first-order kinetics. Analysis in terms of the number of double bonds in the fatty acid chains is valid for total PL of the major head groups and for head groups individually. In this manner we show that, on average, concentrations of saturated or monounsaturated PL decrease in the DRM, whereas concentrations of PL with two or more double bonds (polyunsaturated PL) increase due to cytoskeletal perturbation. We find that these changes are independent of fatty acid chain length. Our mass spectrometric analyses provide a detailed accounting of receptor-activated alterations in the plasma membrane that are regulated by the actin cytoskeleton.

INTRODUCTION

Functional roles for lipid heterogeneity and lipid-based membrane domains in cellular processes have received increasing attention during the past decade [1, 2]. Central to this topic are regions of the plasma membrane containing lipids with liquid ordered (L_o)-like phase behavior, commonly called lipid rafts [1, 3]. Originally identified as a subset of plasma membrane lipids and proteins that are not solubilized by mild detergents such as Triton X-100 [4-6], these membrane domains have been implicated in a variety of cellular functions, including receptor signaling, vesicle trafficking to and from the plasma membrane, and host-pathogen interactions [7-9]. Studies on model membranes show that membrane domains composed predominately of cholesterol and

sphingomyelin or saturated phosphoglycerolipids are in an Lo phase that is sufficient to confer detergent resistance and segregation from liquid disordered (Ld) regions of lipid bilayers [1]. However, because lipid rafts in cells have variable lipid and protein composition, are dynamic, and are difficult to detect by optical microscopy or other non-destructive methods, their true nature and even their existence in live cells has been a subject of controversy [10, 11] and continues to be evaluated with the development of new approaches [12, 13].

Although use of detergent resistance as an indicator for lipid rafts in cells requires careful interpretation, this property continues to serve as a valuable correlative tool [12]. A complementary approach frequently used to visualize coalesced lipid rafts in live cells is to crosslink certain receptors or lipid raft components under conditions that result in large-scale co-clustering of other raft components [14-17]. Results from these fluorescence imaging experiments are generally consistent with predictions from detergent-dependent membrane fractionation [8, 13], and, used together with biological assays, they support the relevance of this biochemical approach to the functional characterization of lipid rafts and associated components. In mast cells, crosslinking of the high affinity IgE receptor, FcεRI, causes its stable association with lipid rafts as assessed by cell lysis with low concentrations of detergent (e.g., 0.05% Triton X-100) and sucrose gradient fractionation. This association is highly correlated with the initiation of cell signaling mediated by native FcεRI [18] or chimeric, single-chain IgE receptors [19].

Under experimental conditions that show co-redistribution of lipid raft components at the cell surface, F-actin is commonly found to co-localize with raft domains by fluorescence microscopy imaging, suggesting a structural relationship between lipid rafts and the cortical cytoskeleton [20-22]. Consistent with this observation, alteration of cholesterol content that inhibits initiation of IgE receptor signaling [17] can also perturb plasma membrane-cytoskeletal interactions [17]. Results in the present study provide new evidence from mass spectrometry for significant coupling between lipid rafts and the actin cytoskeleton.

In a previous study [17], we used Fourier transform mass spectrometry (FTMS) with electrospray ionization (ESI/MS) to characterize the phospholipid (PL) composition of plasma membranes and detergent resistant membranes (DRMs) isolated from RBL mast cells. The unusual FTMS capabilities of resolving power and sensitivity identified unique molecular masses of nearly 100 components, including a number of new species, while mass isolation and dissociation of individual molecular ions provided fragment masses for reliable molecular characterization (24). We showed that both of these membrane preparations are enriched in sphingomyelin and phosphoglycerolipids with saturated or monounsaturated acyl chains, compared to phosphoglycerolipids with polyunsaturated acyl chains. However, the DRM preparations have significantly higher percentages of sphingomyelin and saturated acyl chains, as expected for Lo domains. In contrast, PLs extracted from the whole cells are highly enriched in polyunsaturated species. We discovered that stimulation of RBL cells via FcεRI causes a substantial increase in the ratio of polyunsaturated to saturated plus monounsaturated PLs (P/S+M)

recovered in DRMs. The structural and functional basis for this stimulated change was intriguing but unclear. In the present study, we collect and analyze extensive mass spectrometry data to characterize this DRM lipid compositional change and its temporal trend, and we find that this change follows first-order kinetics and depends on stimulated changes in the actin cytoskeleton. Our results point to sensitive, dynamic regulation of lipid rafts by the actin cytoskeleton that is modulated during receptor-mediated cell activation.

MATERIALS AND METHODS

Cell Stimulation, DRM Vesicle Isolation, and Lipid Extraction.

Methods used are similar to those described by Fridriksson et al. [23], with some modifications. RBL-2H3 cells [24] were sensitized overnight with a 2-5 molar excess over FcεRI of purified anti-DNP IgE [25]. Cells were harvested, washed twice with buffered saline solution (BSS: 135 mM NaCl, 5 mM KCl, 1 mM $MgCl_2$, 1.8 mM $CaCl_2$, 5.6 mM glucose, 20 mM HEPES, pH 7.4, 1 mg/ml BSA) and resuspended at 8 x 10^6 cells/mL. Cells were stimulated with multivalent DNP-BSA (2-5 μg/ml) for 2 to 30 min at 37°C. For some experiments, the Src family tyrosine kinase inhibitor PP1 (BioMol, Plymouth Meeting, PA) was added at 4 μM, 2 min prior to antigen stimulation. For other experiments, jasplakinolide (Invitrogen/Molecular Probes, Eugene, OR) was added at 3 μM for 1 hour at 37°C prior to antigen stimulation. Alternatively, cells were stimulated with 0.9 μM A23187 (Calbiochem, San Diego, CA) for 5 or 15 min, or treated with 0.2-2μM cytochalasin D (Sigma Chemical Co, St. Louis, MO) or 0.2 μM latrunculin A (Invitrogen/Molecular Probes) for 1, 2 or 10 min, all at 37°C.

Following stimulation, cells were lysed by mixing 1:1 with 2x ice-cold lysis buffer (20 mM Tris-HCl, 100 mM NaCl, 2 mM sodium orthovanadate, 60 mM sodium pyrophosphate, 20 mM sodium glycerophosphate, 0.04 U/ml aprotinin, 0.02% sodium azide) containing 0.09% Triton X-100 and 2 mM 4-(2-aminoethyl)benzenesulfonyl fluoride hydrochloride (AEBSF) (Sigma). After 10 min at 4°C, 3.6 pmoles of 1,2-di-nonadecanoyl-sn-glycero-3-phosphatidylcholine (Avanti; PC 38:0) was added as an exogenous lipid standard (accounts for 1-2 Mol% of total lipids detected). Then 10 ml of this cell lysate was mixed 1:1 with 80% sucrose (w/v) in HEPES/saline buffer (25 mM HEPES, 150 mM NaCl and 2 mM EDTA, pH 7.5). These lysates were placed in centrifuge tubes, then 5 ml of 35% sucrose and 5 ml of 5% sucrose in HEPES/saline buffer were carefully layered on top of the 40% sucrose solution containing the cell lysates. Gradients were centrifuged at 100,000 xg for 15-18 hr at 4°C using a Beckman SW-28 rotor in a Sorvall Discovery 100S ultracentrifuge.

After centrifugation, two opaque bands were visible, and the upper band (3 mL), previously identified as containing the DRMs [23], was collected from the interface of the 5% and 35% layers. The contents were diluted with 15 mL phosphate buffered saline (PBS) containing 1 mM EDTA and centrifuged at 300,000 xg for 30 min at 4°C in a Beckman Ti60 rotor. Pellets were resuspended in 400 μl PBS-EDTA, and lipids were extracted using a modified Bligh-Dyer method [26]: the suspended pellets were each mixed with 1.5 mL chloroform/methanol at a 1:2 ratio and vortexed, then 0.5 mL of chloroform was added, and samples were vortexed again. Finally, 0.5 mL of 2N HCl was added, and samples were vortexed and then centrifuged at 2000 xg for 5 min to

achieve phase separation. The lower (chloroform) layer was collected and used for ESI/MS analysis. To determine plasmalogen content of DRMs, pellets were resuspended in 400 μl of 50 mM LiCl, pH 6. 50 mM LiCl was also used in place of 2 N HCL in the extraction process [27].

To determine the percentage of cellular PL recovered in DRMs, 2 X 10^6 cells in BSS were pelleted, resuspended in 400 ml PBS-EDTA and PL were extracted as described for DRMs. For organic phosphate analysis to quantify PL concentrations, extracted PL in chloroform from either DRMs (200 μl) or cells (1 ml) was treated as described previously [28], and the amount of organic phosphate was used as a measure of PL recovered. Comparison of PL recovered per cell equivalent of extracted DRMs and cells permits calculation of the % of PL recovered in DRMs.

Tyrosine Phosphorylation Assay.

RBL-2H3 cells were sensitized overnight with IgE as above, harvested and washed twice with BSS, and then resuspended at 2 x 10^6 cells/ml. Cells were then stimulated with DNP-BSA (0.8 μg/ml) in the presence or absence of 4 μM PP1 at 37°C for times indicated. Samples were quenched by addition of 5x sample buffer (50% glycerol, 0.25 M Tris, pH 6.8), 5% (w/v) SDS, 0.05% (w/v) bromophenol blue) and boiling for 5 min. Samples were electrophoresed and detected by western blotting with 4G10 anti-phosphotyrosine [19].

Cholesterol Content Assay

Free cholesterol in DRMs was assayed using the Amplex Red Cholesterol Assay Kit (Invitrogen/Molecular Probes) following kit instructions, except that cholesterol esterase was omitted from the DRM samples. Following specified incubations, samples were placed on ice, and sample fluorescence was measured with an SLM 8000C spectrofluorometer. We found that 10 μl aliquots of pelleted, resuspended DRMs contain cholesterol values in the linear region of the standard curve.

Quantitative Analysis of Phospholipids Using Electrospray Ionization Mass Spectrometry (ESI/MS).

Spectra were acquired on a modified 6T Finnigan FTMS instrument (Finnigan, Madison, WI) equipped with an electrospray ion source, as described previously [29]. Prior to nanospraying, lipid extracts prepared as described above were diluted 10-fold in 49:49:2 (v/v/v) methanol:chloroform:acetic acid for the positive ion mode and 10-fold in 1:1 (v/v) methanol:chloroform for the negative ion mode [30, 31]. Typically, less than 2 x 10^5 cell equivalents of the lipid extract (<6 nmol of phospholipid) were needed to obtain complete positive and negative mode spectra. For determination of plasmalogen species in the extract, LiOH was added to a final concentration of 2mM prior to the analyses; in the positive ion spectra the lipid species were observed as Li adducts (+ 6 Da). For each sample, four separate aliquots were measured and mol % values (± standard deviation) were determined for each species.

Relative instrument responses (peak intensity per mole of analyte) were determined using a standard mixture of phosphatidylcholine (PC): phosphatidylethanolamine (PE): sphingomyelin (SM): phosphatidylinositol (PI): phosphatidylglycerol (PG): phosphatidylserine (PS): phosphatidic acid (PA) at equimolar ratios for both the positive ion mode and the negative ion mode [23]. Variation of instrument response per mole with acyl chain length and degree of unsaturation was not evaluated, but it is far less than that with headgroups at the low concentration used here [32]. Any such variation will not affect the change of mol% values with experimental parameters on a relative basis. As previously established [33], below 100 μmol total lipids, there are no aggregated ions, and the ion counts are proportional to lipid concentrations in these limits. The detailed ESI/MS data were tabulated as mol% for each PL head group in terms of acyl chain length (number of carbon atoms) and number of double bonds (see Table 1). For kinetic analyses these values are summed for both acyl chains of PC, PE, PS, PI, PG, PA or for the single acyl chain of SM. The mol% data were compiled for samples taken at multiple time points after initiation of a specified treatment. Table 2.1 and Figures 2.3 and 2.5 show representative data from a single experiment. Figures 2.1, 2.2, and 2.4 show data from multiple experiments averaged together.

Kinetic Analysis of PL changes

For systematic analysis over multiple samples and experiments with different treatments, the PL composition data are compared in terms of headgroups, the total number of double bonds in the acyl chains (db0, db1, db2, db3, and db4+), and acyl

chain length. A simple evaluation of time dependent changes monitors acyl chain saturation and represents the mol% abundance data as the lumped ratio P/(S+M), where P corresponds to polyunsaturated (db2, db3, and db4+) acyl chains, S corresponds to saturated (db0) acyl chains, and M corresponds to mono-unsaturated (db1) acyl chains (see Figure 2).

For a comprehensive analysis of compositional changes with time, the mol% values are evaluated with a first-order kinetic model. Useful parameters for comparison are the value of the first order rate constant k together with the direction and magnitude of the concentration change. We consider a species with concentration C(t) that may increase or decrease with time after stimulation; C_i corresponds to the initial (pre-stimulation) concentration and C_f corresponds to the final concentration that stabilizes after stimulation.

$$[C(t) - C_f]/ [C_i - C_f] = \exp(-kt)$$

$$C(t) = (C_i - C_f)\exp(-kt) + C_f \qquad (1)$$

For species with decreasing concentration, $[C_i - C_f] > 0$, and for species with increasing concentration, $[C_i - C_f] < 0$. The direction of the change is given by the value $n = [C_f - C_i]/|C_f - C_i|$ Because of the absolute value in the denominator, n = -1 for species that decrease in concentration, and n= +1 for species that decrease in concentration. The lumped term $k_m = nk$ represents the value of the rate constant and the direction of concentration change.

For sufficiently short times, as compared to the time course of the concentration change, the exponential in Eqn 1 can be replaced by a truncated Taylor series, $\exp(-kt) \simeq 1 - kt$, yielding a linear expression for C(t) vs t and an approximate first order rate constant k_a:

$$C(t) = C_i + (C_f - C_i)k_a t \qquad (2)$$

Note that the slope in this linear approximation, $k_s = (C_f - C_i)k_a$, is a lumped term representing the magnitude and direction of the concentration change *times* the value of k_a. The mol% (C(t)) data are plotted according Eqn 1 (Figure 2.1.A and 2.1.B), or Eqn 2 (Figure 3). From these primary plots, the values of $k_m = nk$ (Figure 2.1.C) or $k_s = (C_f - C_i)k_a$ (Figures 4 and 5) are plotted as a function of the total number of double bonds in the acyl chains with specified headgroups.

Data fitting for exponential curves over longer time periods (Eqn 1; Figures 2.1A and B) and linear approximation curves at short times (Eqn 2; Figure 2.3) was carried out with MATLAB. We determined the linear approximation to be valid for DNP-BSA stimulation by the following comparison: Using mol% at long times (C_f) obtained from fitting the data in Figure 1A with Eqn 1, the value for $(C_f - C_i)$ was determined, and the approximate rate constant k_a was calculated from $(C_f - C_i)k_a$ values obtained from the linear fit (Eqn 2, Figure 3). We find that these k_a values are very similar to k values obtained directly from Figure 1A. Similarly, from a linear fit (Eqn 2) of the 0, 2, 5, 10 min data of Figure 1A, the slope $(C_f - C_i)k$ values were determined. These are also very similar to the $(C_f - C_i)k_a$ values obtained from the slopes in Figure 2.3. This validation of

the linear approximation for DNP-BSA stimulation allowed direct comparison of multiple treatments over the shorter time period (Figure 2.4).

RESULTS

Unsaturated PL Increase in DRM Fractions upon Receptor Mediated Cell Activation

A complete PL analysis was carried out by ESI/MS for DRM samples from cells before and after stimulation with the antigen DNP-BSA at several time points, as represented by the experiment shown in Table 2.1. Notable in these representative data is the high mol% of total SM in DRMs from unstimulated cells (27.6 mol% of the total phospholipids), indicative of highly purified DRM preparations, and similar to SM values of 20-23 mol% for DRM and non-detergent lipid raft preparations from KB cells characterized by Pike et al. [27]. The mol% of SM decreases as a function of stimulation time while total PI increases with stimulation time as exemplified in Table 2.1. A compiled presentation of lipid compositional changes from many different experiments with DNP-BSA stimulation is shown in Figure 2.1.A, where the extensive data are represented in terms of headgroups (separate panels) and for each of these, the mol% of total PL (open circles, right ordinate). These compiled data show that, on average, SM decreased from 28% to 17% after 30 min of antigen stimulation, and PI increased from 17% to 34% within this period; the other major PLs (PC, PE and PS) show relatively small changes in total mol% as a function of stimulation time.

Lipid changes with respect to acyl chain unsaturation were evaluated (Figure 2.1.A, solid symbols, left ordinate). DNP-BSA stimulation time courses were measured

Table 2.1. Normalized mol % of PL in DRMs isolated from cells before and at specified times after DNP-BSA stimulation.

[a]Minutes stimulated with antigen; [b]*xx:y* = total number of carbon atoms in the fatty acid chains: number of double bonds. Standard deviations (*SD*) are shown for the sums within each group. The data are averages over four measurements from a single representative experiment. *Sum S*, *Sum M*, and *Sum P* are the sums of the saturated (S, db0), monounsaturated (M, db1), and polyunsaturated (P, db2 – db4+) phospholipids (PL), respectively, where the degree of saturation refers to the number of double bonds in the the fatty acid chains. The total PL composition for each time point is 100%.

	PC $(M+H)^+$				**SM** $(M+H)^+$				**PE** $(M+H)^+$				**PS** $(M-H)^-$				**PI** $(M-H)^-$				**PG** $(M-H)^-$				**PA** $(M-H)^-$			
Lipid	0[a]	2	5	10	0	2	5	10	0	2	5	10	0	2	5	10	0	2	5	10	0	2	5	10	0	2	5	10
32:0 [b]	1.2	0.6	0.6	0.4																	0.01	0.02	0.02	0.01				
34:0	1.2	0.9	0.7	0.5					1.7	0.9	1.0	0.8	0.1	0.1	0.2	0.2	0.2	0.4	0.3	0.4	0.05	0.07	0.07	0.09				
36:0	0.4	0.3	0.2	0.2					1.8	1.2	1.2	0.8	0.8	0.7	0.6	0.6	0.9	0.6	1.3	1.1	0.04	0.03	0.06	0.05	0.02	0.04	0.03	0.04
40:0									0.7	0.6	0.5	0.9																
16:0					3.6	4.0	3.4	1.8																				
18:0					5.3	4.0	3.4	2.0																				
24:0					8.7	7.4	5.6	3.2																				
sum S	**2.8**	**1.8**	**1.5**	**1.1**	**17.7**	**15.3**	**12.4**	**7.1**	**4.2**	**2.8**	**2.7**	**2.6**	**0.9**	**0.9**	**0.8**	**0.8**	**1.1**	**0.9**	**1.5**	**1.5**	**0.09**	**0.11**	**0.14**	**0.15**	**0.02**	**0.04**	**0.03**	**0.04**
SD	0.3	0.2	0.2	0.3	0.7	2.2	1.7	0.7	1.2	0.4	0.3	0.6	0.0	0.2	0.3	0.1	0.0	0.2	0.8	0.5	0.02	0.03	0.05	0.02	0.00	0.01	0.01	0.03
32:1	1.0	0.6	0.6	0.4																	0.01	0.01	0.01	0.02	0.02	0.04		
34:1	4.7	3.9	3.1	2.1					1.1	0.8	0.8	0.8	0.5	0.8	0.6	0.8	0.7	1.3	1.1	1.8	0.25	0.41	0.34	0.50	0.05	0.10		
36:1	2.8	2.2	1.6	1.4					4.3	3.1	3.2	2.0	5.6	4.9	3.8	3.6	4.3	2.3	4.2	3.8	0.09	0.14	0.19	0.18	0.18	0.28	0.17	0.34
38:1									2.8	2.6	2.3	1.7	0.7	1.1	0.8	1.2	0.2	0.3	0.4	0.4								
24:1					6.1	5.5	4.4	2.7																				
sum M	**8.4**	**6.7**	**5.3**	**3.9**	**6.1**	**5.5**	**4.4**	**2.7**	**8.2**	**6.5**	**6.3**	**4.5**	**6.8**	**6.8**	**5.1**	**5.6**	**5.2**	**3.9**	**5.7**	**6.0**	**0.3**	**0.6**	**0.5**	**0.7**	**0.2**	**0.4**	**0.2**	**0.3**
SD	1.4	0.7	0.8	0.8	0.6	0.6	0.8	0.5	0.8	1.3	0.9	1.4	0.3	1.8	2.0	1.0	0.8	0.8	1.3	2.0	0.1	0.2	0.3	0.2	0.1	0.1	0.1	0.2
sum S+M	**11.2**	**8.6**	**6.9**	**5.0**	**23.8**	**20.9**	**16.8**	**9.8**	**12.3**	**9.3**	**9.1**	**7.0**	**7.7**	**7.7**	**5.9**	**6.4**	**6.4**	**4.9**	**7.2**	**7.5**	**0.4**	**0.7**	**0.7**	**0.9**	**0.3**	**0.5**	**0.2**	**0.4**
SD	1.4	0.9	1.0	1.1	0.5	2.8	2.5	0.2	0.8	1.7	1.2	1.8	0.3	1.9	2.3	1.1	0.8	0.9	2.1	2.4	0.1	0.2	0.3	0.2	0.1	0.1	0.1	0.3
32:2	0.1	0.1	0.1	0.1																					0.02	0.05	0.02	0.02
32:3	0.3	0.5	0.6	0.6																								
34:2	0.5	0.5	0.4	0.3									0.1	0.2	0.2	0.2	0.1	0.2	0.2	0.3		0.16	0.15	0.15	0.02	0.12	0.02	0.05
34:3	0.4	0.7	0.8	0.9									0.1	0.1	0.2	0.2												
34:4	0.4	0.6	0.7	0.8									0.1	0.1	0.1	0.1												
34:5	0.2	0.2	0.2	0.2									0.1	0.2	0.2	0.3												
34:6													0.2	0.4	0.4	0.5												
36:2	1.7	1.5	1.0	1.0					0.9	1.1	0.6	0.4	0.6	0.6	0.5	0.5	1.9	1.0	1.8	1.8	0.05	0.09	0.11	0.11				
36:3	0.7	0.9	1.0	1.3					0.7	1.1	1.2	1.4	0.1	0.1	0.1	0.1												
36:4	1.7	3.0	3.2	4.5					0.6	0.7	0.8	1.0	0.2	0.2	0.2	0.2												
36:5	0.2	0.3	0.3	0.4									0.1	0.1	0.1	0.1												
38:2									1.0	0.9	0.8	0.8	0.6	1.0	0.6	0.9	0.9	0.9	1.4	1.5								
38:3									1.0	1.3	1.6	1.7	0.5	0.6	0.3	0.5	1.8	1.7	2.5	2.8								
38:4	1.0	1.4	1.6	2.1					1.9	2.9	3.5	4.6	0.2	0.3	0.2	0.2	2.3	2.6	3.1	3.4	0.03	0.06	0.04	0.06				
38:5	0.7	0.9	0.9	1.4					1.2	1.0	1.5	1.0	0.1	0.1	0.1	0.1	0.3	0.2	0.4	0.3	0.08	0.07	0.07	0.07				
38:6	0.2	0.2	0.2	0.3																	0.00	0.02	0.03	0.02				
40:3									1.6	0.7	0.8	1.4									0.07	0.22	0.08	0.10				
40:4	0.2	0.3	0.4	0.4					1.5	1.8	2.4	3.1					0.6	1.1	1.0	1.7	0.02	0.05	0.04	0.06				
40:5	0.2	0.3	0.5	0.4					0.9	1.0	0.9	1.3					1.0	1.5	1.5	2.7	0.05	0.09	0.09	0.14				
40:6	0.1	0.2	0.2	0.2									0.3	0.5	0.4	0.5	0.9	1.6	1.7	2.8	0.06	0.12	0.11	0.17				
40:7													0.2	0.3	0.6	0.3					0.12	0.21	0.20	0.34				
40:8													0.2	0.3	0.4	0.3												
42:5																					0.04	0.08	0.09	0.08				
42:6																					0.07	0.21	0.15	0.23				
42:7																					0.07	0.13	0.08	0.13				
18:2					0.4	0.5	0.7	0.7																				
18:3					1.2	1.7	2.5	2.5																				
20:2					0.7	1.0	1.3	1.5																				
20:3					1.5	2.3	3.4	3.5																				
Sum P	**8.7**	**11.6**	**12.0**	**14.7**	**3.8**	**5.5**	**8.0**	**8.2**	**11.3**	**12.5**	**14.1**	**16.7**	**3.7**	**5.2**	**4.7**	**4.8**	**9.7**	**10.8**	**13.5**	**17.3**	**0.7**	**1.5**	**1.2**	**1.7**	**0.0**	**0.2**	**0.0**	**0.1**
SD	1.7	1.5	1.7	1.4	0.9	2.1	1.4	2.4	2.9	0.9	1.2	2.2	0.4	1.3	0.6	0.5	1.5	2.1	2.1	2.0	0.1	0.3	0.2	0.3	0.0	0.0	0.0	0.1
Total	**19.9**	**20.2**	**18.9**	**19.7**	**27.6**	**26.4**	**24.8**	**18.0**	**23.6**	**21.8**	**23.1**	**23.7**	**11.5**	**12.8**	**10.6**	**11.2**	**16.0**	**15.7**	**20.7**	**24.9**	**1.1**	**2.2**	**1.9**	**2.5**	**0.3**	**0.6**	**0.2**	**0.5**
SD	2.7	2.3	2.7	2.1	1.0	3.6	3.5	2.6	3.3	2.0	2.4	2.7	0.4	3.2	2.4	0.6	2.1	2.8	3.9	4.4	0.1	0.3	0.5	0.4	0.1	0.1	0.1	0.3

in multiple experiments for stimulation times of typically 0, 2, 5, 10 min, and in some experiments up to 20 and 30 min. We observe generally that the PL with more unsaturated acyl chains (more double bonds) tend to increase in the DRM fractions with stimulation time, whereas those with saturated or mono-unsaturated acyl chains tend to decrease in these fractions. This is consistent with our previous observations made with DRMs derived from unstimulated cells and cells at a single (5 min) time point after DNP-BSA stimulation [23]. That previous study compared the PL composition simply in terms of acyl chain saturation: saturated (S: 0 double bonds, db0), mono-unsaturated (M: 1 double bond, db1), and polyunsaturated (P: 2 to 4 or more double bonds, db2 - db4+) and compiled the abundance data as the lumped ratio P/(S+M). This type of analysis of data in the present study (Figure 2.2) showed that this simple ratio increases with cell stimulation. For stimulation by DNP-BSA at 37°C (Figure 2.2, solid squares, dark line), the ratio increases approximately 4-fold with a half-time of about 7 min and stabilization by 20 min, whereas there are no changes over 20 min in the absence of stimulant (open squares, dark line). In comparison, DNP-BSA stimulation at 18°C (solid triangles, dark line) results in a somewhat slower, 2-fold increase in the P/(S+M) ratio by 20 min, consistent with the temperature dependence for other antigen-stimulated signaling processes in these cells [34]. Stimulated cellular degranulation is not detectable at 18°C [34], indicating that the lipid changes we observe at this temperature are not a consequence of degranulation.

We evaluated a first-order kinetic model (Eqn 1) for comprehensive evaluation of the detailed mol% data representing PL changes occurring in the DRM fractions after

Figure 2.1. Mol % of phospholipids (PL) in DRMs that contain 0, 1, 2, 3, and ≥ 4 double bonds (db0, db1, db2, db3, db4+, respectively) in the acyl chains *versus* (A) DNP-BSA antigen stimulation time (average of eight independent experiments) or (B) cytochalasin D stimulation time (average of four independent experiments) for each head group summed over head groups. Data points corresponding to specified number of double bonds (each of db0, db1, db2, db3, db4+) are fitted with an exponential decay corresponding to first-order kinetics (Eqn 1). Values of $k_m = nk$ (units of min^{-1}) are listed with each fitted curve. Errors bars show standard deviations from ≥ 4 separate experiments (0 and 10 min), or range of values from two separate experiments (2, 5, and 20 min). Data points with no error bars represent a single experiment (1 and 30 min). (C) The k_m values (units of min^{-1}) from Figures 1A and 1B *versus* the number of double bonds for each head group for DNP-BSA stimulation (squares, left ordinate) compared with cytochalasin D treatment (circles, right ordinate).

Figure 2.1.A

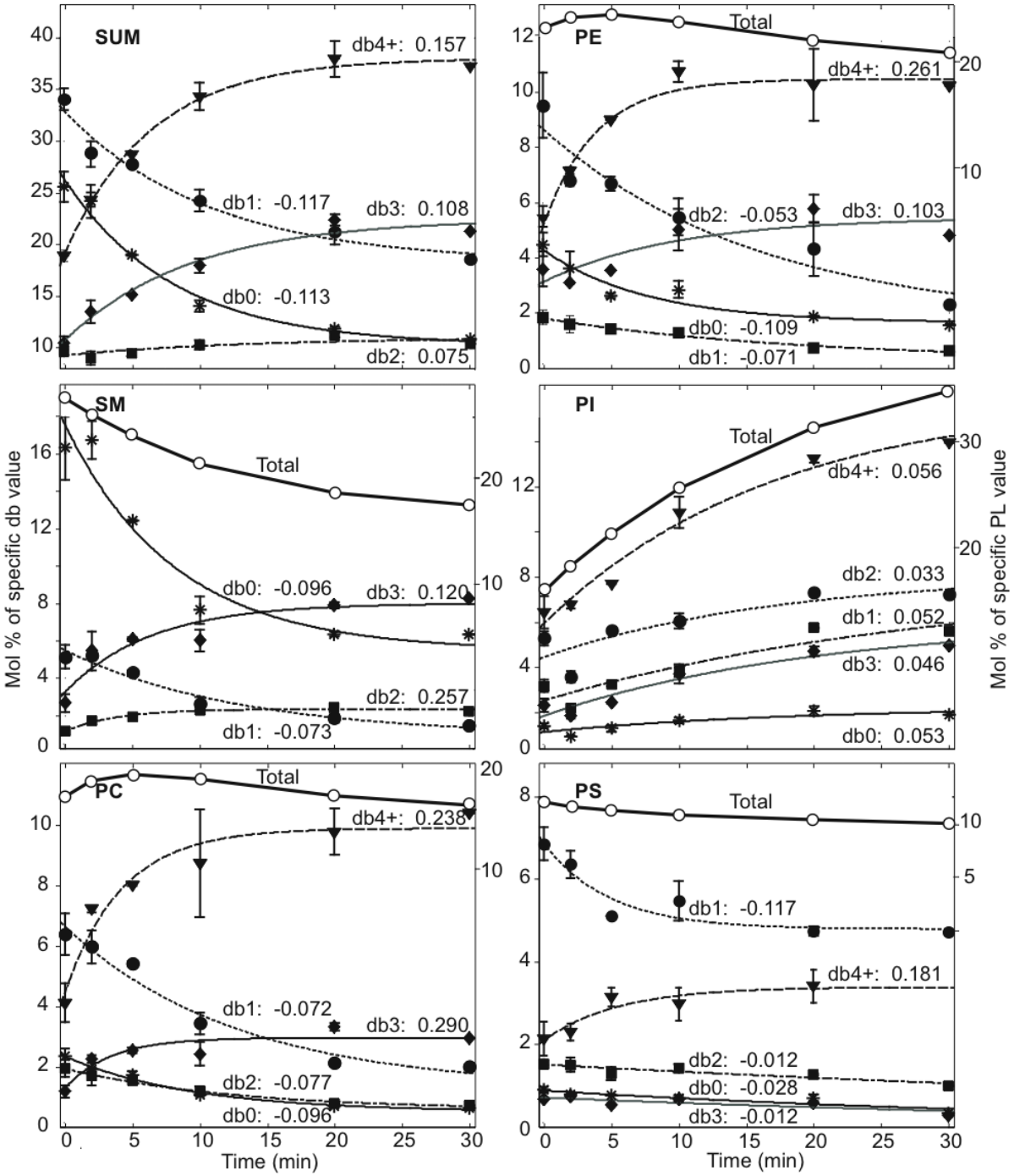
SUM
db4+: 0.157
db1: -0.117
db3: 0.108
db0: -0.113
db2: 0.075
PE
Total
db4+: 0.261
db2: -0.053
db3: 0.103
db0: -0.109
db1: -0.071
SM
Total
db0: -0.096
db3: 0.120
db2: 0.257
db1: -0.073
PI
Total
db4+: 0.056
db2: 0.033
db1: 0.052
db3: 0.046
db0: 0.053
PC
Total
db4+: 0.238
db1: -0.072
db3: 0.290
db2: -0.077
db0: -0.096
PS
Total
db1: -0.117
db4+: 0.181
db2: -0.012
db0: -0.028
db3: -0.012
Mol % of specific db value
Mol % of specific PL value
Time (min)
Time (min)

Figure 2.1.B (continued)

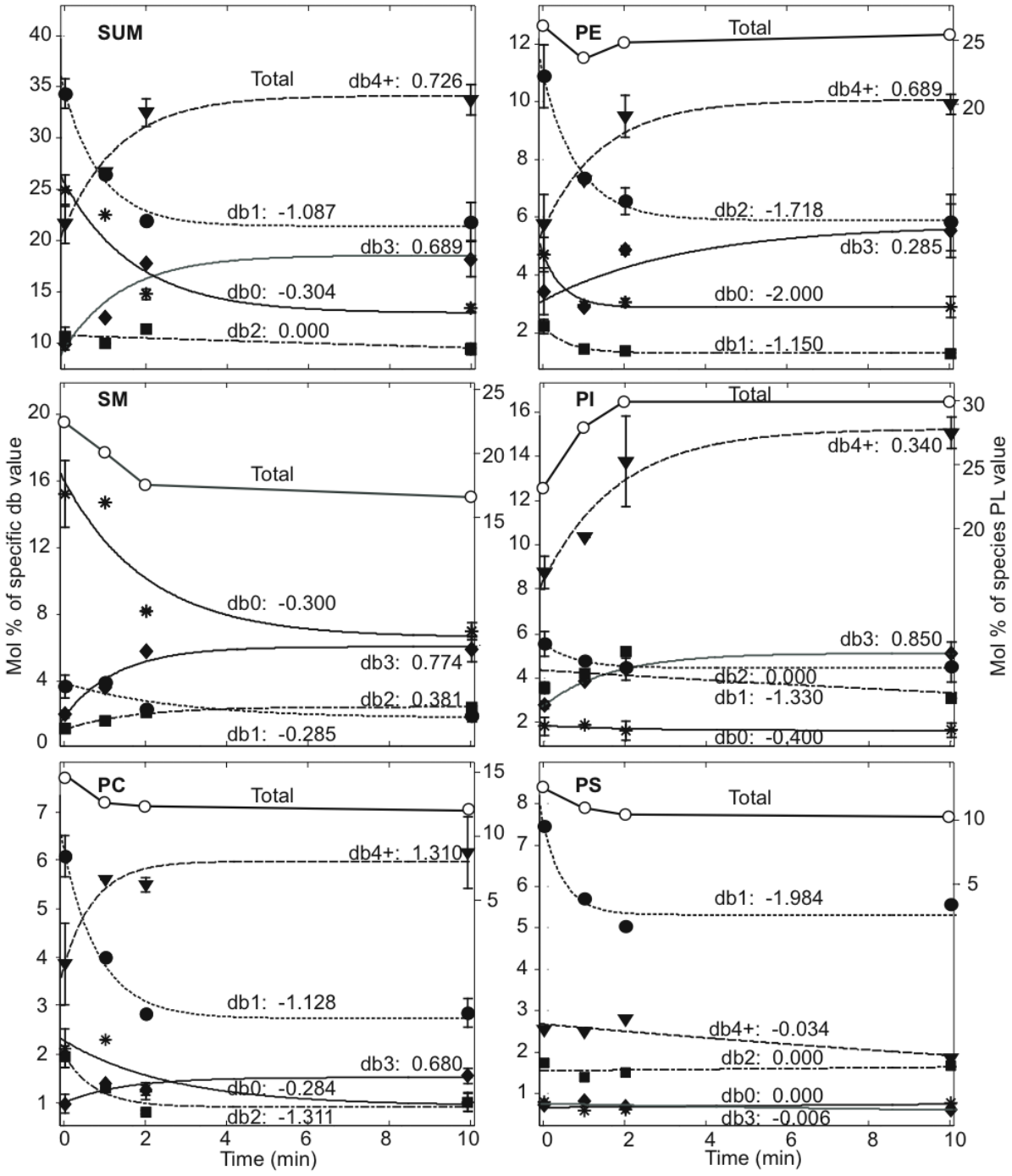

Figure 2.1.C (continued)

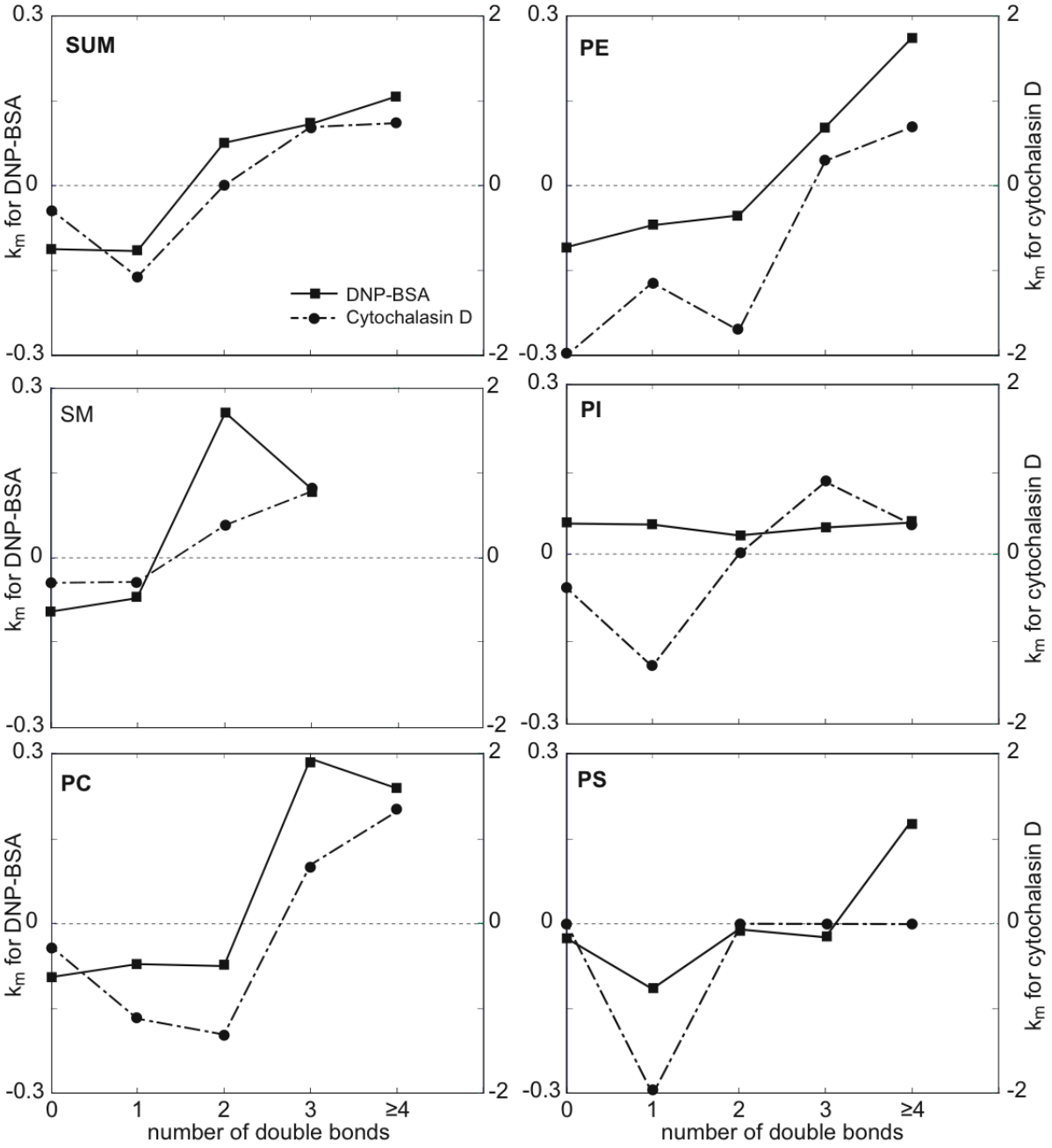

cell stimulation. Figure 2.1A shows first-order kinetic fits for data compiled from eight independent experiments with DNP-BSA stimulation. The data are fitted in terms of the total number of double bonds in the acyl chains (db0, db1, db2, db3, and db4+; left ordinate) associated with each head group (separate panels) (The minor species PG and PA, whose low mol% and corresponding large error bars result in more erratic behavior, are not shown). Data accumulated over 30 min stimulation are fitted with Eqn 1, which applies to species that decrease or increase in concentration. The quality of the fits shows that the compositional changes are consistent with a first-order kinetic model, and this analysis also provides a detailed accounting for our general observation that the degree of acyl chain unsaturation increases in DRM compartments after cells are stimulated with DNP-BSA ([23] and Figure 2.2).

With Eqn 1, the rate constants, k, for each number of double bonds within each head group can be determined from the exponential fits to the data (Figure 2.1.A; solid symbols fit by Eqn 1, left ordinate). The lumped value $k_m = nk$ (where n=+1 or –1 for increasing or decreasing concentration, respectively; see Materials and Methods) are listed with respective curves in Figure 1A. These k_m values for DNP-BSA stimulation are plotted as a function of the number of double bonds for each head group species in Figure 2.1.C (solid squares). These plots summarize succinctly the dependence of stimulated DRM compositional changes on the degree of acyl chain unsaturation. Values of $k = |k_m|$ for each head group and for summed PLs are generally less than 0.3 min^{-1} for DNP-BSA stimulation (Figure 2.1.C, left ordinate). It is notable in these plots that the x-axis is crossed as the k_m values go from negative (decreasing concentration)

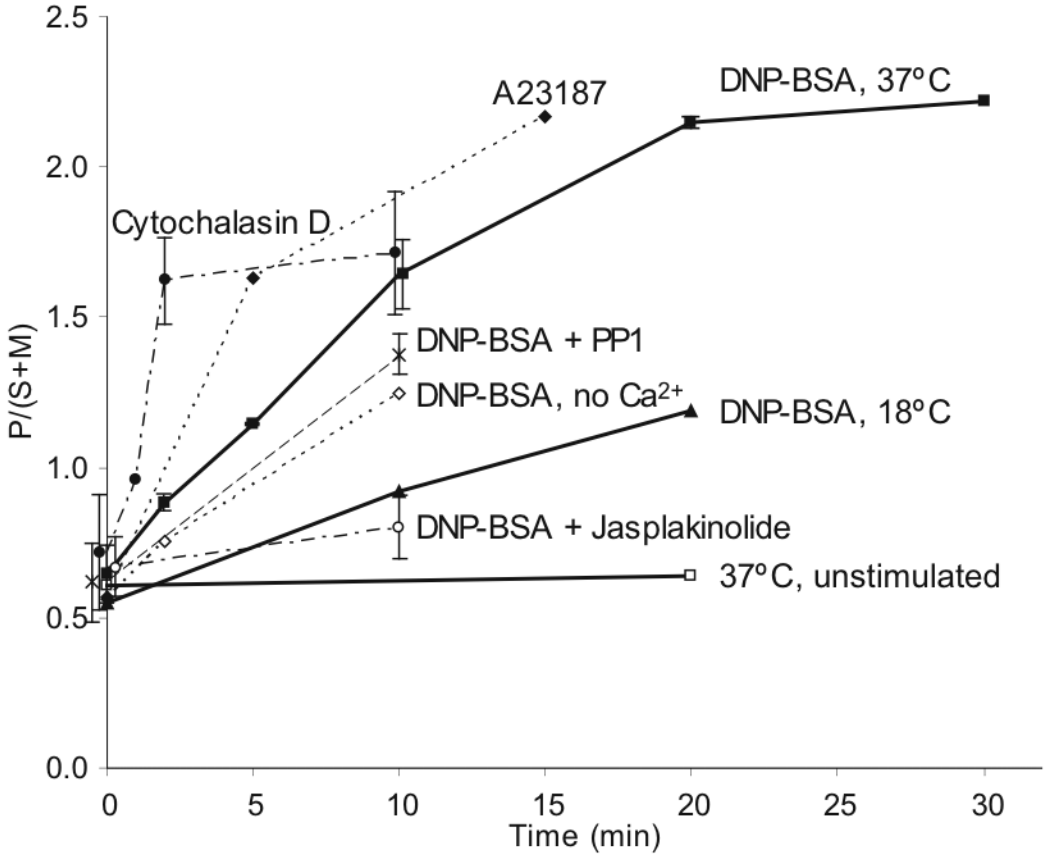

Figure 2.2. Ratio of polyunsaturated (P, db2 – db4+) phospholipids to the sum of saturated (S, db0) and monounsaturated (M, db1) phospholipids (i.e., P/(S+M)) for the time course of stimulation by 5μg/ml DNP-BSA at 37°C (squares, average of eight independent experiments) and 18 °C (triangles), in the presence of 3 mM Jasplakinolide (white circles, average of two independent experiments), 4 μM PP1 (cross, average of two independent experiments), or absence of media Ca^{2+} (white diamonds), or by 2 μM cytochalasin D (circles, average of four independent experiments), 0.9 μM Ca^{2+} ionophore A23187 (diamonds). This ratio, P/(S+M), is also shown for DRMs from unstimulated cells incubated for 20 min at 37°C prior to DRM preparation (white squares). Error bars show standard deviations from ≥ 4 separate experiments or range from two separate experiments for each time point. Data points with no error bars represent only single experiment with that time point.

to positive (increasing concentration). For PC and PE the k_m values go from negative to positive between two and three double bonds. For SM, with a single acyl chain, this change occurs between one and two double bonds. For PI, the concentration increases after DNP-BSA stimulation (positive k_m) for acyl chains with any number of double bonds. When the cumulative data are summed over all the lipid species (upper left panel of Figure 2.1.C) the transition from negative to positive k_m values occurs between one and two double bonds, justifying our choice of the ratio P/(S + M) in the simple data analysis used previously ([23] and Figure 2.2).

A linear approximation to Eqn 1, given by Eqn 2, was also used to evaluate data sets for DNP-BSA stimulation that were collected over shorter time periods (0 – 10 min). As an example, Figure 2.3 presents the data from the representative experiment in Table 1 in terms of the total number of double bonds in the acyl chains (db0, db1, db2, db3, and db4+) associated with each head group (PC, SM, PE, PI, PS, and sum) as a function of stimulation time (0, 2, 5, and 10 min). These data, fitted with Eqn 2, yield a slope corresponding to the apparent rate constant k_a *times* the direction and magnitude of the concentration change (C_f-C_i). These $k_s = (C_f\text{-}C_i)k_a$ values are listed with respective fitted lines in Figure 2.3. As expected from preceding analyses of cumulative data with Eqn 1 (Figures 2.1.A and 2.1.C), the k_s values for each PL head group tend to be more positive for a higher number of double bonds and more negative for a lower number of double bonds.

Figure 2.4 (closed squares, dark line) plots the averaged $k_s = (C_f\text{-}C_i)k_a$ values from five independent experiments with DNP-BSA stimulation as a function of the

Figure 2.3. Representative data (Table 1) plotted as Mol% of DRM phospholipids that contain 0, 1, 2, 3, and ≥ 4 double bonds (db0, db1, db2, db3, and db4+, respectively) in the acyl chains *versus* antigen stimulation time for each head group and summed over head groups. Data points corresponding to each of db0, db1, db2, db3, db4+ are fitted with a linear function corresponding to first-order kinetics at short times (Eqn 2). Values of $k_s = (C_f\text{-}C_i)k_a$ (units of Mol%/ min) are listed with each fitted curve. Error bars show the standard deviations from representative data in Table 1.

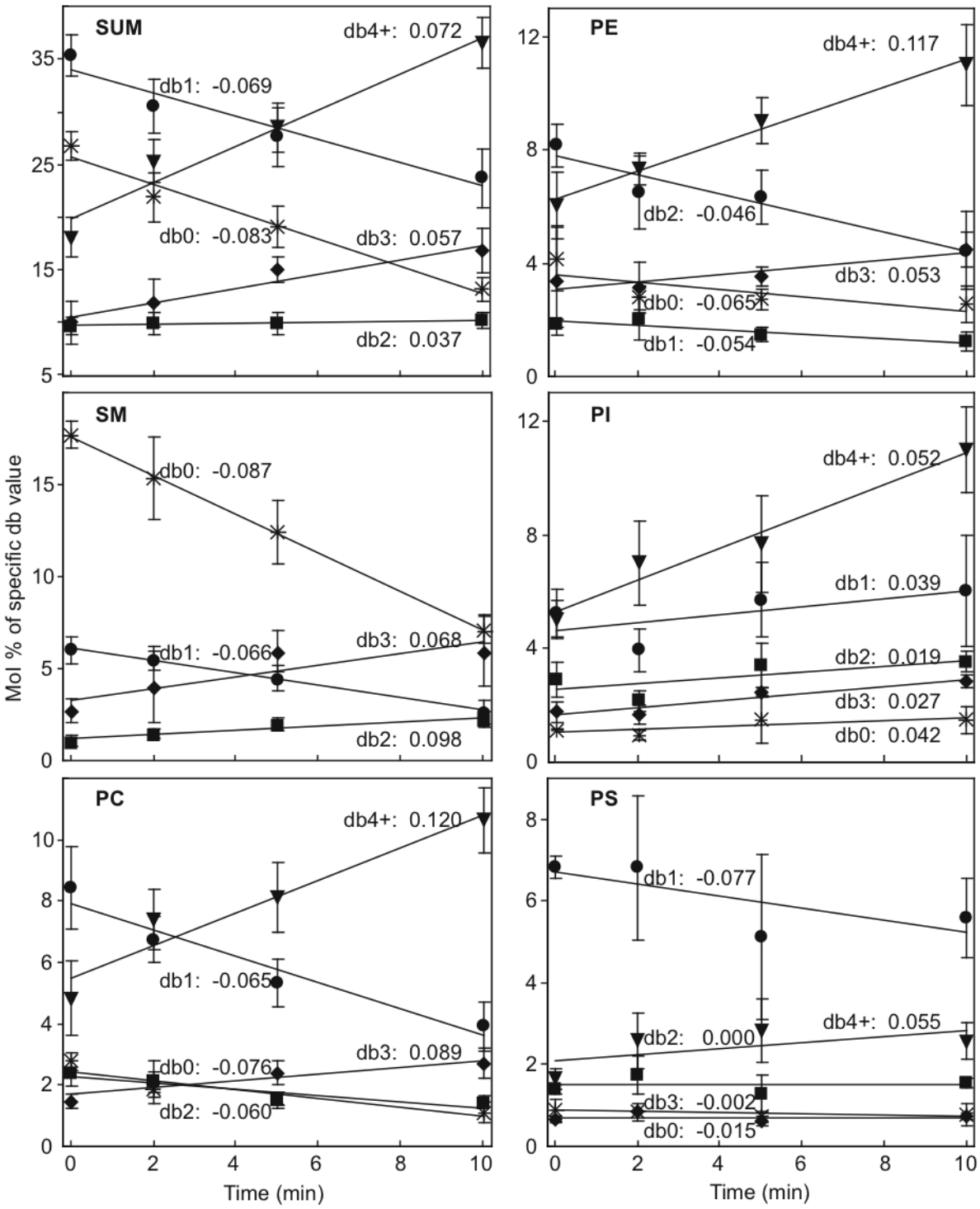
SUM
db4+: 0.072
db1: -0.069
db0: -0.083
db3: 0.057
db2: 0.037
PE
db4+: 0.117
db2: -0.046
db3: 0.053
db0: -0.065
db1: -0.054
SM
db0: -0.087
db3: 0.068
db1: -0.066
db2: 0.098
PI
db4+: 0.052
db1: 0.039
db2: 0.019
db3: 0.027
db0: 0.042
PC
db4+: 0.120
db1: -0.065
db3: 0.089
db0: -0.076
db2: -0.060
PS
db1: -0.077
db4+: 0.055
db2: 0.000
db3: -0.002
db0: -0.015
Mol % of specific db value
Time (min)
Time (min)

number of double bonds for each head group species. As expected these plots reveal the same trend as Figure 2.1.C, i.e. there is a clear dependence of stimulated DRM compositional changes on the degree of acyl chain unsaturation, such that those with higher degrees of unsaturation increase after stimulation. We confirmed that results from Eqns 1 and 2 show good agreement for short time periods ($\leq$ 10 min for DNP-BSA stimulation) as described in Materials and Methods. Therefore, we used the linear approximation (Eqn 2) to compare directly the DRM compositional changes caused by FcεRI mediated activation with multiple other treatments, in many different experiments as described in sections below (Figure 2.4).

We considered alterations in the cholesterol levels or the total PL recovered as factors contributing to our consistent observation of substantial increases in the percentage of unsaturated PL in the DRM compartments after DNP-BSA stimulation. We previously showed under our current experimental conditions that cell lysis is complete and not significantly altered by stimulation [17, 18, 35]. Furthermore, >80% of a GD_{1b} marker is recovered in low density DRM fractions under these conditions [17]. In the present study we found that there is a ~20% increase in cholesterol content of the DRM following stimulation by antigen for 10 min at 37°C, as determined with an enzymatic fluorescence assay for this sterol (Materials and Methods, data not shown). PL recovered in DRMs under the conditions used for their isolation in this study represent 11.2% $\pm$ 2.6 (SD; n=3) of cellular PL, based on organic phosphate analysis of chloroform-soluble PL extracted from DRMs and intact cells (see Materials and Methods). These DRMs contain PL from both plasma membrane and endocytic

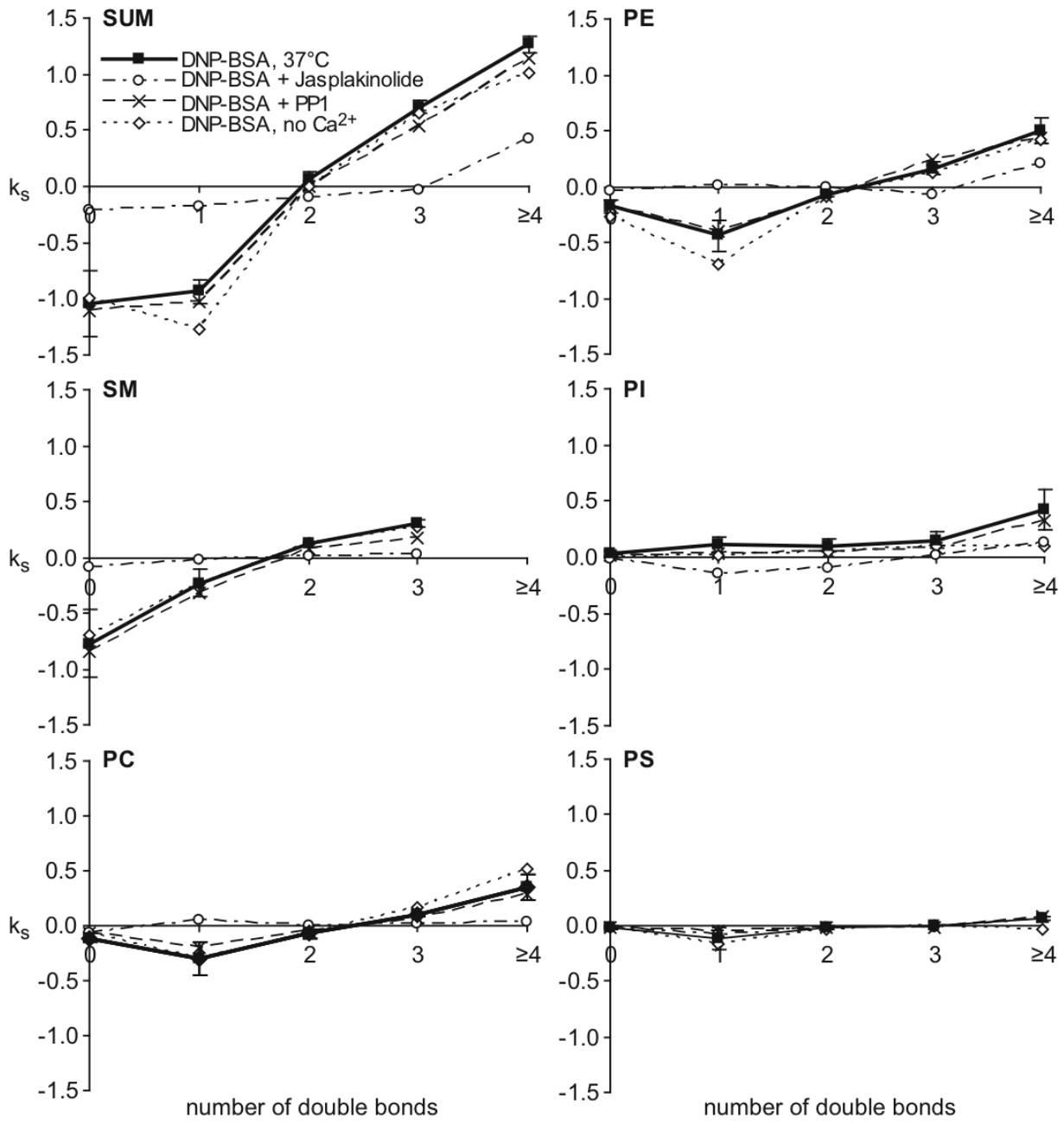

Figure 2.4. Values of $k_s = (C_f\text{-}C_i)k_a$ (Eqn 2; units of Mol%/ min) *versus* number of double bonds in phospholipid fatty acid chains for DNP-BSA stimulation (average of five independent experiments, error bars show standard deviation) compared with antigen stimulation in the presence of PP1, Jasplakinolide, Ca^{2+}-free media (same treatments and number of experiments as in Figure 2).

recycling compartments (N Smith et al., unpublished results). To compare the relative amount of PL recovered in the DRM fraction before and after stimulation, a synthetic phospholipid standard, 1,2-di-nonadecanoyl-sn-glycero-3-phosphatidyl choline, was added to each cell lysate sample at a concentration permitting its co-quantification in ESI/MS analysis of the DRM fraction. As summarized in Table 2.2 (Treatments 1 and 2), this analysis shows that DNP-BSA stimulation causes ~40% molar increase in PLs recovered in the DRM fraction relative to that for unstimulated cells. This is greater than the stimulated increase in DRM cholesterol, suggesting that the stimulated increase in polyunsaturated PLs recovered in DRMs is not due simply to changes in the cholesterol concentration in these compartments. Therefore we investigated involvement of other cellular components in the reorganization of DRM PLs caused by FcεRI-mediated cell activation.

Mechanistic Basis for Observed Changes

To probe the mechanism by which stimulation via FcεRI causes a marked change in the PL composition of DRMs, we examined the effect of the Src family kinase inhibitor, PP1, on these stimulated changes. As shown in the simple analysis of Figure 2.2 (P/(S+M) *vs* time), 4 mM PP1 has a small effect on the DNP-BSA-stimulated response (x, dashed line). At the concentration evaluated, PP1 effectively inhibits most antigen-stimulated tyrosine phosphorylation detected in whole cell western blots, although some FcεRI β and LAT phosphorylation persists ([36] and Figure 2.5). The first-order kinetic analysis summarized in Figure 2.4 ($k_s = (C_f - C_i)k_a$ *vs* db#; based on Eqn 2) shows that this concentration of PP1 present during antigen stimulation causes

Table 2.2. Comparison of relative recoveries of phospholipids (PL) in DRMs isolated after specified treatments of the cells. The value in parentheses indicates the number of experiments for specific treatment. The ratio is the relative amount of total DRM PL to an internal standard lipid (see Materials and Methods) at each condition. This ratio value is averaged from ≥ 2 experiments for treatment 1, 2, and 5, or from single experiment for treatment 3, 4, 6, and 7, and normalized to treatment 1. Standard deviations are from multiple experiments, or for single experiment treatments were calculated from error propagation from standard deviations in four separate measurements.

Treatment	Stimulant	Inhibitor	Ratio
1 (3)	None	None	1.00 ±0.06
2 (3)	DNP-BSA	None	1.39 ±0.11
3 (1)	None	PP1	0.90 ±0.18
4 (1)	DNP-BSA	PP1	1.29 ±0.09
5 (2)	Cytochalasin D	None	1.29 ±0.26
6 (1)	None	Jasplakinolide	0.85 ±0.12
7 (1)	DNP-BSA	Jasplakinolide	0.95 ±0.10

very little difference in PL compositional changes (compare solid squares and x). Table 2.2 (Treatments 3 and 4) shows that this concentration of PP1 causes only a small change in the DNP-BSA stimulated increase in recovery of PL in the DRM fraction. Together, these results suggest that the antigen-stimulated changes in PL composition of DRMs do not depend strongly on the tyrosine phosphorylation cascade that is initiated by FcεRI crosslinking.

Antigen stimulates a robust Ca^{2+} response in RBL mast cells, and this Ca^{2+} mobilization is necessary for degranulation [37, 38]. We investigated stimulated PL changes in DRMs caused by the Ca^{2+} ionophore A23187 that can stimulate RBL cell degranulation (in the absence of DNP-BSA). The simple analysis of Figure 2 shows that a stimulating dose of A23187 (0.9 μM) causes changes in PL composition very similar to those caused by DNP-BSA, but with faster kinetics (compare solid diamonds with solid squares). We also found that DNP-BSA stimulation of cells in buffer without extracellular Ca^{2+} (Figure 2.2, open diamonds) causes attenuation of the antigen-stimulated increase in P/(S+M), but does not prevent it. Under these conditions, antigen stimulates a transient increase in intracellular Ca^{2+} without a sustaining influx of Ca^{2+} from the extracellular medium, which is insufficient in triggering degranulation [37, 38]. In the analysis of Figure 2.4, DNP-BSA stimulation in the absence of extracellular Ca^{2+} (open diamonds) causes PL compositional changes similar to those caused by DNP-BSA in the presence of extracellular Ca^{2+} (solid squares). These results show that a sustained increase in intracellular Ca^{2+} may contribute to, but is not necessary for, the antigen-stimulated changes in DRM lipid composition observed.

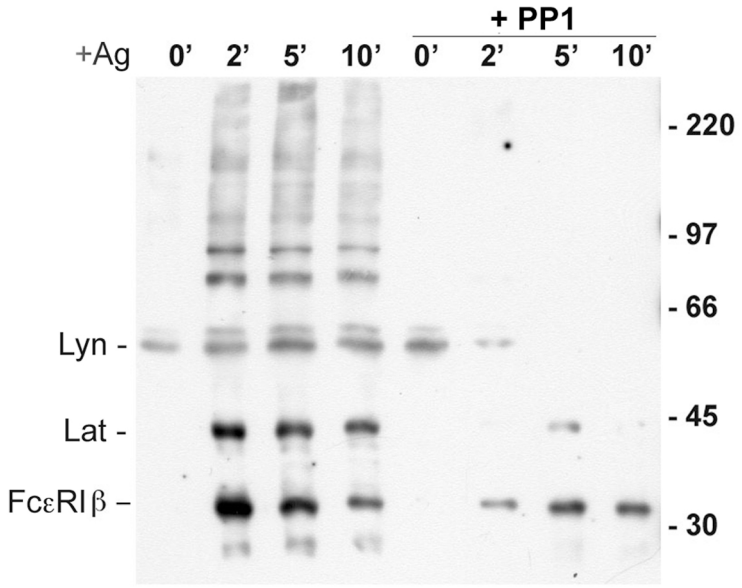

Figure 2.5. PP1 inhibits tyrosine phosphorylation in RBL-2H3 cells. RBL-2H3 cells at a concentration of 2 x 10^6 /ml were stimulated with DNP-BSA (0.8 μg/ml) in the presence or absence of 4 μM PP1 at 37°C for times indicated. Anti-phosphotyrosine western blot of whole cell lysate shows inhibition of antigen-stimulated tyrosine phosphorylation of Lyn, LAT, FcεRIβ and several higher MW proteins.

Role of the Cytoskeleton

Cytochalasin D disrupts the actin cytoskeleton by capping the barbed end of actin microfilaments and preventing elongation, thereby effectively preventing stimulated polymerization of F-actin [39]. This inhibition of actin polymerization has been shown to enhance IgE receptor signaling in RBL mast cells [39, 40]. When testing whether cytochalasin D affects DNP-BSA-stimulated changes in DRM lipid composition, we were surprised to find that cytochalasin D alone causes similar changes, with faster kinetics, as indicated in Figure 2.2 (compare closed circles with closed squares). First-order kinetic analysis of cytochalasin effects provides detailed accounting of PL compositional changes according to headgroup and double bonds (Figure 2.1.B). A summary of this analysis in terms of k_m=nk values (eqn 1) reveals that, compared with antigen stimulation (Figure 2.1.C, squares, left ordinate), treatment of RBL cells with 2 μM cytochalasin D (Figure 2.1.C, circles, right ordinate) causes significantly faster changes in DRM lipid composition for each head group: The k_m values are as much as 6-fold larger for cytochalasin D stimulation. Figure 2.1.C also shows that the dependence of k_m values on the acyl chain unsaturation is similar to DNP-BSA for all the major PL head groups, with some differences for PI. Latrunculin A is another inhibitor of actin polymerization that disrupts the actin cytoskeleton by a different mechanism: sequestration of monomeric G-actin to inhibit its incorporation into polymeric F-actin [41]. Changes similar to those for 2 μM cytochalasin D (Figure 2.1.C, circles) also occurred with 0.2 μM latrunculin A or with cytochalasin D at doses as low as 0.2 μM (data not shown). Only very small changes in net F-actin content occur under these

conditions of cytochalasin D treatment [39], indicating that the DRM lipid composition is sensitive to relatively subtle changes in F-actin.

Overall, our results indicate that the mechanistic basis for the antigen-stimulated change in PL composition of DRMs may be stimulated depolymerization of cortical F-actin, which partially redistributes to other intracellular locations [42]. To test this explanation, we examined the effect of jasplakinolide, which is known to stabilize F-actin [43], on antigen-stimulated changes in the PL composition of DRMs. We found that 3 μM jasplakinolide has no discernible effect on DRM composition in the absence of stimulation (Figure 2.2, open circle at 0 min). However, this reagent effectively inhibits the antigen-stimulated changes in PL composition as shown in Figure 2.2 (open circle at 10 min) and in Figure 2.4 (open circles). Consistent with these observations, jasplakinolide inhibits the antigen-stimulated increase in the relative amount of PLs fractionating with DRMs (Table 2.2, Treatments 1, 2, 6 and 7), whereas cytochalasin D causes PL increase similarly to antigen stimulation (Table 2.2, Treatment 1, 2 and 5). Our results show that the actin cytoskeleton regulates the structural composition and stability of plasma membrane domains that fractionate as DRMs. Correspondingly, we conclude that antigen and IgE receptor mediated changes in the distribution of F-actin substantially modify the composition and/or stability during cell signaling of these membrane domains represented by the DRMs.

Dependence of DRM Compositional Change after Antigen Stimulation on Length of Acyl Chains

Compositional changes in terms of acyl chain length associated with each head group were also evaluated after DNP-BSA stimulation with the first-order kinetic model. For this purpose, acyl chains associated with all head groups were evaluated according to Eqn 2, in terms of both combined length of their acyl chains and total number of double bonds. These results are summarized for a single representative experiment (Table 2.1) in Figure 2.6, which compiles the chain length results for the major phospholipids PC, PE, PI (SM with one rather than two acyl chains gave similar results). Compared on this same graph is the dependence of total DRM lipid compositional changes on the number of double bonds (solid squares and dark line reproduced from upper left panel in Figure 2.4). Whereas the dependence of lipid compositional change on the number double bonds is pronounced, as described above, there is negligible dependence on the chain length.

DISCUSSION

Our detailed PL analysis in the present study builds on previous observations to further our understanding of the interactions between lipid raft membrane domains and the actin cytoskeleton, and the regulation of these interactions by IgE receptor (FcεRI) signaling. Published studies on structural and functional roles for lipid rafts in cell biology number in the thousands, strongly implicating their critical participation in cellular homeostasis and stimulated responses. Yet these compartments remain elusive to

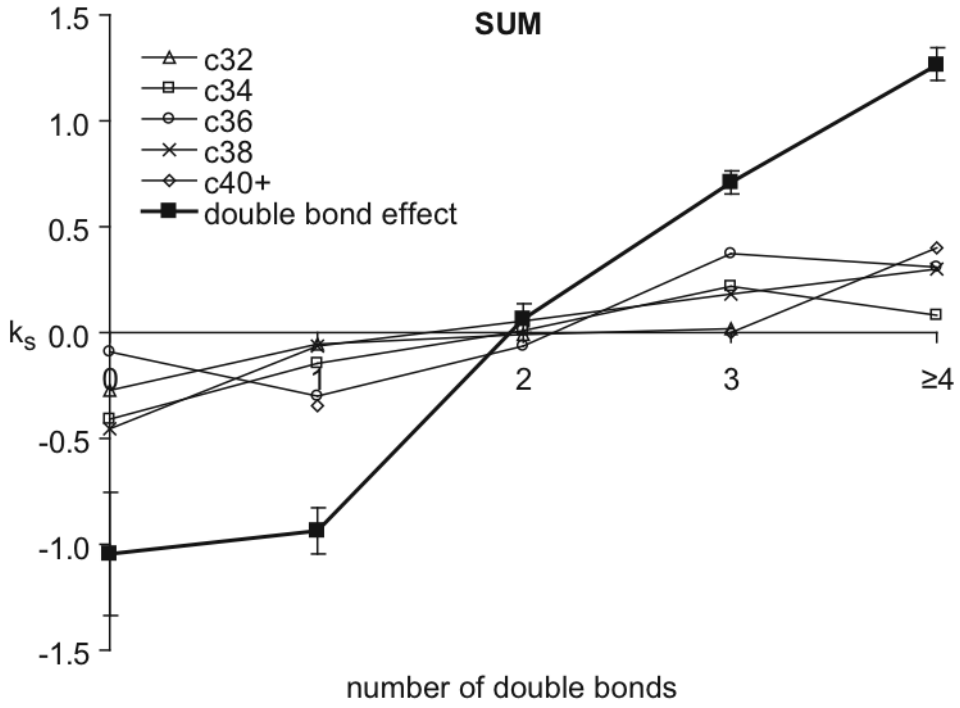

Figure 2.6. Representative data (Table 1) evaluated for cells stimulated with DNP-BSA and dependence of DRM phospholipid compositional changes on total acyl chain length. Values of $k_s = (C_f\text{-}C_i)k_a$ (Eqn 2; units of Mol%/ min) versus number of double bonds are shown for separate chain lengths corresponding to 32, 34, 36, 38, and ≥ 40 carbons in both acyl chains (c32, c34, c36, c38, c40+, respectively, summed over seven head groups). The solid squares and dark line correspond to k_s values *versus* number of double bonds summed over all head groups (double bond effect; duplicated from the upper left panel of Figure 4)

experimental definition because of their lipid and protein heterogeneity and their dynamic nature in living cells. Biochemical isolation of subcellular components is an essential part of structure-function analysis in live cells, even while recognizing that the procedures involved perturb their structures relative to those in live cells. Isolation of lipid rafts by detergent fractionation or other methods suffers the same pitfalls of this general approach, but it provides the necessary means for molecular characterization that can be further tested and refined in live cell experiments. DRM preparations have proven to be a useful correlative tool in elucidating the functional role of lipid rafts in FcεRI signaling [8].

We showed previously with ESI/MS that DRM preparations from RBL mast cells contain ~100 distinct PL species [23], highlighting the complexity that exists in these membranes. In the present study we confirmed and extended our initial observation that antigen-crosslinking of IgE receptors stimulates changes in the PL composition of DRMs isolated before and after this cell activation. Furthermore, we discovered that this substantial compositional change depends on stimulated alterations in the actin cytoskeleton, and appears largely independent of the tyrosine phosphorylation cascade that is activated in parallel to these cytoskeletal changes. This finding is surprising, as it indicates that the PL composition of detergent-resistant lipid rafts is much more sensitive to cytoskeletal regulation than to various phospholipases whose activation is stimulated by tyrosine phosphorylation [44, 45]. Consistent with this, only small changes in the total PL composition of RBL mast cells are detected due to antigen stimulation [46], indicating that net gain or loss of specific PL species due to stimulated PL turnover

is likely to provide a relatively minor contribution to the large changes in DRM PL composition that we observe.

Our results implicate the actin cytoskeleton as strongly influencing the PL composition of DRM preparations. Relatively small changes in net F-actin content caused by cytochalasin D or latrunculin A cause large and rapid changes in this composition, and antigen-stimulated changes are prevented by jasplakinolide. We observe net increases in the amount of PLs isolated as DRMs, and preferential increases in polyunsaturated lipids caused by inhibitors of F-actin polymerization or by antigen stimulation. These results suggest that membrane interactions with the actin cytoskeleton limit recovery of detergent-resistant lipids in resting cells, and that cell stimulation or direct inhibition of F-actin polymerization reduces these interactions. Although antigen stimulation causes a net increase in stimulated actin polymerization [39], it is possible that spatially localized actin depolymerization [41] is chiefly responsible for the increase in detergent resistant PL that are recovered under these conditions.

Our detailed kinetic analysis of extensive mass spectrometry data for DRMs provides a comprehensive means for investigating and comparing temporal changes in lipid composition that are initiated by various stimulants in the signaling pathway. This analysis compares mol % content of individual lipid species within the total lipids collected in the isolated membranes, and thereby structural and physical changes that accompany specific cell stimulating conditions. In a previous study [47], Milne et al. described a lipid array study using ESI-MS coupled with computational approaches to

identify lipid pattern of total cellular lipids, and changes in the pattern as indicated by the relative change in peak abundance over the defined time course of antigen stimulation in B cells. Our kinetic study presents an effective way to characterize lipid compositional change in the context of functionally relevant membrane domains and pinpoints subtle changes related to specific stimulating conditions. Thus, our kinetic approach should be a valuable tool for lipidomic studies towards understanding membrane signaling.

Our ESI/MS analysis is carried out on DRMs isolated after cell lysis in relatively low concentration of TX-100 (0.045%). These conditions were chosen because they discriminate between crosslinked and uncrosslinked IgE receptors as DRM components, whereas other components of lipid rafts, such as the GPI-anchored protein Thy-1, are efficiently recovered in DRMs in the presence or absence of IgE receptor crosslinking [17, 18, 48]. It is possible that different sensitivity to antigen stimulation or F-actin inhibitors would be observed at higher concentrations of detergent, but substantial detergent interference under these conditions precludes accurate mass spectrometric analysis of the PL composition [23]. Special LiCl extraction conditions gave essentially the same results, with no indication of plasmalogen species at m/z of 720.5, 722.5, 770.6, and 774.6 as reported by others [27, 49, 50]. This may reflect differences in the membrane preparations or cell growth conditions. It is notable that cytochalasin D does not change the % recovery of crosslinked IgE receptors with DRMs under the conditions of our experiments. However, this treatment does decrease the density of detergent-resistant FcεRI-containing membranes, as separated in sucrose

gradients, consistent with cytoskeletal interactions by these detergent-resistant receptors in the absence of cytochalasin D [21].

The changes in DRM PL composition we observe are stimulated by the Ca^{2+} ionophore, A23187 (Figure 2). They are also stimulated by antigen in the absence of extracellular Ca^{2+} (Figures 2 and 4), a condition that inhibits degranulation and most signaling processes downstream of FcεRI [37, 51]. Interestingly, activation of permeabilized mast cells by either micromolar Ca^{2+} or GTPγ-S in the presence of EGTA results in redistribution of F-actin from the periphery to the cell interior in a process that is similar to that stimulated in intact mast cells [52, 53]. These results suggest that F-actin redistribution from the cell cortex can be elicited by both Ca^{2+}-dependent and Ca^{2+}-independent stimuli, and this may be relevant to the PL changes in DRM that we observe.

A model to explain our results is that loss of F-actin proximal to the plasma membrane caused by antigen activation or by inhibitors of actin polymerization perturbs the structural regulation of nanoscopic Ld/Lo-like phase separation. This could result in lipid redistributions that enhance the recovery of polyunsaturated PLs, particularly those with PI head groups, in DRM fractions. Preferential interactions of polyphosphatidylinositol PLs with the actin cytoskeleton at the inner leaflet of the plasma membrane [54, 55] may be relevant to this process, and the negative charge of PI may also contribute to these interactions. In this scenario, disruption of interactions between PI and structural proteins by antigen stimulation or by inhibitors of actin polymerization could result in increased recovery of PI in detergent–resistant, low density membranes.

Future efforts are aimed at detecting in intact cells the membrane structural changes manifested by our ESI/MS analysis of DRM PLs. To this end, biophysical methods such as resonance energy transfer [56, 57], fluorescence correlation spectroscopy [58], and electron spin resonance [59] are proving use to be useful approaches to studying membrane lipid heterogeneity in live cells.

CONTRIBUTIONS AND ACKNOWLEDGEMENTS

X. Han and N. L. Smith share first authorship for this work. Research designed by X. Han, N. L. Smith, D. A. Holowka, F. W. McLafferty and B. A. Baird; X. Han performed mass spectrometry and analysis; N. L. Smith prepared experimental samples and performed biochemical experiments; D. Sil performed analysis. Paper written by X. Han, N. L. Smith and B. A. Baird. Research supported by National Institutes of Heath Grants AI018306 (B. A. Baird and D. A. Holowka) and GM016609 (F. W. McLafferty) and in part by the Nanobiotechnology Center (NSF-ECS-9876771).

REFERENCES

1. Brown, D.A., *Lipid Rafts: From Model Membranes to Cells.* Biochim Biophy Acata, 2005. **1746**((1-2)): p. 182-95.

2. Mukherjee, S. and F.R. Maxfield, *Membrane domains.* Annu Rev Cell Dev Biol, 2004. **20**: p. 839-66.

3. Simons, K. and D. Toomre, *Lipid rafts and signal transduction.* Nat Rev Mol Cell Biol, 2000. **1**(1): p. 31-9.

4. Brown, D.A. and J.K. Rose, *Sorting of GPI-anchored proteins to glycolipid-enriched membrane subdomains during transport to the apical cell surface.* Cell, 1992. **68**(3): p. 533-44.

5. Cinek, T. and V. Horejsi, *The nature of large noncovalent complexes containing glycosyl-phosphatidylinositol-anchored membrane glycoproteins and protein tyrosine kinases.* J Immunol., 1992. **149**(7): p. 2262-70.

6. Simons, K. and E. Ikonen, *Functional rafts in cell membranes.* Nature, 1997. **387**(6633): p. 569-72.

7. Anderson, R.G., *The caveolae membrane system.* Annu Rev Biochem, 1998. **67**: p. 199-225.

8. Holowka, D., et al., *Lipid segregation and IgE receptor signaling: a decade of progress.* Biochim Biophy Acata, 2005. **1746**(3): p. 252-9.

9. Smith, A.E. and A. Helenius, *How viruses enter animal cells.* Science, 2004. **304**(5668): p. 237-42.

10. Edidin, M., *The state of lipid rafts: from model membranes to cells.* Annu Rev Biophys Biomol Struct, 2003. **32**: p. 257-83.

11. Munro, S., *Lipid rafts: elusive or illusive?* Cell, 2003. **115**(4): p. 377-88.

12. Brown, D.A., *Lipid rafts, detergent-resistant membranes, and raft targeting signals.* Physiology (Bethesda), 2006. **21**: p. 430-9.

13. Sengupta, P., B. Baird, and D. Holowka, *Lipid rafts, fluid/fluid phase separation, and their relevance to plasma membrane structure and function.* Semin Cell Dev Biol, 2007. **18**(5): p. 583-90.

14. Harder, T., et al., *Lipid domain structure of the plasma membrane revealed by patching of membrane components.* J Cell Biol, 1998. **141**(4): p. 929-42.

15. Janes, P.W., S.C. Ley, and A.I. Magee, *Aggregation of lipid rafts accompanies signaling via the T cell antigen receptor.* J Cell Biol, 1999. **147**(2): p. 447-61.

16. Pyenta, P.S., D. Holowka, and B. Baird, *Cross-correlation analysis of inner-leaflet-anchored green fluorescent protein co-redistributed with IgE receptors and outer leaflet lipid raft components.* Biophys J., 2001. **80**(5): p. 2120-32.

17. Sheets, E.D., D. Holowka, and B. Baird, *Critical role for cholesterol in Lyn-mediated tyrosine phosphorylation of FCepsilonRI and their association with detergent-resistant membranes.* J Cell Biol., 1999. **145**(4): p. 877-87.

18. Field, K.A., D. Holowka, and B. Baird, *Compartmentalized activation of the high affinity immunoglobulin E receptor with membrane domains.* J Biol Chem, 1997. **272**(7): p. 4276-80.

19. Gosse, J.A., et al., *Transmembrane sequences are determinants of immunoreceptor signaling.* J Immunol., 2005. **175**(4): p. 2123-31.

20. Harder, T. and K. Simons, *Clusters of glycolipid and glycosylphosphatidylinositol-anchored proteins in lymphoid cells: accumulation of actin regulated by local tyrosine phosporylation.* Eur J Immunol, 1999. **29**(2): p. 556-62.

21. Holowka, D., E.D. Sheets, and B. Baird, *Interactions between Fc(epsilon)RI and lipid raft components are regulated by the actin cytoskeleton.* J Cell Sci., 2000. **113**(Pt 6): p. 1009-19.

22. Wu, M., et al., *Visualization of plasma membrane compartmentalization with patterned lipid bilayers.* Proc Natl Acac Sci, 2004. **101**(38): p. 13798-803.

23. Fridriksson, E.K., et al., *Quantitative analysis of phospholipids in functionally important membrane domains from RBL-2H3 mast cells using tandem high-resolution mass spectrometry.* Biochemistry, 1999. **38**(25): p. 8056-63.

24. Barsumian, E.L., et al., *IgE-induced histamine release from rat basophilic leukemia cell lines: isolation of releasing and nonreleasing clones.* Eur J Immunol, 1981. **11**(4): p. 317-23.

25. Posner, R.G., et al., *Aggregation of IgE-receptor complexes on rat basophilic leukemia cells does not change the intrinsic affinity but can alter the kinetics of the ligand-IgE interaction.* Biochemistry, 1992. **31**(23): p. 5350-6.

26. Bligh, E.G. and W.J. Dyer, *A rapid method of total lipid extraction and purification.* Can J Biochem Physiol, 1959. **37**(8): p. 911-7.

27. Pike, L.J., et al., *Lipid rafts are enriched in arachidonic acid and plasmenylethanolamine and theri composition is independent of caveolin-1 expression: a quantitative electrospray ionization/mass spectrometric analysis.* Biochemistry, 2002. **41**(6): p. 2075-2088.

28. Kingsley, P.B. and G.W. Feigenson, *The synthesis of a perdeuterated phospholipid: 1,2-dimyristoyl-sn-glycero-3-phosphocholine-d72.* Chem. Phys. Lipids., 1979. **24**: p. 135-147.

29. Beu, S.C., et al., J. Am. Soc. Mass. Sectrom., 1993. **4**: p. 557-565.

30. Wilm, M.S. and M. Mann, *Electrospray and Taylor-Cone theory, Dole's beam of macromolecules at last?* International Journal of Mass Spectrometry and Ion Processes, 1994. **136**(2-3): p. 167-180.

31. Wilm, M.S. and M. Mann, *Analytical properties of the nanoelectrospray ion source.* Anal. Chem., 1996. **68** p. 1-8.

32. Kim, H.Y., T.C. Wang, and Y.C. Ma, *Liquid chromatography/mass spectrometry of phospholipids using electrospray ionization.* Anal Chem, 1994. **66**(22): p. 3977-82.

33. Han, X. and R.W. Gross, *Electrospray ionization mass spectroscopic analysis of human erythrocyte plasma membrane phospholipids.* Proc Natl Acad Sci U S A, 1994. **91**(22): p. 10635-9.

34. WoldeMussie, E., K. Maeyama, and M.A. Beaven, *Loss of secretory response of rate basophilic leukemia (2H3) cells at 40 degrees C is associated with reversible supression of inositol phospholipid breakdown and calcium signals.* J Immunol., 1986. **137**(5): p. 1674-80.

35. Field, K.A., D. Holowka, and B. Baird, *Structural aspects of the association of FcepsilonRI with detergent-resistant membranes.* J Biol Chem, 1999. **274**(3): p. 1753-8.

36. Amoui, M., P. Draber, and L. Draberova, *Src family-selective tyrosine kinase inhibitor, PP1, inhibits both Fc epsilonRI- and Thy-1-mediated activation of rat basophilic leukemia cells.* Eur J Immunol, 1997. **27**(8): p. 1881-6.

37. Beaven, M.A., et al., *The mechanism of the calcium signal and correlation with histamine release in 2H3 cells.* J Biol Chem, 1984. **259**(11): p. 7129-36.

38. Mohr, F.C. and C. Fewtrell, *Depolarization of rat basophilic leukemia cells inhibits calcium uptake and exocytosis.* J Cell Biol, 1987. **104**(3): p. 783-92.

39. Frigeri, L. and J.R. Apgar, *The role of actin microfilaments in the down-regulation of the degranultion response in RBL-2H3 mast cells.* J Immunol., 1999. **162**(4): p. 2243-50.

40. Narasimhan, V., D. Holowka, and B. Baird, *Microfilaments regulate the rate of exocytosis in rat basophilic leukemia cells.* Biochem Biophys Res Commun, 1990. **171**(1): p. 222-9.

41. Coue, M., et al., *Inhibition of actin polymerization by latrunculin A.* FEBS Lett, 1987. **213**(2): p. 316-8.

42. Koffer, A., P.E. Tatham, and B.D. Gomperts, *Changes in the state of actin during the exocytotic reaction of permeabilized rat mast cells.* J Cell Biol., 1990. **111**(3): p. 919-27.

43. Bubb, M.R., et al., *Effects of jasplakinolide on the kinetics of actin polymerization. An explanation for certain in vivo observations.* J Biol Chem, 2000. **275**(7): p. 5163-70.

44. Beaven, M.A. and H. Metzger, *Signal transduction by Fc receptors: the Fc epsilon RI case.* Immunol Today, 1993. **14**(5): p. 222-6.

45. Field, K.A., et al., *Mutant RBL mast cells defective in Fc epsilon RI signaling and lipid raft biosynthesis are reconstituted by activated Rho-family GTPases.* Mol Biol Cell, 2000. **11**(10): p. 3661-73.

46. Cohen, J.S., *The role of phospholipid metabolism in regulated secretion in RBL mast cells.* 2001, Cornell University: Ithaca. p. 105.

47. Milne, S.B., Forrester, P. T., Ivanova, P. T., Armstrong, M. D., Brown, H. A., *Multiplexed lipid arrays of anti-immunoglobulin M-induced changes in the glycerophospholipid composition of WEHI-231 cells.* AfCS Reports (www.signaling-gateway.org/reports/vl/DA0011/DA0011.htm), 2003. **11**.

48. Field, K.A., D. Holowka, and B. Baird, *Fc epsilon RI-mediated recruitment of p53/56lyn to detergent-resistant membrane domains accompanies cellular signaling.* Proc Natl Acad Sci U S A, 1995. **92**(20): p. 9201-5.

49. Pike, L.J., X. Han, and R.W. Gross, *Epidermal growth factor receptors are localized to lipid rafts that contain a balance of inner and outer leaflet lipids: a shotgun lipidomics study.* J Biol Chem, 2005. **280**(29): p. 26796-804.

50. Surviladze, Z., et al., *FcepsilonRI and Thy-1 domains have unique protein and lipid compositions.* J Lipid Res, 2007. **48**(6): p. 1325-35.

51. Beaven, M.A. and R. Ludowyke, *Stimulatory signals for secretion in mast cells and basophils*, in *Advances in Regulation of Cell Growth*, M. J.J., C. J.C., and W. A, Editors. 1989, Raven Press: New York. p. 245-285.

52. Ludowyke, R.I., K. Kawasugi, and P.W. French, *PMA and calcium ionophore induce myosin and F-actin rearrangement during histamine secretion from RBL-2H3 cells.* Cell Motil Cytoskeleton, 1994. **29**(4): p. 354-65.

53. Norman, J.C., et al., *Actin filament organization in activated mast cells is regulated by heterotrimeric and small GTP-binding proteins.* J Cell Biol, 1994. **126**(4): p. 1005-15.

54. Kwik, J., et al., *Membrane cholesterol, lateral mobility, and the phosphatidylinositol 4,5-bisphosphate-dependent organization of cell actin.* Proc Natl Acad Sci U S A, 2003. **100**(24): p. 13964-9.

55. Raucher, D., et al., *Phosphatidylinositol 4,5-bisphosphate functions as a second messenger that regulates cytoskeleton-plasma membrane adhesion.* Cell, 2000. **100**(2): p. 221-8.

56. Zacharias, D.A., et al., *Partitioning of lipid-modified monomeric GFPs into membrane microdomains of live cells.* Science, 2002. **296**(5569): p. 913-6.

57. Sengupta, P., D. Holowka, and B. Baird, *Fluorescence resonance energy transfer between lipid probes detects nanoscopic heterogeneity in the plasma membrane of live cells.* Biophys J, 2007. **92**(10): p. 3564-74.

58. Bacia, K., et al., *Fluorescence correlation spectroscopy relates rafts in model and native membranes.* Biophys J, 2004. **87**(2): p. 1034-43.

59. Swamy, M.J., et al., *Coexisting domains in the plasma membranes of live cells characterized by spin-label ESR spectroscopy.* Biophys J, 2006. **90**(12): p. 4452-65.

CHAPTER THREE

Sphingosine Derivatives Inhibit Cell Signaling by Electrostatically Neutralizing Polyphosphoinositides at the Plasma Membrane[1]

SUMMARY

Mast cell stimulation via IgE receptors causes activation of multiple processes, including Ca^{2+} mobilization, granule exocytosis, and outward trafficking of recycling endosomes to the plasma membrane. We used fluorescein-conjugated cholera toxin B (FITC-CTxB) to label GM_1 in recycling endsomes and to monitor antigen-stimulated trafficking to the plasma membrane in both fluorimeter and imaging-based assays. We find that the sphingosine derivatives D-sphingosine and N,N'-dimethylsphingosine effectively inhibit this outward trafficking response, whereas a quarternary ammonium derivative, N,N',N''-trimethylsphingosine, does not inhibit. This pattern of inhibition is also found for Ca^{2+} mobilization and secretory lysosomal exocytosis, indicating a general effect on Ca^{2+}-dependent signaling processes. This inhibition correlates with the capacity of sphingosine derivatives to flip to the inner leaflet of the plasma membrane that is manifested as changes in plasma membrane-associated FITC-CTxB fluorescence and cytoplasmic pH. Using a fluorescently labeled MARCKS effector domain to monitor plasma membrane-associated polyphosphoinositides, we find that these sphingosine derivatives displace the electrostatic binding of this MARCKS effector domain to the plasma membrane in parallel with their capacity to inhibit Ca^{2+}-dependent

---

[1] Published as N. L. Smith, S. Hammond, D. Gadi, A. Wagenknecht-Wiesner, B. Baird and D. Holowka, *Sphingosine Derivatives Inhibit Cell Signaling by Electrostatically Neutralizing Polyphosphoinositides at the Plasma Membrane*. Self/Nonself , 2010. **1**(2): p.133-43. Reprinted with permission.

signaling. Our results support roles for plasma membrane polyphosphoinositides in Ca^{2+} signaling and stimulated exocytosis, and they illuminate a mechanism by which D-sphingosine regulates signaling responses in mammalian cells.

INTRODUCTION

Mast cells play important roles in inflammation and allergic disease. In response to antigen-mediated crosslinking, IgE receptors, FcεRI, initiate a complex signaling cascade that results in exocytosis of secretory lysosomes and stimulated production of numerous cytokines in these cells [1]. Previously, our laboratory developed a fluorescence assay for trafficking of recycling endosomes in RBL mast cells that monitors pH-dependent changes in the fluorescence of FITC-CTxB and FITC-anti-transferrin receptor mAb, and we showed that antigen stimulates increased recycling endosomal trafficking to the plasma membrane [2]. This trafficking response was found to be largely insensitive to inhibitors of downstream enzymes in secretory lysosomal exocytosis, including PI3-kinase and protein kinase C, but was reduced by the absence of extracellular Ca^{2+} and by U73122, an inhibitor of inositol 1,4,5-triphosphate production leading to Ca^{2+} mobilization [3].

Recycling endosomes were first identified as a perinuclear pool of tubular and vesicular membranes containing transferrin receptors [4]. This membrane pool is mildly acidic and is distinct from the early and sorting endosomes as well as from the Golgi complex [5]. It has been shown to participate in regulating the directionality of epithelial cell migration [6] and the maintenance of cell polarity [7, 8], as well as in phagocytosis [9] and cytokinesis [10]. Furthermore, there is evidence that recycling endosomes play

roles in various diseases, including enhancement of HIV viral particle release [11] and influence neuro-degenerative diseases such as Alzheimer's disease [12]. Studies have also provided evidence for their role in stimulated secretion of cytokines in hematopoietic cells [13].

In the course of investigating selective inhibition of stimulated recycling endosome trafficking to the plasma membrane, we found that certain sphingosine derivatives are particularly effective inhibitors of this process in RBL mast cells. This inhibition correlates with inhibition of stimulated Ca^{2+} mobilization that is important for exocytosis of recycling enodsomes as well as secretory lysosomes. Furthermore, this inhibition depends on the capacity of sphingosine bases to flip to the inner leaflet of the plasma membrane and to mediate electrostatic neutralization of polyphosphoinositides at this cytoplasmic interface. These results confirm an important role for Ca^{2+} signaling in stimulation of recycling endosomal trafficking, and they provide new insights into the mechanism by which both exogenous and endogenous sphingosines can regulate stimulated signaling in eukaryotic cells.

MATERIALS AND METHODS

Reagents

FITC-cholera toxin B subunit (FITC-CTxB), D-sphingosine, cytochalasin D, 4-methylumbelliferyl-N-acetyl-β-D-glucosaminide, and nigericin were obtained from Sigma –Aldrich Chem. Co. (Saint Louis, MO USA). BCECF-AM, indo-1 AM, and Alexa488-CTxB were purchased from Invitrogen Corp. (Carlsbad, CA USA). A23187 was from EMD (San Diego, CA USA). N,N'-dimethylsphingosine and N,N',N''-trimethylsphingosine

were purchased from Avanti Polar Lipids (Alabastar, AL, USA). Mouse monoclonal anti-dinitrophenyl (DNP) IgE was purified as previously described [14]. Multivalent antigen, DNP-BSA, contained an average of 15 DNP groups as previously described [2].

Cell Culture

RBL-2H3 mast cells were cultured in minimum essential media with 20% fetal bovine serum (Atlanta Biologicals) and 10 μg/ml gentamicin sulfate (RBL Media) as described previously [15]. All tissue culture reagents were obtained from Invitrogen unless otherwise noted. For antigen stimulation, cells were sensitized with 2-5 fold molar excess of anti-DNP IgE for 2-24 hr prior to experiments. Confluent cells were harvested with 135 mM NaCl, 5mM KCl, 20 mM Hepes, 1.5 mM EDTA, pH 7.4, and resuspended in either buffered saline solution (BSS: 135 mM NaCl, 5 mM KCL, 1.8 mM $CaCl_2$, 1 mM $MgCl_2$, 5.6 mM glucose, 1 mg/ml BSA and 20 mM HEPES, pH 7.4) or RBL media with 20 mM HEPES.

Cholera Toxin B Trafficking

For steady state spectrofluorimeter experiments, RBL-2H3 cells were harvested and resuspended at 4 $x10^6$ cells/ml in RBL media with 20 mM Hepes. FITC-CTxB was added to a final concentration of 3 μg/ml and incubated at 37°C for 2 hours. Cells were washed 2 times and resuspended at a final concentration of 2 x 10^6 cells/ml in BBS, stirred continuously in an acrylic cuvette and maintained at a temperature of 37°C. Fluorescence measurements were made with and SLM 8000C fluorescence spectrophotometer as previously described [2]. Following additions as indicated in figure legends, cells were stimulated with either 4 μg/ml DNP-BSA in the presence or absence

of 2 mM cytochalasin D or with 1 μM calcium ionophore A23187, and changes in FITC fluorescence were monitored.

For analysis, Excel (Microsoft) software was used. Briefly, using recorded pre-stimulation data, the TREND function was used to generate a linear baseline prediction that extended over the stimulation time course. This baseline was then subtracted from the stimulated data and the resulting data were normalized for variations in initial fluorescence.

Degranulation

IgE-sensitized RBL-2H3 cells were harvested and resuspended in BSS at $2x10^6$ cells/ml with 2 μM cytochalasin D. Cells were incubated with sphingosine derivatives for 5 minutes prior to stimulation. Stimulated cells were incubated in a water bath with shaking at 37°C for 1 hr, then placed on ice for 10 minutes, and centrifuged for 5 minutes at 900 rpm at 4°C as previously described [16]. Following centrifugation, 25 μl cell supernatants were plated in triplicate in black flat bottomed 96 well plates (Costar) with 100 μl substrate solution (1.2 mM 4-methylumbelliferyl-N-acetyl-β-D-glucosaminide in acetate buffer (0.12 M acetic acid, pH 4.4) and processed for measurement of b-hexosaminidase activity as previously described [17].

Measurement of Intracellular pH

RBL cells were harvested and resuspended in BSS at $1x10^7$cells/ml and equilibrated to 37°C. BCECF-AM (3.3. μg/ml) was loaded into cells by incubating for 1-1.5 minutes, then diluting to $2x10^6$ cells/ml and rotating slowly for 30 minutes at 37°C.

Washed cells were used at a final concentration of $1x10^6$ cells/ml, and fluorescence was measured using SLM 8000C fluorescence spectrophotometer, with excitation at 490 nm and emission at 510 nm. Changes in pH were determined using a calibration curve generated by dilution of cells into calibration buffer at pH values of 6, 6.5, 7, 7.5 and 8 in the presence of 10 μM nigericin [18].

Measurement of Intracellular Ca^{2+}

Stimulated Ca^{2+} responses were monitored as described previously [15]. Briefly, RBL cells were loaded with the calcium indicator indo-1 AM, washed, and calcium mobilization in response to stimulation was measured using SLM 8000C fluorescence spectrophotometer. Time-integrated responses were determined as the area under the stimulated timecourse minus the baseline over 400 sec, normalized to the maximal response in Triton X-100 lysed cells [19].

Confocal Fluorescence Microscopy

Cells were labeled with Alexa488-CTxB as described for FITC-CTxB above, incubated with or without sphingosine derivatives in BSS for 10 min at 37°C, then fixed in 4% paraformaldehyde for 15 minutes at room temperature. Fixed cells were imaged with a BioRad MRC 600 confocal system and a Zeiss Axiovert 10 microscope and 100x objective.

For detection of interactions between sphingosine derivatives and polyphosphoinositdes at the plasma membrane, mRFP-MARCKS ED^{SA3} was expressed in RBL cells by transient transfection with Fugene HD (Roche Diagnostics, Indianapolis,

IN) as previously described [20]. mRFP-MARCKS ED^{SA3} was made from YFP-MARCKS ED [21] (Construct a gift from Dr. Tobias Meyer (Stanford University)) by exchanging YFP for mRFP by using the Nhe I and Hind III restriction sites. Subsequently, the QuikChange Site-Directed Mutagenesis Kit (Stratagene) was used to insert successive mutations of serines 159, 163 and 170 (full length MARCKS notation) to alanines. Changes were confirmed by DNA sequence analysis. For these experiments, transfected cells in MatTek 35mm culture dishes (MatTek Corp., Ashland, MA) were treated with sphingosine derivatives or other agents as described in Results, then fixed and imaged as above using a 63x achromatically corrected objective (NA 1.4). Line scan analysis of equatorial confocal sections with Image J (NIH) was used to determine the ratio of plasma membrane to cytoplasmic localization for mRFP-MARCKS ED^{SA3} after various treatments. Ratios determined for each sample are averages of 15-20 cells in 4-5 images.

To monitor GM_1 trafficking to the plasma membrane by quantitative confocal imaging, RBL cells in MatTek culture dishes were first incubated with 5 μg/ml unlabeled CTxB and 2 μg/ml DiI-C16 (Molecular Probes/Invitrogen) for 5 min at 25°C to block plasma membrane-associated GM_1 and to label the plasma membrane. Cells washed in BSS were then imaged in the presence of 1 μg/ml Alexa488-CTxB and 2 μM cytochalasin D, with or without 8 μM D-sphingosine, and stimulated by 4.8 μM A23187 at 25°C to minimize label exchange and internalization. Confocal images were acquired using a Leica TCS SP2 upright microscope system (Leica Microsystems, Exton, PA) with a 63x, 0.9 NA HCX APO LU-V-I water immersion objective. Green and red images

were collected sequentially to minimize bleed-through, with a rate of 3 sec/frame. For Alexa488-CTxB, I_{ex}=488, I_{em}=500-550; for DiI-C16, I_{ex}=543, I_{em}=560-630. Image analysis was carried out as previously described [22]. This method uses the plasma membrane-localized DiI-C16 label to create a binary plasma membrane mask that is used to define the Alexa488 fluorescence of interest. The average intensity of Alexa488-CTxB fluorescence in this region is calculated for each frame and plotted as a function of time.

RESULTS

Sphingosine derivatives cause transient increases in surface FITC-CTxB fluorescence that correlates with insertion and flipping in the plasma membrane.

In our previous study of recycling endosome trafficking, we determined that Ca^{2+} influx is necessary for sustained outward trafficking of recycling endosomes in RBL mast cells [2]. Ca^{2+} mobilization during IgE-FcεRI-mediated signaling involves both release of Ca^{2+} from stores and influx via the store-operated Ca^{2+} entry (SOCE) channel Orai1/CRACM1 [23, 24]. It was shown previously that sphingosine derivatives effectively block SOCE [25], so we examined the effects of several sphingosine derivatives on outward trafficking of FITC-CTxB in RBL cells.

In initial experiments, we found that addition of 8 μM D-sphingosine or N,N'-dimethylsphingosine (DMS) to cells labeled with FITC-CTxB at 37°C caused a rapid increase in FITC fluorescence that decayed back to its original intensity after ~10 min (Figure 3.1A and data not shown). To determine whether this response is due to stimulated outward trafficking of CTxB from recycling endosomes, cells were labeled at 4°C to confine labeling to the plasma membrane [2]. Under these conditions, a similar

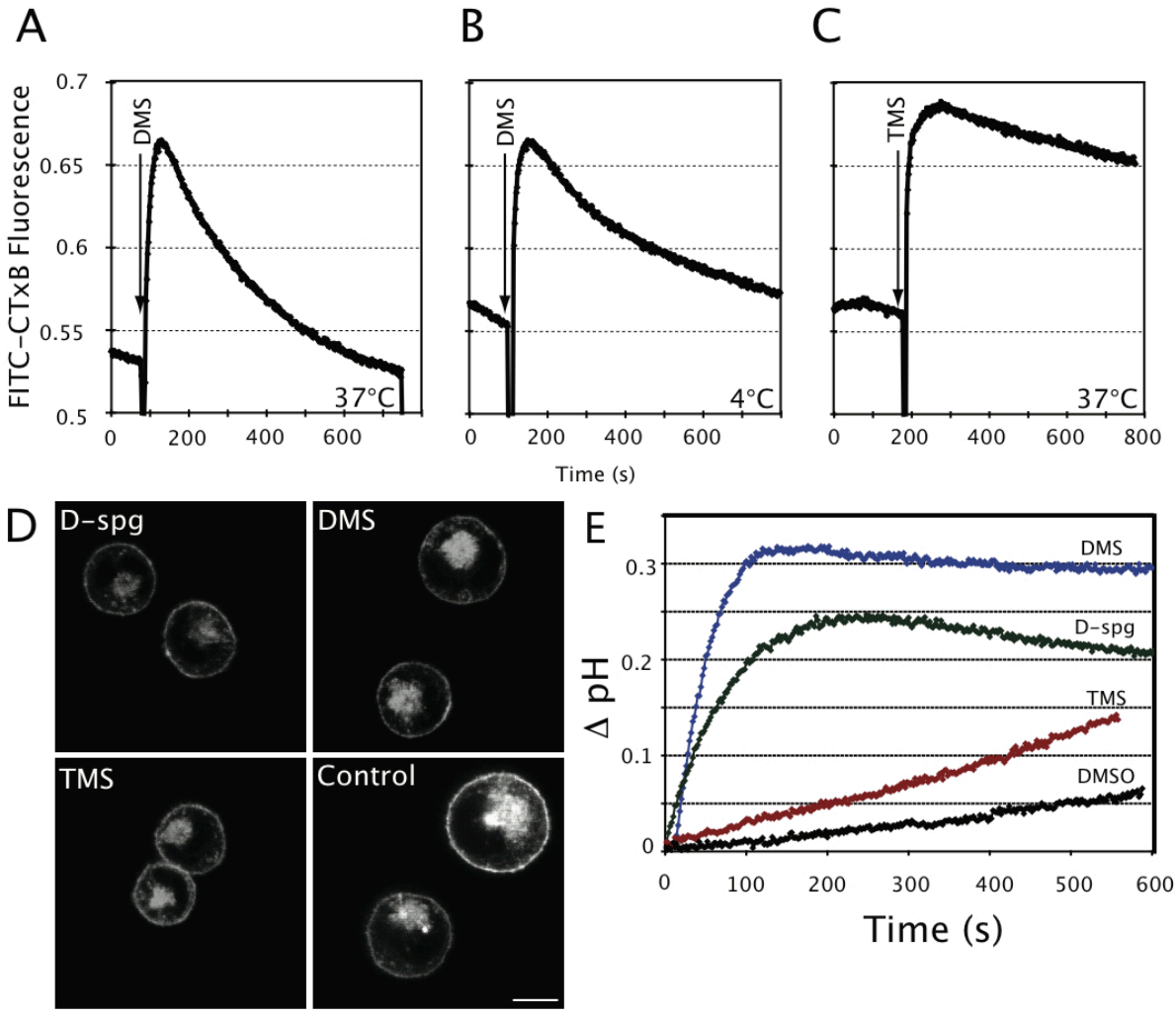

Figure 3.1. Sphingosine derivatives cause transient increases in the fluorescence of FITC-CTxB bound to GM_1 that correlates with cytoplasmic alkalinization. (A-C) RBL-2H3 cells were labeled with FITC-CTxB 37°C or 4°C, and 8 μM DMS or TMS were added as indicated. (D) Confocal equatorial images of RBL-2H3 cells labeled with Alexa488-CTxB for 2 hr at 37ºC, then treated with 8 μM D-sphingosine (D-spg), DMS, or TMS for 10 minutes prior to fixation and imaging Scale bar = 10 μm. (E) Changes in BCECF fluorescence in labeled RBL-2H3 cells in response to sphingosine derivatives (8 μM) or solvent (0.05%v/v DMSO) alone. Data in A-E are representative of at least 3 independent experiments.

transient increase in FITC fluorescence was observed upon addition of these derivatives, with no detectable change in the cellular distribution of label (Figure 3.1B and data not shown), indicating that this reflects a change in plasma membrane-associated FITC fluorescence. By comparison, addition of, N,N',N''-trimethylsphingosine (TMS), the quaternary ammonium derivative, to cells labeled with FITC-CTxB at 37^{o}C causes a similar rapid increase in FITC-CTxB fluorescence, but this higher level of fluorescence is more sustained over the same timescale (Figure 3.1C). Under these conditions, none of these sphingosine derivatives cause visible changes in the distributions of FITC-CTxB or Alexa488-CTxB (Figure 3.1D) at the plasma membrane and the recycling endosomal pool.

In other experiments, we found that cells labeled with pH-insensitive Alexa488-CTxB showed a similar, transient increase fluorescence in response to DMS, suggesting that it represents transient relief of self-quenching of the CTxB conjugates at the cell surface, rather than a pH-dependent effect on FITC fluorescence (data not shown). Furthermore, these sphingosine derivatives do not alter the fluorescence of CTxB conjugates in solution or that of FITC-IgE bound to FcεRI at the cell surface (data not shown), indicating an effect that depends on the specific protein ligand (CTxB) bound to GM_1 at the cell surface.

These results suggest that the increase in fluorescence observed is due to the insertion of the sphingosine compounds into the outer leaflet of the plasma membrane, which relieves FITC-CTxB self-quenching at the cell surface. D-sphingosine and DMS in Triton X-100 micelles and lipid bilayers have pKa values of 8.5 [26] and 8.8 [27],

respectively, and thus exist largely as protonated, positively charged species at pH 7.2, whereas the quarternary amine derivative TMS is positively charged at all pH values. Because of this charge, the latter derivative has a very low probability of flipping to the inner leaflet of the plasma membrane at any time [28], whereas this probability is significant for DMS and D-sphingosine, which both undergo deprotonation at a small but finite probability at pH 7.2. Thus, the biphasic nature of the FITC-CTxB fluorescence change induced by DMS and D-sphingosine is likely due to their insertion, then time-dependent flipping to the inner leaflet of the plasma membrane. In this process, the uncharged sphingosine species would regain a proton at the inner leaflet as dictated by its pKa and the cytoplasmic pH (~7.4).

To test this hypothesis, we loaded RBL-2H3 cells in suspension with cell permeable BCECF-AM, a fluorescein-based pH sensor [18], and monitored BCECF fluorescence during addition of sphingosine derivatives. As shown in Figure 3.1E, 8 μM D-sphingosine and DMS both caused a time-dependent increase in the cytoplasmic pH by 0.2-0.3 pH units that becomes maximal after 100-200 sec. By comparison, the same concentration of TMS caused a much slower increase in BCECF fluorescence that was only a little larger than the baseline change in the presence of solvent alone. These results indicate that the transient increase in FITC-CTxB fluorescence caused by D-sphingosine and DMS can be accounted for by their insertion into the plasma membrane, followed by their flipping to its inner leaflet upon deprotonation, where they become reprotonated and thereby increase the cytoplasmic pH. For TMS, the slow decline of FITC-CTxB fluorescence following its rapid increase, and the slow, small

increase in BCECF fluorescence following addition of TMS that are observed (Figs. 3.1C and E) may be due to impurities in this preparation, such as small amounts of DMS.

D-sphingosine and DMS inhibit outward trafficking of FITC-CTxB-labeled recycling endosomes.

As previously described, antigen stimulates a rapid increase in FITC fluorescence from RBL cells that are sensitized with IgE and labeled with FITC-CTxB at 37^{o}C (Figure 3.2A, left panel), and this was shown to reflect stimulated outward trafficking of labeled recycling endosomes [2]. As illustrated in Figure 3.2A, right panel, addition of the inhibitor of actin polymerization, cytochalasin D, prior to stimulation enhances the magnitude and duration of the stimulated trafficking response [2]. Because cytochalasin D provides a stronger, more sustained response to antigen, we carried out subsequent trafficking experiments under these conditions. To evaluate the effects of sphingosine derivatives on stimulated trafficking of FITC-CTxB-labeled recycling endosomes, RBL cells sensitized with IgE and labeled with FITC-CTxB at 37^{o}C were treated with different sphingosine derivatives for 10 min prior to addition of cytochalasin D and antigen. The fluorescence baseline was monitored for several minutes subsequent to addition of cytochalasin D, and this was extrapolated and subtracted as described in Materials and Methods.

As shown in Figure 3.2B, both D-sphingosine and DMS substantially reduce the trafficking response to antigen, with some differences in the time courses of these attenuated responses. In contrast, TMS does not alter the magnitude or kinetics of the

Figure 3.2. D-sphingosine and DMS, but not TMS, inhibit antigen-stimulated FITC-CTxB/GM_1 trafficking. (A) RBL cells exhibit outward trafficking of FITC-CTxB due to antigen (left panel) that is enhanced by cytochalasin D (Cyto D; right panel). (B) Representative time courses for stimulated trafficking in the presence or absence of sphingosine derivatives (8 μM) as indicated. (C) Summary of the effects of sphingosines on trafficking responses integrated for 420 s. Data are averages from 4 independent experiments, +/- SD.

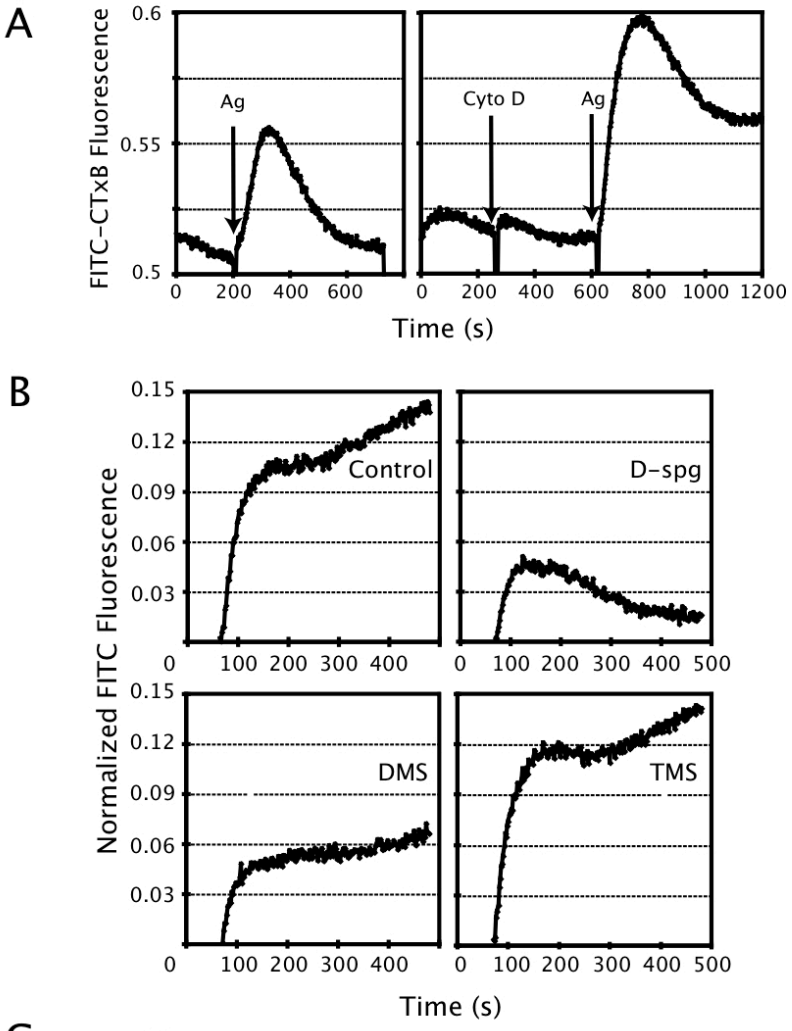
A
FITC-CTxB Fluorescence
0.6
0.55
0.5
Ag
Cyto D
Ag
0
200
400
600
800
1000
1200
Time (s)
B
Normalized FITC Fluorescence
0.15
0.12
0.09
0.06
0.03
Control
D-spg
DMS
TMS
0
100
200
300
400
500
Time (s)
C
Ag-stimulated CTxB Trafficking
1.2
1
0.8
0.6
0.4
0.2
0
-
+D-Spg
+DMS
+TMS

stimulated response. Figure 3.2C compares the integrated responses to Ag in the presence and absence of these sphingosine derivates as averages of four independent experiments. As indicated, 8 μM D-sphingosine or DMS both inhibit this integrated response by ~60%. In other experiments, we found that lower concentrations of these derivatives inhibit to lesser extents: 4 μM D-sphingosine causes less than half of the inhibition observed at 8 μM (data not shown). At concentrations of these derivatives greater than 10 μM, some cell lysis is variably detected, as indicated by progressive leakage of the Ca^{2+} indicator, indo-1 (data not shown). In subsequent experiments, we compared the effects of these sphingosine derivatives at the optimal dose of 8 μM. In other experiments, we found that the stereoisomer of D-sphingosine, L-sphingosine, inhibits the outward trafficking of FITC-CTxB bound to GM_1 to a similar extent at similar concentrations (data not shown), suggesting that stereospecific binding to a target protein is unlikely to be the mechanism of inhibition.

We subsequently tested the effects of sphingosine derivatives on outward trafficking of FITC-CTxB/GM_1 stimulated by the Ca^{2+} ionophore A23187. A23187 is a mobile carrier of divalent cations that increases intracellular Ca^{2+} levels in the absence of inositol 1,4,5-trisphosphate (IP_3)-dependent antigen-stimulated Ca^{2+} release from intracellular stores, thereby allowing us to bypass early signaling steps. In initial experiments we found that stimulation with A23187 caused robust outward trafficking, even in the absence of cytochalasin D (Fig. 3.3A). Under these conditions, D-sphingosine and DMS substantially inhibit outward trafficking of FITC-CTxB bound to GM_1, and DMS is somewhat more effective than D-sphingosine (Fig. 3.3A and B). The

Figure 3.3 Sphingosine derivatives inhibit recycling endosome trafficking triggered by calcium ionophore. (A) Representative time courses showing that D-sphingosine and DMS, but not TMS, inhibit calcium ionophore-stimulated trafficking of FITC-CTxB/GM1. RBL cells were stimulated with 1 mM A23187 in the presence or absence of 8 μM sphingosine derivatives. (B) Summary of inhibitory effects averaging 3 independent experiments, +/- SD.

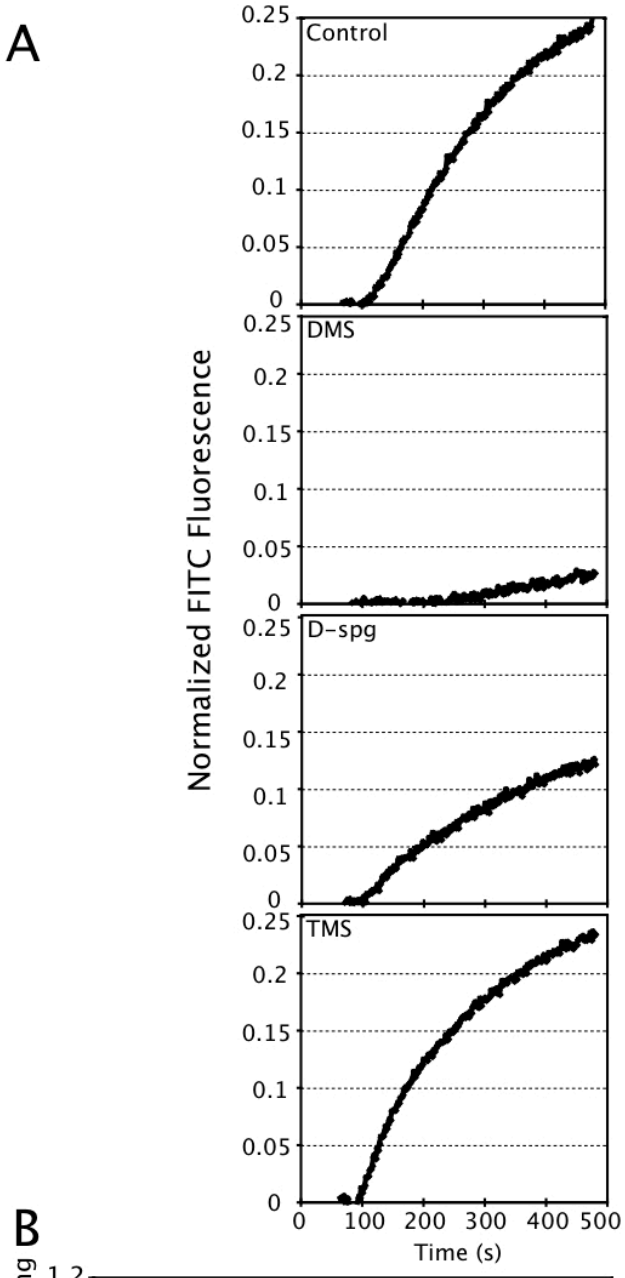
A
Control
DMS
D-spg
TMS
Normalized FITC Fluorescence
0.25
0.2
0.15
0.1
0.05
0
0 100 200 300 400 500
Time (s)

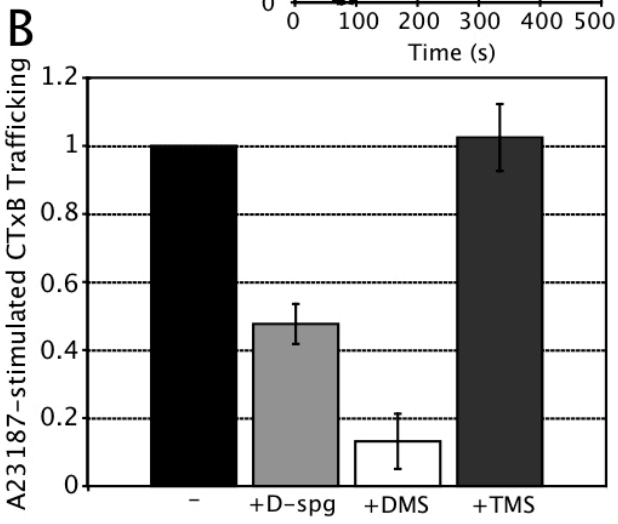
B
A23187-stimulated CTxB Trafficking
1.2
1
0.8
0.6
0.4
0.2
0
-
+D-spg
+DMS
+TMS

basis for this difference is unclear. Similarly, we found that D-sphingosine and DMS inhibit outward trafficking of FITC-CTxB stimulated by thapsigargin, which stimulates SOCE by inhibiting SERCA pumps in the endoplasmic reticulum (ER; data not shown). Together, these results indicate that sphingosine derivatives inhibit FITC-CTxB trafficking downstream from the earliest signaling events stimulated by FcεRI. In fact, no significant change in stimulated phosphorylation of FcεRI β and γ subunits is detected following addition of the sphingosine derivatives tested in this study (data not shown).

To evaluate whether outward trafficking of recycling endosomes occurs in adherent RBL mast cells, we developed an imaging method to detect this process. For these experiments, we first blocked GM_1 at the plasma membrane with unlabeled CTxB, then stimulated cells in the presence of excess Alexa488-CTxB and monitored its binding to newly-trafficked GM_1 at the plasma membrane using an imaging analysis method that we previously developed [22]. As shown in Figure 3.4A, A23187 stimulates a significant increase in the trafficking of GM_1 to the plasma membrane in adherent RBL cells. Furthermore, D-sphingosine inhibits this stimulated outward trafficking of GM_1 by ~60% under these conditions (Fig. 3.4B), consistent with results for stimulated trafficking of FITC-CTxB bound to GM_1 in suspended RBL cells (Fig. 3.3). Thus, GM_1 outward trafficking is stimulated in adherent RBL cells, indicating that this process is not restricted to suspended cells or to CTxB/GM_1 complexes. Furthermore, these results establish an alternative, single cells imaging assay for stimulated outward trafficking of recycling endosomes.

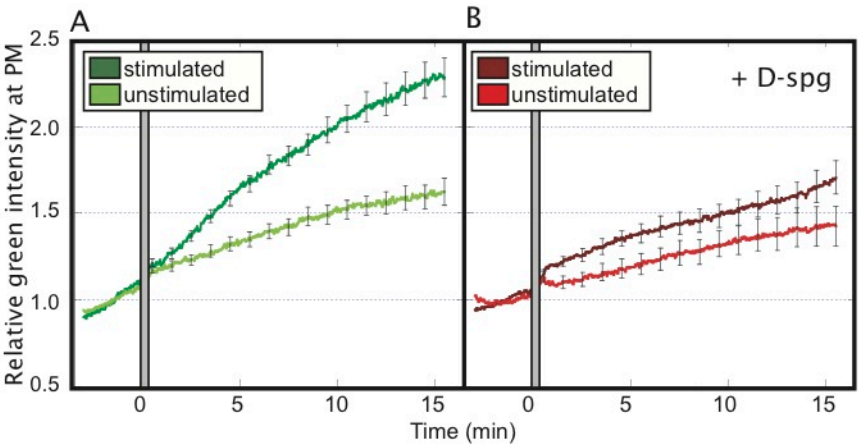

Figure 3.4. Live cell imaging of GM_1 trafficking to the plasma membrane in response to stimulation by calcium ionophore. Dynamics are monitored as mean plasma membrane fluorescence of Alexa488-CTxB in the absence (A) or presence (B) of 8 μM D-sphingosine, normalized to each pre-stimulation average. Gray bars indicate time of A23187 addition. Each condition represents average data for 15-28 individual cells from 4-5 independent experiments. Error bars show SEM.

Degranulation of secretory lysosomes is inhibited by sphingosine derivatives.

To determine whether sphingosines inhibit stimulated release of secretory lysosomes in these cells, we carried out degranulation assays with suspended RBL-2H3 cells in the presence of cytochalasin D to match the conditions used in our FITC-CTxB recycling endosome trafficking experiment. As shown in Figure 3.5, both D-sphingosine and DMS inhibit degranulation responses similar to the extents that they inhibit FITC-CTxB outward trafficking. As in the previous trafficking experiments, TMS had little effect on the degranulation response, consistent with its incapacity to flip to the inner leaflet of the plasma membrane.

Sphingosine derivatives inhibit Ca^{2+} mobilization in stimulated RBL mast cells.

Because DMS and D-sphingosine inhibit both RE trafficking and degranulation responses, it is likely that they inhibit a signaling step that is important for both. Although Ca^{2+} mobilization and protein kinase C (PKC) activation are important for secretory granule exocytosis in these cells [29, 30], inhibition of PKC has little effect on CTxB/GM_1 outward trafficking [2]. Ca^{2+} mobilization has two well-identified phases in RBL-mediated signaling: release from intracellular stores via IP_3 and IP_3 receptors on the ER followed by extracellular Ca^{2+} influx through Orai1 [31].

To evaluate whether sphingosine derivatives affect stimulated Ca^{2+} release from stores as well as influx, we stimulated RBL cells in the absence of extracellular Ca^{2+}, then replenished Ca^{2+} after several hundred seconds. In untreated cells, antigen addition causes a rapid increase in the intracellular Ca^{2+} concentration that returns to baseline following store depletion (Figure 3.6A). When Ca^{2+} is added back into the

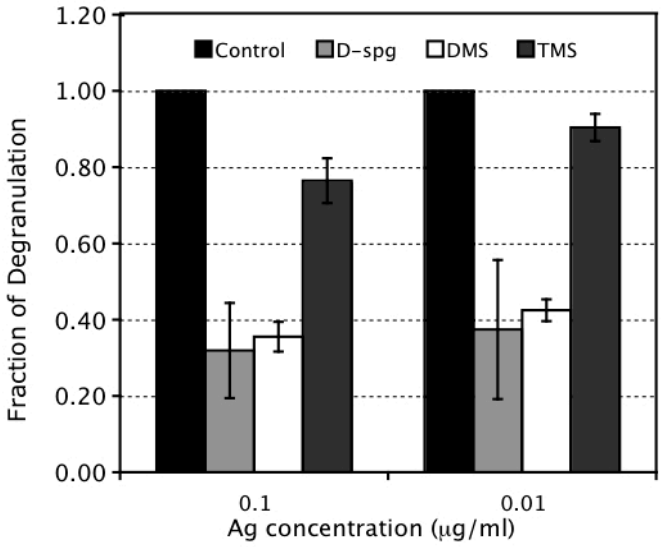

Figure 3.5. Degranulation responses in RBL-2H3 cells are similarly inhibited by D-sphingosine and DMS, but not TMS. Degranulation measured by β-hexosaminidase release following antigen stimulation at concentrations indicated in the presence of 2 μM cytochalasin D +/- sphingosine derivatives, expressed as fraction of control (antigen-stimulated) cell degranulation. Average of 3 independent experiments, +/- SD.

Figure 3.6. Sphingosine derivatives inhibit release from Ca^{2+} stores in addition to blocking Ca^{2+} influx. (A-D) RBL cells labeled with indo-1, then washed into Ca^{2+}-free buffer, were treated with sphingosine derivatives (8 μM), followed by antigen (0.8 μg/ml DNP-BSA) and Ca^{2+} (2 mM) as indicated. Data are representative of 2-4 independent experiments. (E) Summary of indo-1-monitored time-integrated responses to antigen in the presence of extracellular Ca^{2+}, with or without 8 μM sphingosine derivatives. Data are averages from 4-5 independent experiments, +/- SD.

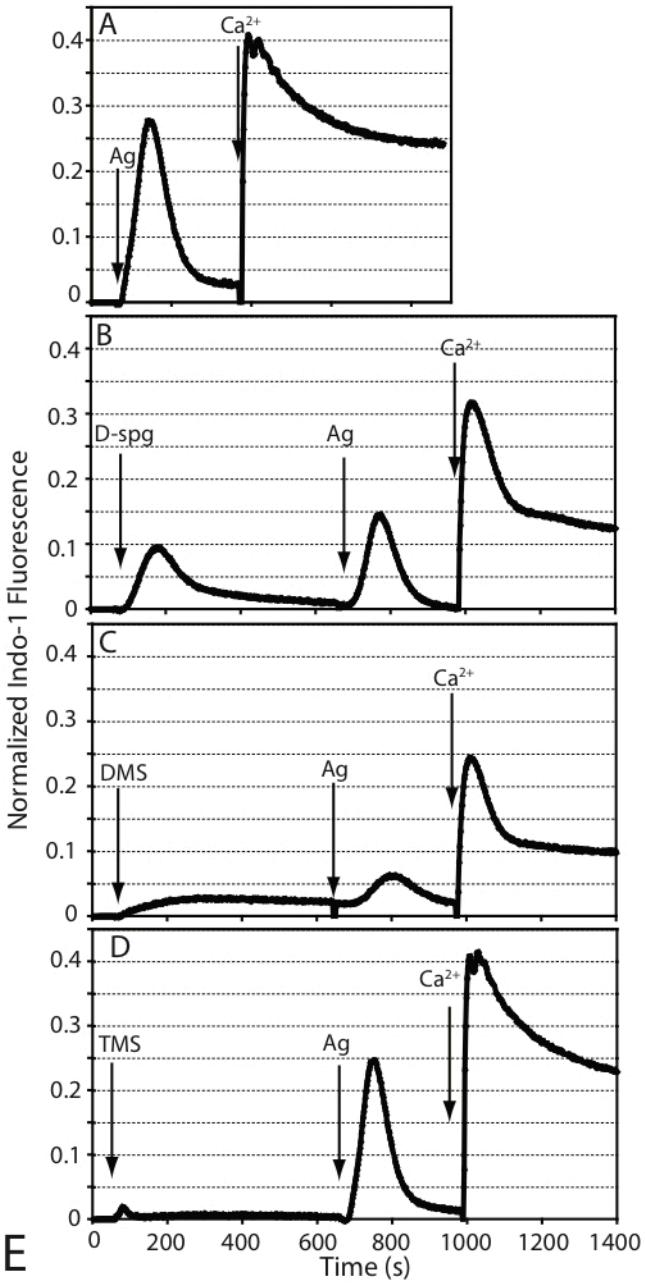
A
B
C
D
E
Ag
D-spg
DMS
TMS
Ca2+
Normalized Indo-1 Fluorescence
Time (s)
0
200
400
600
800
1000
1200
1400
0.1
0.2
0.3
0.4

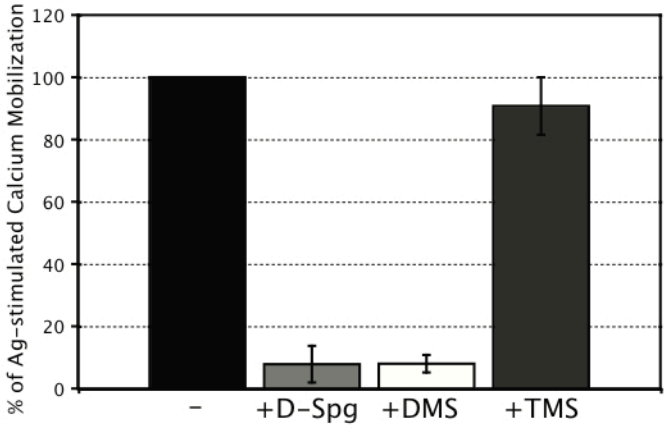
% of Ag-stimulated Calcium Mobilization
0
20
40
60
80
100
120
–
+D-Spg
+DMS
+TMS

extracellular buffer, stimulated Ca^{2+} influx results in a sustained increase in cytoplasmic Ca^{2+}. Addition of D-sphingosine or DMS to unstimulated cells causes small and/or transient increases in cytoplasmic Ca^{2+}, and subsequent addition of antigen results in reduced stimulated release from stores. In four separate experiments with 8 μM D-sphingosine, antigen-stimulated Ca^{2+} release from stores was reduced by 85 +/- 19% (SD). Similar to trafficking and degranulation responses, treatment with TMS has negligible effects on antigen-induced calcium release from stores (Figure 3.6D). Addition of Ca^{2+} subsequent to antigen for D-sphingosine and DMS-treated cells results in smaller responses than with antigen alone, whereas the antigen response in TMS-treated cells is identical to that of untreated cells (Fig. 3.6, A-D). These results indicate that D-sphingosine and DMS inhibit both antigen-stimulated Ca^{2+} release from stores, as well as stimulated Ca^{2+} influx.

To quantify effects of sphingosine derivatives on Ca^{2+} responses in the presence of extracellular Ca^{2+}, we compared time-integrated Ca^{2+} responses to antigen. As summarized in Figure 3.6E, both D-sphingosine and DMS block much of the antigen-stimulated Ca^{2+} response when compared to either untreated cells or those treated with TMS. These results, together with others described above, make it likely that D-sphingosine and DMS inhibit degranulation and outward trafficking of recycling endosomes at least in part by inhibiting Ca^{2+} mobilization, which is important for these more downstream exocytotic processes. Consistent with this, we find that these derivatives similarly inhibit the sustained, influx phase of A23187-mediated Ca^{2+} mobilization and A23187-stimulated degranulation (data not shown). These results are

accountable by the inhibition of store-operated Ca^{2+} entry by these long chain bases, as this process is activated by A23187, as well as by antigen and thapsigarin, and is important for stimulated degranulation in mast cells [24].

D-Sphingosine and DMS displace the polybasic MARCKS effector domain from interactions with polyphosphtidylinositols at the plasma membrane.

To investigate the mechanism by which D-sphingosine and DMS inhibit Ca^{2+} mobilization and Ca^{2+}-dependent secretory processes, we utilized the polybasic myristoylated, alanine-rich PKC substrate effector domain (MARCKS ED), which is a 25 amino acid sequence containing 13 basic residues that binds tightly to the plasma membrane via interactions with acidic phospholipids [32]. Meyer and colleagues showed that this association with the inner leaflet of the plasma membrane is dependent on interactions with polyphosphatidylinositides (see discussion, [21]). Full-length MARCKS dissociates from the plasma membrane in response to PKC-mediated phosphorylation of three serine residues in the effector domain. We mutated these residues to alanines to prevent this dissociation and used this MARCKS ED^{SA3} as an inhibitor of phosphoinositide accessibility (Gadi et al., submitted for publication).

As shown in Figure 3.7A, MARCK ED^{SA3}, tagged with a monomeric red fluorescent protein (mRFP), associates preferentially with the plasma membrane, with some additional label in the cytoplasm and nucleus to varying extents. Consistent with expectations, activation of PKC by 8 nM phorbol 12-myristate 13-acetate causes dissociation of mRFP-MARCKS ED from the plasma membrane but does not induce the dissociation of mRFP-MARCKS ED^{SA3} (Gadi et al., submitted for publication). To

quantify the partitioning of mRFP-MARCKS ED^{SA3} between the plasma membrane and the cytoplasm, we measured the intensity profile of a line across individual cells as illustrated in Figure 3.7A and described in Materials and Methods. In six separate experiments in which the ratio of plasma membrane to cytoplasmic intensity of mRFP-MARCKS ED^{SA3} was quantified in at least 15 cells per sample for each experiment, the average value for this ratio in control cells is 7.0 +/- 0.9 (SEM).

To establish whether mRFP-MARCKS ED^{SA3} could be displaced from the plasma membrane by perturbations known to alter polyphosphatidylinositide levels, we measured its plasma membrane to cytoplasmic fluorescence ratio to evaluate the effects of antigen stimulation and pharmacological inhibitors of polyphosphoinositide kinases (Figure 3.7). Wortmannin is a potent inhibitor of phosphatidylinositol (PI)3-kinases [33], but at a concentration sufficient to completely inhibit this enzyme family (200 nM), wortmannin did not induce detectable dissociation of mRFP-MARCKS ED^{SA3} from the plasma membrane (data not shown). At higher concentrations, wortmannin is an effective inhibitor of Type II PI4-kinases [34], with Ki's of ~100 nM. As shown in Figure 3.7B, treatment of these cells with 10 μM wortmannin for 10 min at 37^{o}C reduced the association of mRFP-MARCKS ED^{SA3} with the plasma membrane by ~30%, suggesting that PI4-P contributes to the binding of this probe to the plasma membrane.

Antigen stimulation of PI 4,5-bisphosphate (PIP_2) hydrolysis is expected to reduce the effective concentration of PIP_2 at the plasma membrane and thereby reduce the binding of MARCKS ED [21, 31]. However, antigen stimulation of RBL cells causes them to ruffle and flatten [35], making it difficult to quantify mRFP-MARCKS ED^{SA3} at the

A

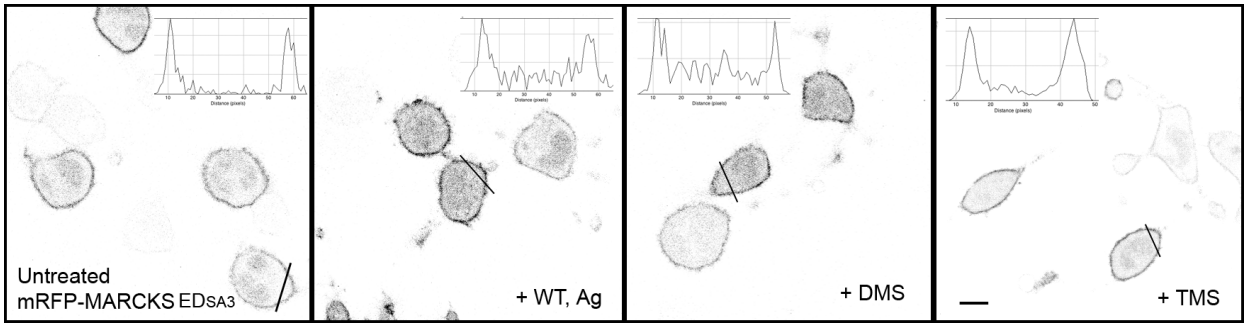

B

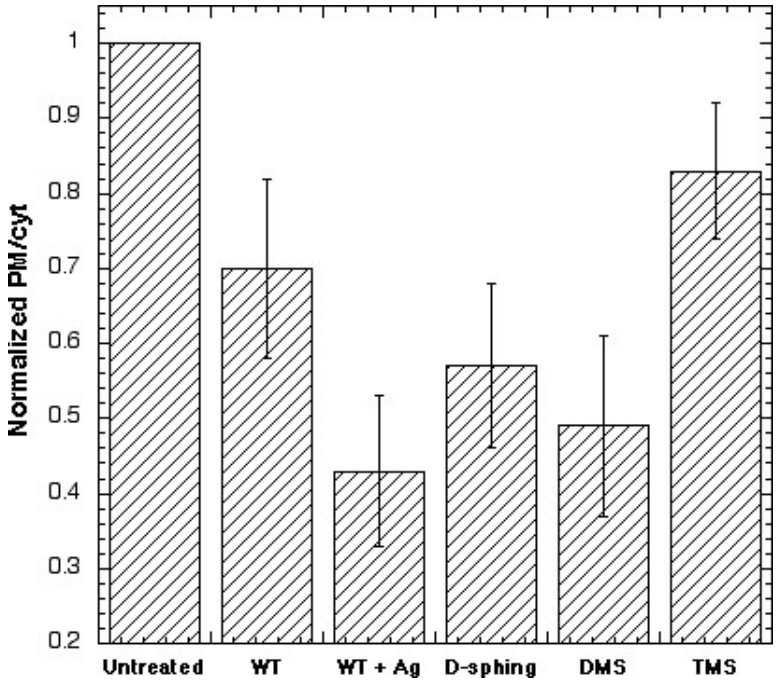

Figure 3.7. Dissociation of mRFP-MARCKS ED^{SA3} from the plasma membrane due to various treatments. A) Representative inverted confocal images showing mRFP-MARCKS ED^{SA3}-expressing RBL cells in the absence (first (left) panel) or following treatment with 10 mM wortmannin (WT) and 0.8 mg/ml antigen (second panel), 8 mM DMS (third panel), or 8 mM TMS (fourth panel). Lines through cells in each panel illustrate sections chosen for line scan analysis, and profiles for these are shown as inserts in each panel. (B) Summary of effects of various treatments on the normalized ratio of mRFP-MARCKS ED^{SA3} fluorescence at the plasma membrane to average cytoplasmic fluorescence determined as described in Materials and Methods. Data represents the average of 3-4 experiments per sample (>50 cells total per sample), +/- SD.

plasma membrane. Wortmannin prevents these morphological changes while permitting stimulated hydrolysis of PIP_2, as evidenced by antigen-stimulated, IP_3-dependent Ca^{2+} mobilization under these conditions (data not shown). As shown in Figure 3.7B, antigen stimulation in the presence of 10 μM wortmannin further reduces the association of mRFP-MARCKS ED^{SA3} at the plasma membrane compared to wortmannin alone, consistent with sensitivity of this association to PIP_2 hydrolysis.

We next determined whether sphingosine derivatives can displace mRFP-MARCKS ED^{SA3} from the plasma membrane under conditions in which these long chain bases inhibit signaling. As shown in Figure 3.7B, addition of 8 μM D-sphingosine for 10 min at 37°C causes substantial displacement of mRFP-MARCKS ED^{SA3} from the plasma membrane, and DMS at the same concentration causes a slightly larger displacement of ~50%, similar to that causes by 10 μM wortmannin + antigen. In contrast, TMS causes a relatively small reduction (<20%) in the plasma membrane to cytoplasmic ratio of mRFP-MARCKS ED^{SA3}. This effect may be due in part to impurities in the TMS preparation that can flip to the inner leaflet or, alternatively, to an increased plasma membrane surface area that is induced when TMS partitions into the outer leaflet (Figure 3.1).

Taken together, these results provide evidence that sphingosine derivatives that flip from the outer to the inner leaflet of the plasma membrane substantially reduce the binding of mRFP-MARCKS ED^{SA3} to the plasma membrane. Because of the electrostatic basis for this association, it is likely that the positively charged headgroups of D-sphingosine and DMS provide electrostatic neutralization of polyphosphoinositides

at the inner leaflet of the plasma membrane, thus competing with mRFP-MARCKS ED^{SA3} for binding to these negatively charged phospholipids.

DISCUSSION

The plasma membrane is a dynamic organelle, with continuous turnover of lipids and proteins mediated by membrane trafficking and other processes. Recycling endosomes, also know as the endosomal recycling compartment, provide a pool of readily available membrane components that can be trafficked to the cell surface under resting and stimulatory conditions [2, 36]. The small GTPases Rab11 and Arf6 have been identified as regulators of recycling endosomes [37-39]. Mutation of Rab11 to an inactive GTPase inhibits trafficking of transferrin-containing recycling endosomes [40], whereas an analogous mutation in Arf6 inhibits trafficking of GM_1, but not transferrin receptors, from recycling endosomes to the plasma membrane, suggesting that at least two distinct subsets of recycling endosomes participate in these processes [41].

Although much is now known about the proteins and signaling pathways that regulate trafficking of recycling endosomes, the roles of this trafficking in cell physiology are poorly understood in most cell types. To begin to investigate these roles in mast cells, we characterized the effects of sphingosine derivatives on antigen-stimulated outward trafficking of FITC-CTxB-labeled recycling endosomes. We found that D-sphingosine and DMS are similarly effective inhibitors of this process, and this inhibition correlates with their capacity to flip from the outer leaflet of the plasma membrane to its inner leaflet, as monitored by both transient relief of FITC-CTxB self-quenching at the plasma membrane, and by a time-dependent increase in cytoplasmic pH. In contrast to

these sphingosines, most TMS remains in the outer leaflet of the plasma membrane, as monitored by a more sustained increase in FITC-CTxB fluorescence and a smaller, more slowly developing increase in cytoplasmic pH (Figure 3.1). Consistent with these differences, TMS does not inhibit stimulated outward trafficking of FITC-CTxB-labeled recycling endosomes (Figure 3.2 and 3.3). Similarly, D-sphingosine and DMS inhibit antigen-stimulated degranulation responses by ~60% under these conditions, whereas TMS inhibits this response to a much smaller extent (Figure 3.5). Recently, D-sphingosine has been shown to inhibit exocytotic release of insulin and Glut4 expression at the plasma membrane of beta cells, and a similar electrostatic mechanism of inhibition has been implicated [42].

Similar trends are observed for the effects of these derivatives on antigen-stimulated Ca^{2+} responses. These results are consistent with a previous study that demonstrated inhibition of IP_3- and thapsigargin-stimulated, Ca^{2+} release-activated Ca^{2+}(CRAC) channels by D-sphingosine and DMS [25]. In a more recent study, we showed that these derivatives inhibit store-operated Ca^{2+} entry by interfering with the coupling between the CRAC channel, Orai1, and the ER Ca^{2+} sensor protein, STIM1 [20]. However, we now find that these sphingosine derivatives inhibit antigen-stimulated Ca^{2+} release from ER stores, indicating an additional effect on antigen-stimulated Ca^{2+} responses at a step that precedes store-operated Ca^{2+} entry (Figure 3.6). Similar to results for stimulated outward trafficking of recycling endosomes and degranulation, we find that TMS fails to inhibit both antigen-stimulated Ca^{2+} release from stores and Ca^{2+}

influx, suggesting that the redistribution of D-sphingosine and DMS to the inner leaflet of the plasma membrane are important for their inhibitory effects.

In some previous studies, inhibition of Ca^{2+} mobilization and other signaling processes by DMS was suggested to be due to inhibition of the production of sphingosine-1-phosphate by sphingosine kinases [43, 44]. From our present results and those of Mathes et al. [25], this explanation seems unlikely, as both DMS and the substrate for sphingosine-1-kinase, D-sphingosine, similarly inhibit Ca^{2+} mobilization and exocytosis of both recycling endosomes and secretory lysosomes. Although more complex mechanisms, such as substrate inhibiton of sphingosine 1-kinase, cannot be excluded [45], the simplest explanation for our results is that sphingosine derivatives inhibit antigen-stimulated signaling processes by a different mechanism than interference with sphingosine-1-phosphate production. In this regard, Olivera et al. showed that knockout of sphingosine kinase 2, which inhibits Ca^{2+} mobilization in mast cells, significantly increases intracellular levels of D-sphingosine [46]. Thus, we suggest that alterations in endogenous levels of D-sphingosine may directly modulate Ca^{2+} and other signaling processes.

One mechanism by which basic lipids such as sphingosines might alter signaling pathways is electrostatic neutralization of acidic lipids. These lipids, including polyphosphatidylinositides, are preferentially localized at the inner leaflet of the plasma membrane, and they serve multiple roles in cell signaling [47]. PIP_2, for example, serves as a substrate for phospholipase C-mediated production of IP_3 in the initiation of store-operated Ca^{2+} entry [48], and it has also been implicated in exocytotic processes via

plasma membrane targeting of Ca^{2+}-sensing proteins such as synaptotagmins [49]. As described above, Meyer and colleagues investigated the roles of polyphosphoinositides in plasma membrane-targeting of various signaling proteins, and they showed that the strong association of the polybasic effector domain of the PKC substrate MARCKS with the plasma membrane is largely due to electrostatic interactions with polyphosphatidylinositides [21]. We took advantage of these observations to test whether sphingosines can compete for electrostatic interactions between polyphosphatidylinositides at the plasma membrane and mRFP-MARCKS ED that is mutated to prevent its PKC-mediated dissociation. We found that both D-sphingosine and DMS substantially reduce the plasma membrane-to-cytoplasmic ratio of mRFP-MARCKS ED^{SA3}, whereas TMS causes a smaller decrease in this ratio (Figure 3.7).

Interestingly, wortmannin at a concentration that effectively inhibits PI3-kinases (200 nM) does not significantly reduce association of mRFP-MARCKS ED^{SA3}, whereas 10 μM wortmannin, which also inhibits PI4-P synthesis [34], causes substantial dissociation that is enhanced by antigen, most likely due to stimulated PIP_2 hydrolysis (Figure 3.7B). These results suggest that PI4-P contributes to the electrostatic association of mRFP-MARCKS ED^{SA3} with the plasma membrane, in addition to the contribution of PIP_2. The similar extent of mRFP-MARCKS ED^{SA3} dissociation caused by D-sphingosine and DMS compared to that caused by 10 μM wortmannin and antigen suggests that these sphingosine derivatives effectively compete with mRFP-MARCKS ED^{SA3} for binding to PIP_2 and PI4-P at the plasma membrane.

These results, taken together, indicate that D-sphingosine and DMS are effective inhibitors of FcεRI-mediated signaling because of their capacity to compete electrostatically with proteins for binding to polyphosphatidylinositols at the inner leaflet of the plasma membrane. However, we cannot exclude roles for electrostatic neutralization of other classes of negatively charged phospholipids by these sphingosine derivatives for their inhibitory effects on Ca^{2+} mobilization leading to stimulated exocytosis of recycling endosomes and secretory lysosomes. Further studies will be necessary to assess more directly the phospholipid specificity of these inhibitory effects. None-the-less, our results show that electrostatic neutralization of negatively charged phospholipids, including polyphosphoinositides, is likely to be relevant to a large number of studies in which sphingosine derivatives have been shown to be effective inhibitors of cell signaling.

CONTRIBUTIONS AND ACKNOWLEDGEMENTS

Research designed by N. L. Smith, D. A. Holowka, B. A. Baird and S. Hammond; N. L. Smith performed and analyzed recycling endosomal trafficking and calcium experiments; S. Hammond performed and analyzed microscopy experiments to examine RE trafficking; D. Gadi and A. Wagenknecht-Wiesner generated and characterized mRFP-MARCKS ED^{SA3} construct; D. Holowka performed and analyzed microscopy with mRFP-MARCKS ED^{SA3} construct. Paper written by N. L. Smith, D. A. Holowka and B. A. Baird. Research supported by National Institutes of Heath Grants R01 AI022449 (B. A. Baird and D. A. Holowka).

We thank Ms. Carol Bayles for maintaining the Cornell Microscopy and Imaging Facility.

REFERENCES

1. Gilfillan, A.M. and J. Rivera, *The tyrosine kinase network regulating mast cell activation.* Immunol Rev, 2009. **228**(1): p. 149-69.

2. Naal, R.M., et al., *Antigen-stimulated trafficking from the recycling compartment to the plasma membrane in RBL mast cells.* Traffic, 2003. **4**(3): p. 190-200.

3. Taylor, C.W. and L.M. Broad, *Pharmacological analysis of intracellular Ca2+ signalling: problems and pitfalls.* Trends Pharmacol Sci, 1998. **19**(9): p. 370-5.

4. Hopkins, C.R. and I.S. Trowbridge, *Internalization and processing of transferrin and the transferrin receptor in human carcinoma A431 cells.* J Cell Biol, 1983. **97**(2): p. 508-21.

5. Yamashiro, D.J., et al., *Segregation of transferrin to a mildly acidic (pH 6.5) para-Golgi compartment in the recycling pathway.* Cell, 1984. **37**(3): p. 789-800.

6. Prigozhina, N.L. and C.M. Waterman-Storer, *Decreased polarity and increased random motility in PtK1 epithelial cells correlate with inhibition of endosomal recycling.* J Cell Sci, 2006. **119**(Pt 17): p. 3571-82.

7. Ang, A.L., et al., *Recycling endosomes can serve as intermediates during transport from the Golgi to the plasma membrane of MDCK cells.* J Cell Biol, 2004. **167**(3): p. 531-43.

8. Cresawn, K.O., et al., *Differential involvement of endocytic compartments in the biosynthetic traffic of apical proteins.* Embo J, 2007. **26**(16): p. 3737-48.

9. Murray, R.Z., et al., *A role for the phagosome in cytokine secretion.* Science, 2005. **310**(5753): p. 1492-5.

10. Dyer, N., et al., *Spermatocyte cytokinesis requires rapid membrane addition mediated by ARF6 on central spindle recycling endosomes.* Development, 2007. **134**(24): p. 4437-47.

11. Varthakavi, V., et al., *The pericentriolar recycling endosome plays a key role in Vpu-mediated enhancement of HIV-1 particle release.* Traffic, 2006. **7**(3): p. 298-307.

12. Zhang, M., et al., *Presenilin/gamma-secretase activity regulates protein clearance from the endocytic recycling compartment.* Faseb J, 2006. **20**(8): p. 1176-8.

13. Stow, J.L., et al., *Cytokine secretion in macrophages and other cells: Pathways and mediators.* Immunobiology, 2009.

14. Posner, R.G., et al., *Aggregation of IgE-receptor complexes on rat basophilic leukemia cells does not change the intrinsic affinity but can alter the kinetics of the ligand-IgE interaction.* Biochemistry, 1992. **31**(23): p. 5350-6.

15. Gidwani, A., et al., *Disruption of lipid order by short-chain ceramides correlates with inhibition of phospholipase D and downstream signaling by FcepsilonRI.* J Cell Sci, 2003. **116**(Pt 15): p. 3177-87.

16. Mohr, F.C. and C. Fewtrell, *The relative contributions of extracellular and intracellular calcium to secretion from tumor mast cells. Multiple effects of the proton ionophore carbonyl cyanide m-chlorophenylhydrazone.* J Biol Chem, 1987. **262**(22): p. 10638-43.

17. Naal, R.M., et al., *In situ measurement of degranulation as a biosensor based on RBL-2H3 mast cells.* Biosens Bioelectron, 2004. **20**(4): p. 791-6.

18. Kamp, F., et al., *Rapid flip-flop of oleic acid across the plasma membrane of adipocytes.* J Biol Chem, 2003. **278**(10): p. 7988-95.

19. Field, K.A., et al., *Mutant RBL mast cells defective in Fc epsilon RI signaling and lipid raft biosynthesis are reconstituted by activated Rho-family GTPases.* Mol Biol Cell, 2000. **11**(10): p. 3661-73.

20. Calloway, N., et al., *Molecular clustering of STIM1 with Orai1/CRACM1 at the plasma membrane depends dynamically on depletion of Ca2+ stores and on electrostatic interactions.* Mol Biol Cell, 2009. **20**(1): p. 389-99.

21. Heo, W.D., et al., *PI(3,4,5)P3 and PI(4,5)P2 lipids target proteins with polybasic clusters to the plasma membrane.* Science, 2006. **314**(5804): p. 1458-61.

22. Das, R., et al., *Real-time cross-correlation image analysis of early events in IgE receptor signaling.* Biophys J, 2008. **94**(12): p. 4996-5008.

23. Hewavitharana, T., et al., *Role of STIM and Orai proteins in the store-operated calcium signaling pathway.* Cell Calcium, 2007. **42**(2): p. 173-82.

24. Vig, M., et al., *Defective mast cell effector functions in mice lacking the CRACM1 pore subunit of store-operated calcium release-activated calcium channels.* Nat Immunol, 2008. **9**(1): p. 89-96.

25. Mathes, C., A. Fleig, and R. Penner, *Calcium release-activated calcium current (ICRAC) is a direct target for sphingosine.* J Biol Chem, 1998. **273**(39): p. 25020-30.

26. Bottega, R., R.M. Epand, and E.H. Ball, *Inhibition of protein kinase C by sphingosine correlates with the presence of positive charge.* Biochem Biophys Res Commun, 1989. **164**(1): p. 102-7.

27. Lau, B. and P.M. Macdonald, *Determination of the pKa of membrane-bound N,N-dimethylsphingosine using deuterium NMR spectroscopy.* Biochim Biophys Acta, 1995. **1237**(1): p. 37-42.

28. Devaux, P.F., *Static and dynamic lipid asymmetry in cell membranes.* Biochemistry, 1991. **30**(5): p. 1163-73.

29. Wolfe, P.C., et al., *Differential effects of the protein kinase C activator phorbol 12-myristate 13-acetate on calcium responses and secretion in adherent and suspended RBL-2H3 mucosal mast cells.* J Biol Chem, 1996. **271**(12): p. 6658-65.

30. Taurog, J.D., et al., *Noncytotoxic IgE-mediated release of histamine and serotonin from murine mastocytoma cells.* J Immunol, 1977. **119**(5): p. 1757-61.

31. Ma, H.T. and M.A. Beaven, *Regulation of Ca2+ signaling with particular focus on mast cells.* Crit Rev Immunol, 2009. **29**(2): p. 155-86.

32. McLaughlin, S. and A. Aderem, *The myristoyl-electrostatic switch: a modulator of reversible protein-membrane interactions.* Trends Biochem Sci, 1995. **20**(7): p. 272-6.

33. Yano, H., et al., *Inhibition of histamine secretion by wortmannin through the blockade of phosphatidylinositol 3-kinase in RBL-2H3 cells.* J Biol Chem, 1993. **268**(34): p. 25846-56.

34. Balla, A. and T. Balla, *Phosphatidylinositol 4-kinases: old enzymes with emerging functions.* Trends Cell Biol, 2006. **16**(7): p. 351-61.

35. Pfeiffer, J.R., et al., *Membrane and cytoskeletal changes associated with IgE-mediated serotonin release from rat basophilic leukemia cells.* J Cell Biol, 1985. **101**(6): p. 2145-55.

36. Maxfield, F.R. and T.E. McGraw, *Endocytic recycling.* Nat Rev Mol Cell Biol, 2004. **5**(2): p. 121-32.

37. D'Souza-Schorey, C., et al., *ARF6 targets recycling vesicles to the plasma membrane: insights from an ultrastructural investigation.* J Cell Biol, 1998. **140**(3): p. 603-16.

38. Green, E.G., et al., *Rab11 is associated with transferrin-containing recycling compartments in K562 cells.* Biochem Biophys Res Commun, 1997. **239**(2): p. 612-6.

39. Sonnichsen, B., et al., *Distinct membrane domains on endosomes in the recycling pathway visualized by multicolor imaging of Rab4, Rab5, and Rab11.* J Cell Biol, 2000. **149**(4): p. 901-14.

40. Ren, M., et al., *Hydrolysis of GTP on rab11 is required for the direct delivery of transferrin from the pericentriolar recycling compartment to the cell surface but not from sorting endosomes.* Proc Natl Acad Sci U S A, 1998. **95**(11): p. 6187-92.

41. Balasubramanian, N., et al., *Arf6 and microtubules in adhesion-dependent trafficking of lipid rafts.* Nat Cell Biol, 2007. **9**(12): p. 1381-91.

42. Williams, D., et al., *Evidence that electrostatic interactions between vesicle-associated membrane protein 2 and acidic phospholipids may modulate the fusion of transport vesicles with the plasma membrane.* Mol Biol Cell, 2009. **20**(23): p. 4910-9.

43. Jolly, P.S., et al., *Transactivation of sphingosine-1-phosphate receptors by FcepsilonRI triggering is required for normal mast cell degranulation and chemotaxis.* J Exp Med, 2004. **199**(7): p. 959-70.

44. Itagaki, K. and C.J. Hauser, *Sphingosine 1-phosphate, a diffusible calcium influx factor mediating store-operated calcium entry.* J Biol Chem, 2003. **278**(30): p. 27540-7.

45. Prieschl, E.E., et al., *The balance between sphingosine and sphingosine-1-phosphate is decisive for mast cell activation after Fc epsilon receptor I triggering.* J Exp Med, 1999. **190**(1): p. 1-8.

46. Olivera, A., et al., *The sphingosine kinase-sphingosine-1-phosphate axis is a determinant of mast cell function and anaphylaxis.* Immunity, 2007. **26**(3): p. 287-97.

47. Di Paolo, G. and P. De Camilli, *Phosphoinositides in cell regulation and membrane dynamics.* Nature, 2006. **443**(7112): p. 651-7.

48. Rhee, S.G., *Regulation of phosphoinositide-specific phospholipase C.* Annu Rev Biochem, 2001. **70**: p. 281-312.

49. Paddock, B.E., et al., *Ca2+-dependent, phospholipid-binding residues of synaptotagmin are critical for excitation-secretion coupling in vivo.* J Neurosci, 2008. **28**(30): p. 7458-66.

CHAPTER FOUR

Recycling Endosomal Contribution to the Secretion of IL-4 and TNFα in RBL Mast Cells

SUMMARY

In mast cells, crosslinking of FcεRI-IgE by multivalent antigen results in a complex signaling cascade that culminates in the secretion of preformed allergic mediators from secretory granules. Additionally, this signaling cascade activates the transcription of various gene products, including cytokines, which play important roles in the adaptive immune response. Our ELISA measurements show that cytokines IL-4 and TNFα are secreted following stimulation. Confocal microscopy shows that cytokine IL-4 is produced *de novo* in RBL mast cells following multivalent antigen stimulation. We observe intracellular localization of IL-4 with both Golgi and recycling endosomal markers, but not with markers for secretory lysosomes. Using pharmacological inhibitors, we find that PI3-kinases, and protein kinase C (PKC) isoforms are necessary for initiation of signaling by FcεRI that leads to cytokine secretion, but the two enzymes are dispensible for the sustained secretory phase. In contrast, secretion of IL-4 and TNFα is enhanced to different extents by both inhibition of actin polymerization and by siRNA knockdown of the GTPase Rab11A. These results support a role for recycling endosomal (RE) trafficking of newly synthesized cytokines in stimulated mast cells. We are developing tools such as a GFP-tagged TNFα construct and specific inactivation of RE trafficking to further test this hypothesis and to address other questions regarding the regulation and function of recycling endosomes.

INTRODUCTION

Signaling in mast cells, initiated by antigen-mediated cross-linking of FcεRI/IgE complexes, triggers multiple effector functions. The most commonly associated result of mast cell signaling is the rapid release of preformed mediators, such as histamine, from secretory granules. On longer time scales, this signaling also activates the production of a number of immunologically relevant molecules, from eicosanoids to cytokines. Mast cell signaling is predominately associated with allergic disease, inflammation, and asthma [1], but it is also important in host defense to helminths [2], in innate immunity [3] and, in some cases, in limiting inflammation [4].

It is widely accepted that cytokines play crucial roles in the orchestration and regulation of immune responses. In immune cells, cytokine synthesis is triggered through activation of a number of receptor families including multichain immune recongition receptors (MIRR), cytokine receptors and Toll-like receptors (TLR). The various signal transduction cascades that emanate from these receptors have been extensively studied.

Less well studied are the mechanisms that control and regulate cytokine secretion. The protein biosynthetic pathway generally involves protein synthesis on ER-associated ribosomes, protein modification in the ER, and transport to the Golgi for further post-translational modification prior to plasma membrane trafficking and secretion. The precise mechanisms that regulate secretion of cytokines via vesicular transport downstream of the Golgi have recently gained attention, and they highlight a

role for RE for cytokine secretion [5]. RE containing TNFα have been shown to traffic to sites of phagocytosis in macrophages [6]. Furthermore, there is evidence that subcompartments of the RE may differentially traffic IL-6 and TNFα [7]. This is reminiscent of a study by Huse et al. in which activated T cells show spatially discrete cytokine secretion patterns [8]. Recently, cytokine secretion in NK cells was shown to be dependent on RE trafficking but functionally independent of granule exocytosis [9]. Similarly, our laboratory has shown that RE outward trafficking is spatially distinct from granule exocytosis in mast cells [10].

Mast cells predominantly secrete cytokines associated with Th2-mediated immunity, such as IL-3, IL-4, IL-13 and TNFα [2]. Determining the intracellular mechanisms that control both the spatial and temporal aspects of cytokine export in mast cells may lead to new therapies for managing the damaging effects of allergy-associated inflammation that occurs as a result of mast cell signaling.

To this end, we used RBL mast cells to begin to probe the intracellular pathways that govern cytokine secretion. We began by confirming that RBL mast cells secrete both IL-4 and TNFα in response to stimulation by multivalent antigen. Furthermore, we show visual evidence that newly synthesized IL-4 localizes to RE following antigen stimulation. Pharmacological inhibition of PI3 kinase and PKC reveal these kinases are essential for FcεRI early signaling events leading to cytokine secretion but are dispensable at later timepoints. IL-4 and TNFα secretion have differential sensitivity to cytochalasin D, suggesting the actin cyotskeleton may contribute to cytokine secretion in multiple ways. Cytokine secretion is also halted by D-sphingosine, an inhibitor of RE

trafficking. Similar to other immune cell types, our results suggest that mast cell cytokine secretion is a regulated process that involves RE. Furthermore, our results point to future directions for probing the involvement of RE in cytokine secretion.

MATERIALS AND METHODS

Chemicals and Reagents

FITC-cholera toxin B (FITC-CTxB), cytochalasin D, diaminobenzidine and all other chemicals, unless otherwise indicated, were purchased from Sigma-Aldrich. All tissue culture reagents were obtained from Invitrogen Corp. Transferrin-HRP was purchased from Rockland. Anti-DNP IgE was purified as described previously [11]. The following antibodies were purchased: anti-rat IL-3β (Peprotech), anti-rat IL-4 (R&D Biosystems), anti-rat CD63, anti-rat GM130 and anti-rat transferrin (BD Biosciences). AlexaFluor-conjugated secondary antibodies were purchase from Invitrogen Corp.

Cell Culture

RBL mast cells were passed weekly to maintain a monolayer culture as described previously [12]. For experiments, cells were sensitized with 1 μg/ml anti-DNP IgE over night.

For knockdown experiments, Rab11A siRNA sequences (Ambion, Inc. catalog numbers AM16708A siRNA IDs 189852 (#1) and 53555 (#2)), or a negative control sequence was used (target sequence NNUUAACCUUACCGAGGGUCGAA) (Darmacon, Inc) were used. siRNA was introduced by electroporation of 1 μM siRNA

into cells at a concentration of $1x10^7$/ml. Transfected cells were plated in complete RBL media (minimum essential media (MEM) with L-glutamine containing 20% fetal bovine serum and 50 μg/ml Gentamicin) for 48 hours prior to experiments.

For transient transfections, cells were sparsely plated ($1\text{-}3x10^5$/ml) on no. 1.5 coverslips or in 35 mm glass bottom dishes (MatTek). After overnight culture, media was replaced by OPTIMEM and cells were transfected using 2 ug DNA and 8 μl Fugene HD (Roche Diagnostics) per ml media for 1 hour followed by addition of 1 ng/ml phorbol 12,13-dibutyrate for 3-5hr [13]. Samples were then washed into complete RBL media and incubated 16-24 hours to allow for protein expression.

ELISAs

IgE-sensitized cells were plated in triplicate at a concentration of 3 $x10^5$ cells/ well in a 96 well plate overnight. Stimulation with 10 ng/ml DNP-BSA was performed in complete RBL media buffered with 20 mM HEPES. Some experiments were conducted in the presence of wortmannin (200 nM), bisindolyl malemide (BIM, 100 μM) or 2 μM cytochalasin D. These agents were added either just prior to or one hour after initiation of antigen stimulation in order to differentiate between early signaling and downstream effector functions. To assay cytokine secretion, IL-4 and TNFα ELISA kits (BD Biosciences) and tetramethylbenzidine (TMB) substrate (KPL, Inc.) were used according to manufacturers instructions. Plates were read with a Spectra Fluor plate reader (Tecan, Inc.).

Generation of GFP-TNFα Construct

The AcGPF-TNFα construct was generated using rat TNFα cDNA (Open Biosystems/ThermoFisher). The TNFα sequence was cloned into pAcGFP-C1 Clonetech, Inc) using the HindIII and EcoRI restrictions sites within the multiple cloning site, producing and N-terminal GFP-tagged TNFα construct. This construct was generated in collaboration with Dr. Alice Wagenknecht-Wiesner (Cornell University). Construct was assessed by confocal microscopy using the fixation protocol described below.

Confocal Microscopy

To assess *de novo* cytokine production, sensitized RBL cells plated on 35 mm glass bottom dishes (MatTek) were stimulated with 10 ng/ml DNP-BSA for 3 hours followed by fixation with 4% paraformaldehyde and 0.1% glutaraldehyde in phosphate buffered saline (PBS; 10 minutes at room temperature). Excess fixative was quenched with 10 mg/ml BSA in PBS with 0.01% azide. Samples were images on a on a SP2 confocal system (Leica).

RE Inactivation and RE Trafficking Assay

Specific inactivation of RE was performed using a method described previously [7, 14]. Briefly, transferrin-HRP (10 μg/ml) was added to sensitized RBL cells ($6x10^6$/ml) that had been labeled with FITC-CTxB for one hour. Surface-bound transferrin-HRP was removed by 2 brief washes with 150 mM NaCl with 20 mM citric acid (pH 5) and then washed into BSS (135 mM NaCl, 5 mM KCL, 1 mM $MgCl_2$, 1.8 mM

$CaCl_2$, 5.6 mM glucose 20 mM HEPES, pH 7.4, 1 mg/ml BSA). 0.1 mg/ml Diaminobenzidine (DAB) and 0.025% H_2O_2 was added to samples and allowed to incubate on ice and protected from light for 1 hour. Cells were washed into BSS and FITC-CTxB trafficking was assessed by fluorimetry [15].

Statistical Analyses

Statistical analysis was performed with Prism software (Graphpad). All bar graphs display mean ± SD unless otherwise noted. Statistical significance was determined by 1-way ANOVA (Analysis of Variance) followed by Tukey's post-test. Level of significance is denoted as follows: * $P<0.05$, ** $P<0.01$, *** $P<0.001$ and **** $P<0.0001$.

RESULTS

RBL mast cells synthesize and secrete IL-4 and TNFα in response to antigen stimulation.

IL-4 is synthesized as a soluble molecule, whereas TNFα is synthesized as a type II transmembrane protein and later cleaved. We hypothesized that these differences in synthesis would result in differential biosynthetic trafficking, therefore we chose to compare IL-4 and TNFα secretion upon antigen stimulation. Figure 4.1 shows secretion of each cytokine in response to antigen stimulation. For IL-4, secretion starts two hours after receptor cross-linking and continues to occur for at least 4 to 8 hours (Figure 4.1A). In contrast, the majority of TNFα secretion occurs on a slightly accelerated timescale, and most of the secretion occurs within two hours of stimulation

at considerably lower levels than IL-4 (Figure 4.1B). Results may suggest that the kinetic differences in secretion of these two cytokines are due to differential biosynthetic trafficking, but we cannot exclude the possibility that the regulation is occurring at the level of transcription or translation.

To assess the intracellular pathway for IL-4 prior to secretion, we used immunofluorescence confocal microscopy. In the absence of stimulation, we see no cytokine label in these cells. Following stimulation by multivalent antigen we detect IL-4 in a subset (<10%) of RBL cells (Figure 4.2, left panels). We observe some colocalization with GM130 labeling in cis-Golgi (Figure 4.2B), as one might expect for a protein traveling the biosynthetic pathway following gene transcription and protein translation. Furthermore, this label is partially coincident with CTxB marking RE (Figure 4.2A), suggesting, in agreement with other studies [6, 9], that RE may play a role in cytokine secretion. In contrast, these cytokines show no overlap with lysosomal marker CD63 (Figure 4.2C), indicating that is not likely that they are exported via secretory lysosomes. We see similar sub-cellular distribution of another cytokine, IL-3β (Figure 4D-F). We attempted to look at TNFα synthesis following antigen stimulation in RBL cells by microscopy but were unable to find an antibody that labeled under standard fixation and labeling protocols. We conclude that cytokine production is largely due to new synthesis, not preformed stores, and our data suggest that IL-4 follows a biosynthetic pathway that takes it through the Golgi complex and RE, but not via secretory lysosomes.

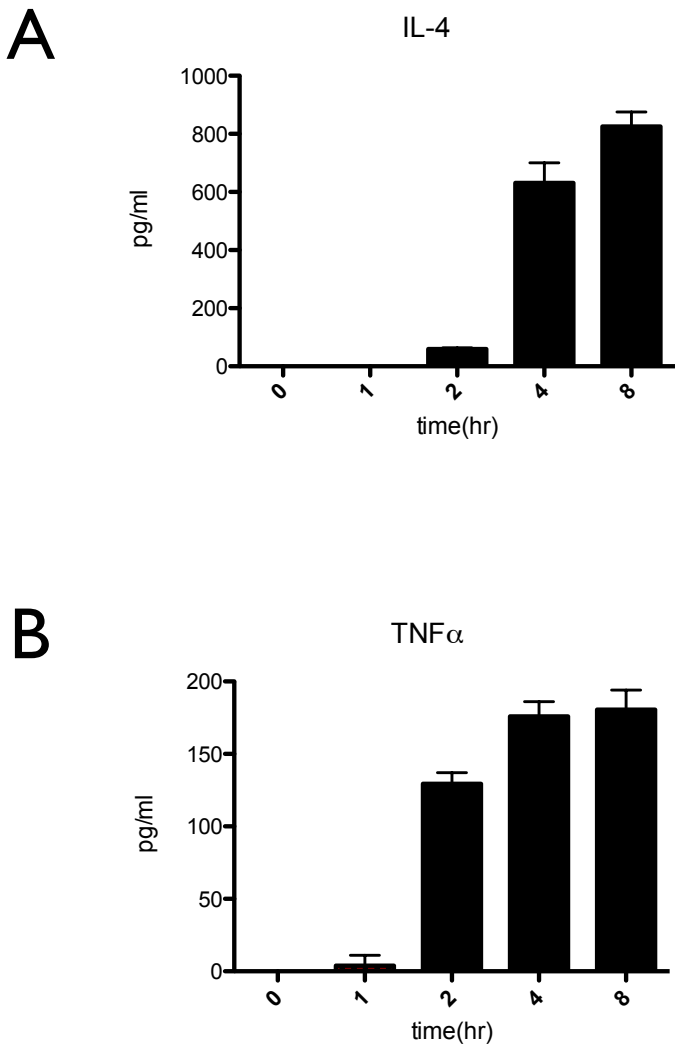

Figure 4.1. RBL mast cells secrete newly synthesized IL-4 and TNFα following antigen stimulation. Histograms show representative ELISA measurements of (A) IL-4 and (B) TNFα secretion following stimulation with DNP-BSA. Error bars represent SD.

Figure 4.2. Newly synthesized IL-4 is detected in the perinuclear RE/golgi region following antigen stimulation. Confocal microscopy images of RBL cells fixed 3 hours post stimulation show relative overlap with (A) Alexa 555-CTxB (recycling endosomes, red), (B) anti-GM-130 (Golgi, red) or (C) anti-CD63 (lysosome, red). In all cases, IL-4 is immuno-labeled (green). IL-3β is also synthesized in response to antigen stimulation in RBL mast cells. Confocal microscopy images show relative overlap with (D) Alexa 555-CTxB (RE, red), (E) anti-GM-130 (golgi, red) or (F) anti-CD63 (lysosome, red). In all cases, IL-3β is immuno-labeled (green). Scale bar is 10 μm.

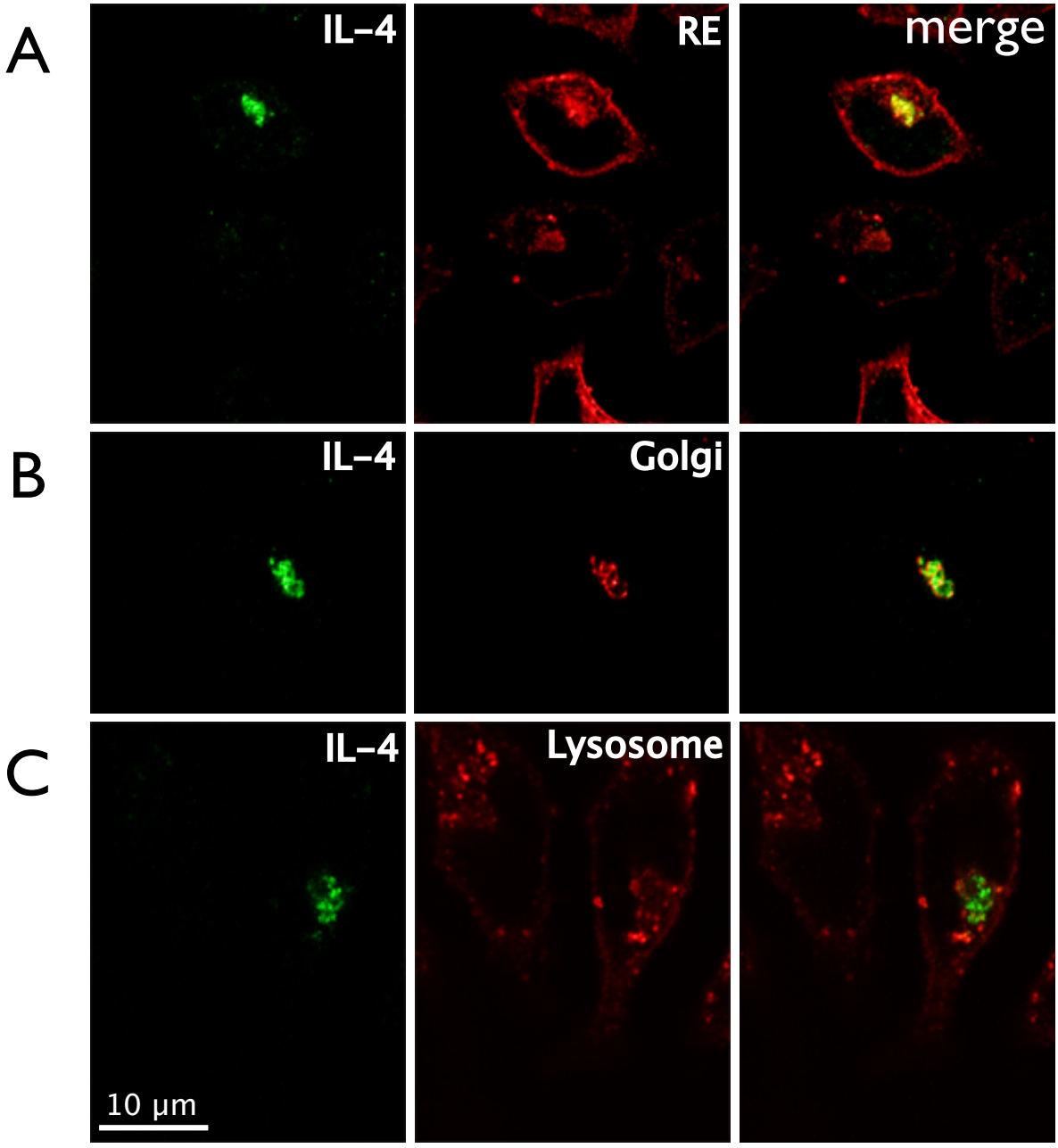
A
IL-4
RE
merge
B
IL-4
Golgi
C
IL-4
Lysosome
10 μm

Figure 4.2. (continued)

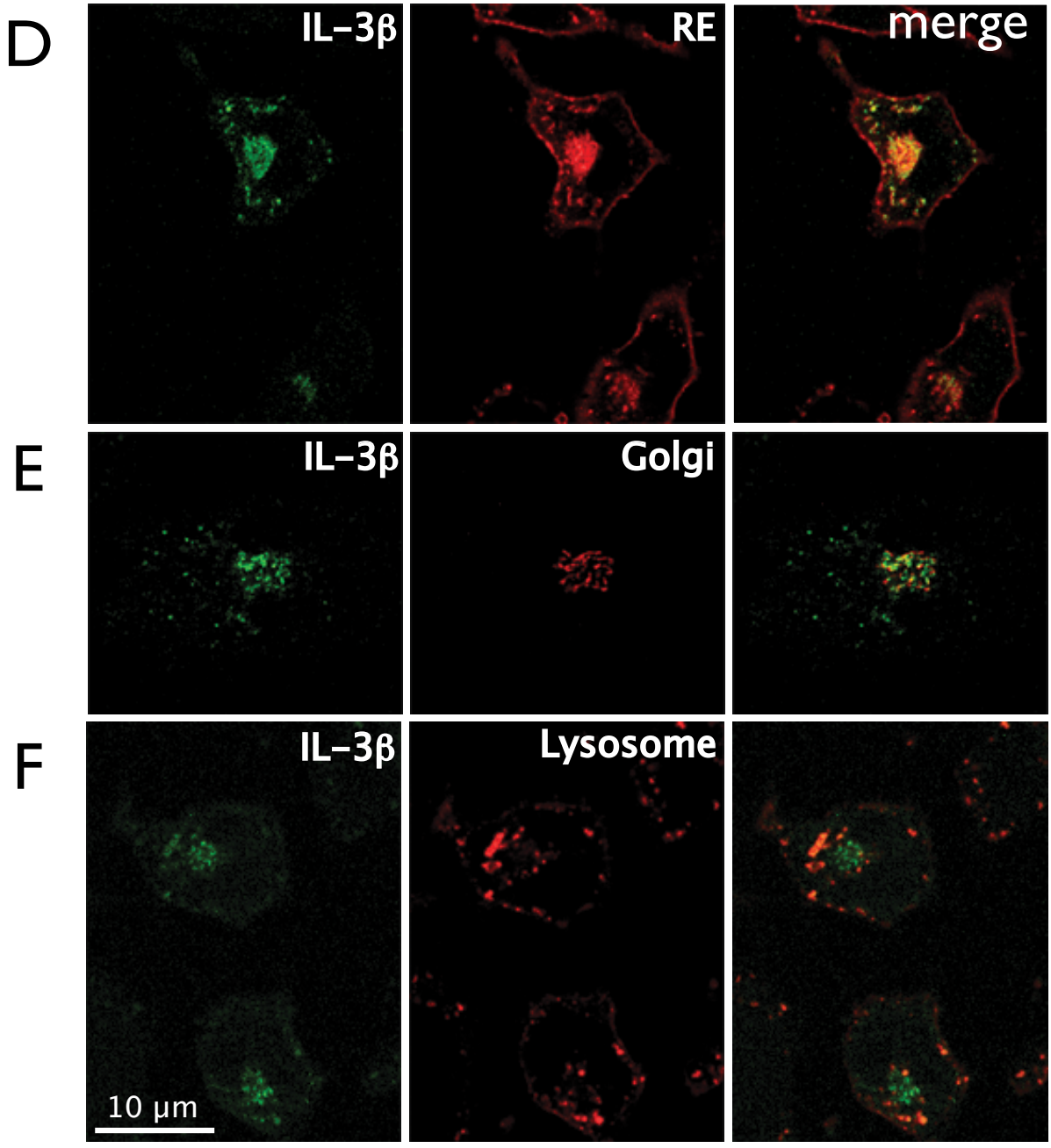

Pharmacologic Inhibitors reveal temporal requirements for PI3 kinases and PKC in cytokine secretion.

To begin to determine requirements for cytokine secretion resulting from signaling through the IgE/FcεRI receptor system, we used a variety of known inhibitors of key signaling components. Treatment with the Src-family kinase inhibitor, PPI, prior to antigen stimulation blocks cytokine secretion (data not shown), consistent with phosphorylation of FcεRI by Lyn kinase as a necessary signal. Treatment with either 200 nM wortmannin, a dose that specifically inhibits PI3 kinases, or with the PKC inhibitor bisindolyl maleimide (BIM; 100 μM) prior to receptor engagement also results in nearly complete abrogation of IL-4 secretion (Figure 4.3, BIM Pre and wortmannin Pre). These results indicate that the early signaling steps involving PI3 kinase and PKC, which are likewise important for RBL mast cell degranulation, are also important for cytokine secretion. A possible explanation is that these kinases are necessary for the initiation of gene transcription of cytokines. To address this issue, we added these inhibitors one hour after the addition of antigen to allow for the initiation gene transcription. Under this condition, IL-4 secretion occurs, but PKC inhibition still results in significant reduction of IL-4 secretion (Figure 4.3, BIM Post). We observe similar trends in TNFα secretion (data not shown), although the quantity of TNFα secreted under these conditions approaches the lower detection limits of our ELISA, precluding robust data analysis. These results suggest that following the initiation of signal transduction, inhibition of these kinases has little or no effect on cytokine secretion,

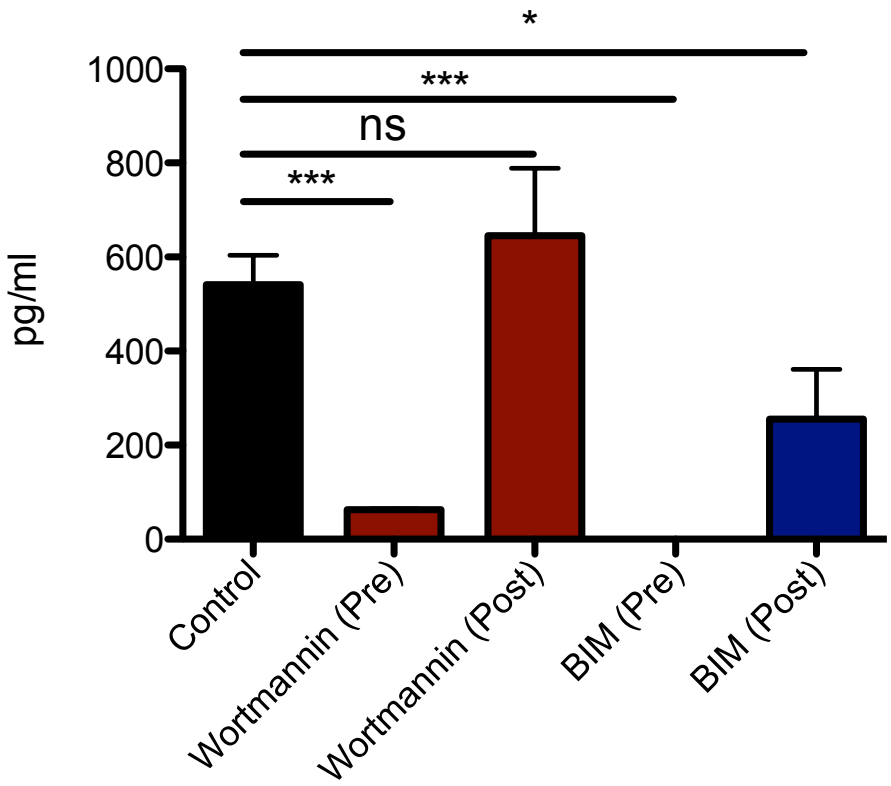

Figure 4.3. Pharmacological manipulation of IL-4 secretion reveals early requirement for PI3K and PKC activity. Representative ELISA measurements showing the effects of 200 nM wortmannin (brown) and 100 uM bis-indolyl maleimide (BIM, blue) added either just prior to (Pre) or 1 hour after (Post) antigen stimulation. All supernatant samples collected 4 hours post stimulation. Error bars represent SD, * denotes $p< 0.05$ and *** denotes $p<0.001$.

indicating that PI3 kinases and PKC are not essential for the biosynthetic export of these cytokines.

Blocking actin polymerization selectively enhances cytokine secretion.

Cytochalasin D blocks actin polymerization by binding monomeric G actin, thereby preventing filament formation. It is known that treating RBL cells with cytochalasin D enhances FcεRI receptor tyrosine phosphorylation [16], degranulation [17], and stimulated recycling endosomal trafficking [18]. In the context of IL-4 secretion, we find that either cytochalasin D pre-treatment (Figure 4.4A, white bars) or addition following antigen stimulation (Figure 4.4A, green bars) robustly enhances secretion. Similarly, pre-treatment with cytochalasin D significantly enhances secretion of TNFα at two and four hours post stimulation (Figure 4.4B, white bars). However, when cytochalasin D is added after the initiation of signaling, there are no significant changes in TNFα secretion at either timepoint (Figure 4.4B. green bars). That cytochalasin D added after the initiation of signaling shows differential effects on IL-4 and TNFα secretion suggests that actin dynamics differentially affects exocytosis of these two cytokines.

Rab11A siRNA knockdown modestly enhances cytokine secretion.

Our initial interest in the regulation of cytokine secretion was prompted by the possible involvement of RE trafficking in cytokine secretion [6]. Rab11A is a GTPase known to be involved in the regulation of transferrin (TfR) receptor trafficking via RE [19]. Therefore, we used RNA interference (RNAi) techniques to probe the involvement

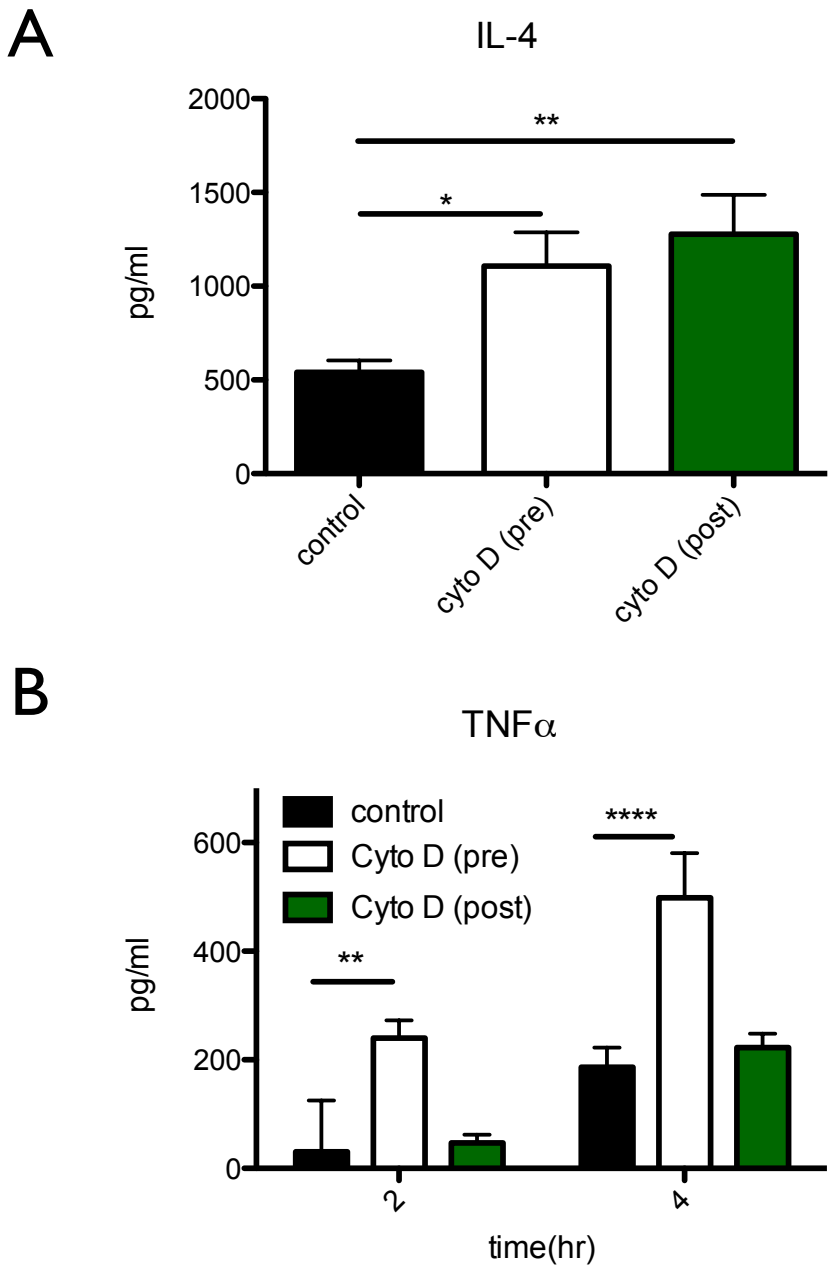

Figure 4.4. Addition of cytochalasin D either before or after antigen stimulation enhances IL-4 secretion, while only pretreatment enhances TNFα secretion. Representative IL-4(A) and TNFα (B) ELISA measurements of antigen-stimulated RBL cells pretreated (pre, white) or following antigen stimulation (1 hour) (post, green) with cytochalasin D (Cyto D). For IL-4 treatments, samples were collected 4 hours after stimulation. Error bars represent SD, * denotes $p<0.05$, * denotes $p<0.01$ and **** denotes $p<0.0001$.

of Rab11A in RBL cell cytokine secretion. Figure 4.5A demonstrates that we were able to use two different siRNA sequences (see Material and Methods) and get efficient knockdown of Rab11A protein. When these cells were used in cytokine secretion assays, we see that both IL-4 (Figure 4.5B) and TNFα (Figure 4.5C) secretion are modestly enhanced by Rab11A knockdown. This enhancement is slightly more pronounced for TNFα secretion. Consistent with these results, antigen-stimulated RE trafficking monitored using FITC-CTxB is modestly enhanced in siRNA treated cells (Figure4.5D). The enhancement may be partially explained by a modest acceleration in the growth rate of siRNA treated cells (data not shown).

Characterization of GFP-TNFα construct and RE inactivation assays.

Our results are consistent with a role for RE in cytokine secretion in that treatments that modulate RE trafficking also modulate cytokine secretion, but additional work is needed to confirm the involvement of this organelle in cytokine secretion. To this end, we generated a GFP-TNFα construct (see schematic in Figure 4.6A) for use in live microscopy experiments. When this construct is expressed in RBL cells, it is generally localized at the plasma membrane and to small vesicular structures throughout the cytoplasm, perhaps with some peri-nuclear localization (Figure 4.6, left panels). In some cells, we can see partial localization with RE markers CTxB (Figure 4.6B) and TfR (Figure 4.6C). Additionally, it is excluded from the Golgi complex (Figure 4.6D).

Another useful technique we have begun to utilize is specific inhibition of RE trafficking by chemically inactivating RE. This is a method developed in the laboratory of

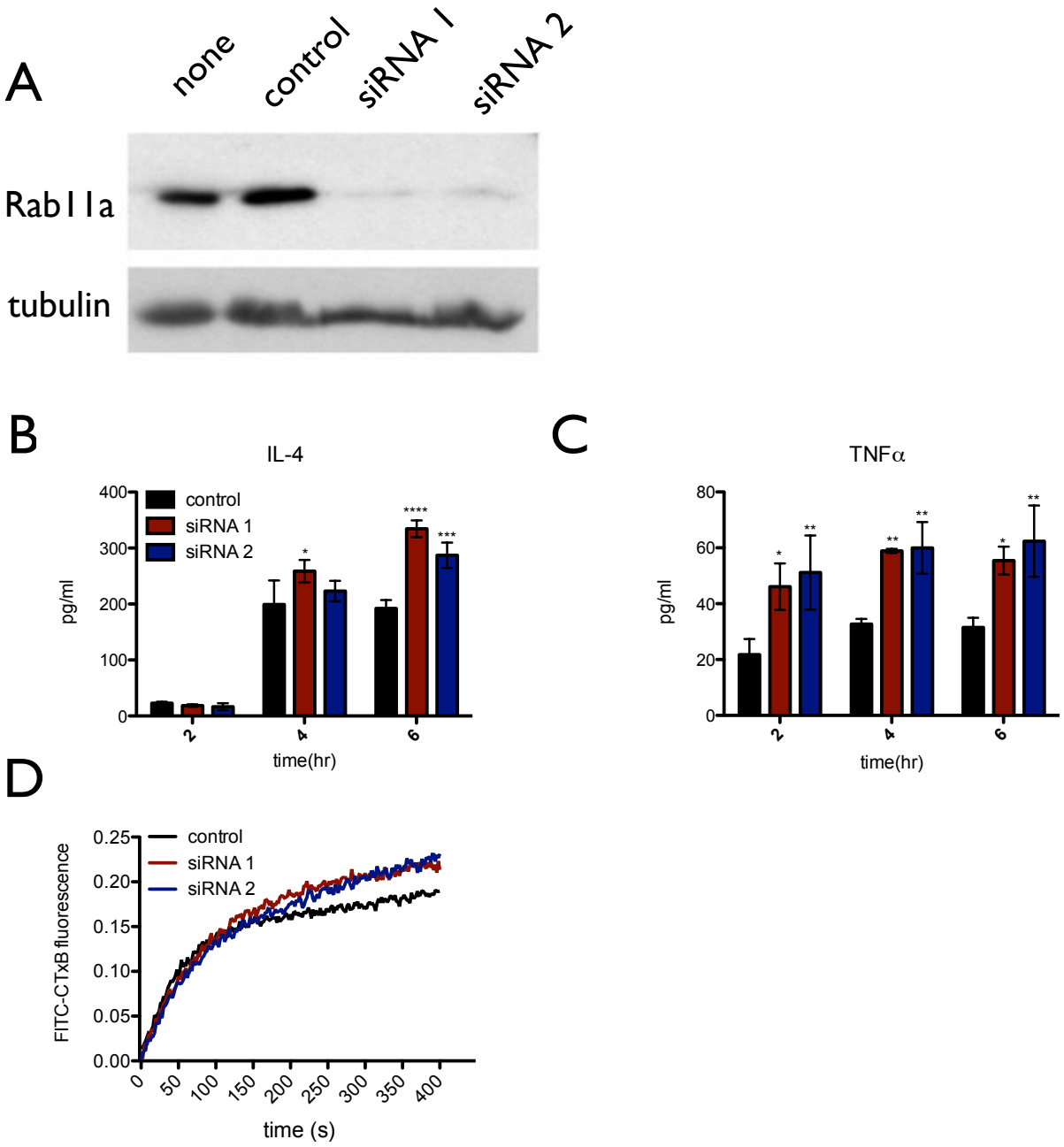

Figure 4.5. Rab11A knockdown potentiates cytokine secretion. (A) Western blotting shows the efficiency of siRNA knockdown of endogenous Rab11A by two different siRNA sequences, 1 and 2, compared to cells transfected with either nothing (none) or a control siRNA sequence (control). (B) Representative ELISA measurements comparing IL-4 secretion in control siRNA (black), siRNA 1 (red) or siRNA 2 (blue). (C) TNFα secretion in parallel samples. (D) Plot of antigen mediated RE trafficking in Rab11A knockdown cells (representative of 2 experiments). Error bars represent SD, * denotes $p<0.05$, ** denotes $p<0.01$, *** denotes $p<0.001$ and **** denotes $p<0.0001$.

Figure 4.6. Initial GFP-TNFα construct characterization by confocal microscopy. (A) Schematic of construct. (B) Two representative images of GFP-TNFα (green) showing relative overlap with RE labeled by Alexa555-CTxB. (C) representative images showing extent of GFP-TNFα colocalization with TfR or GM-130 immunolabeled with primary antibodies followed with Alexa555 secondary antibodies.

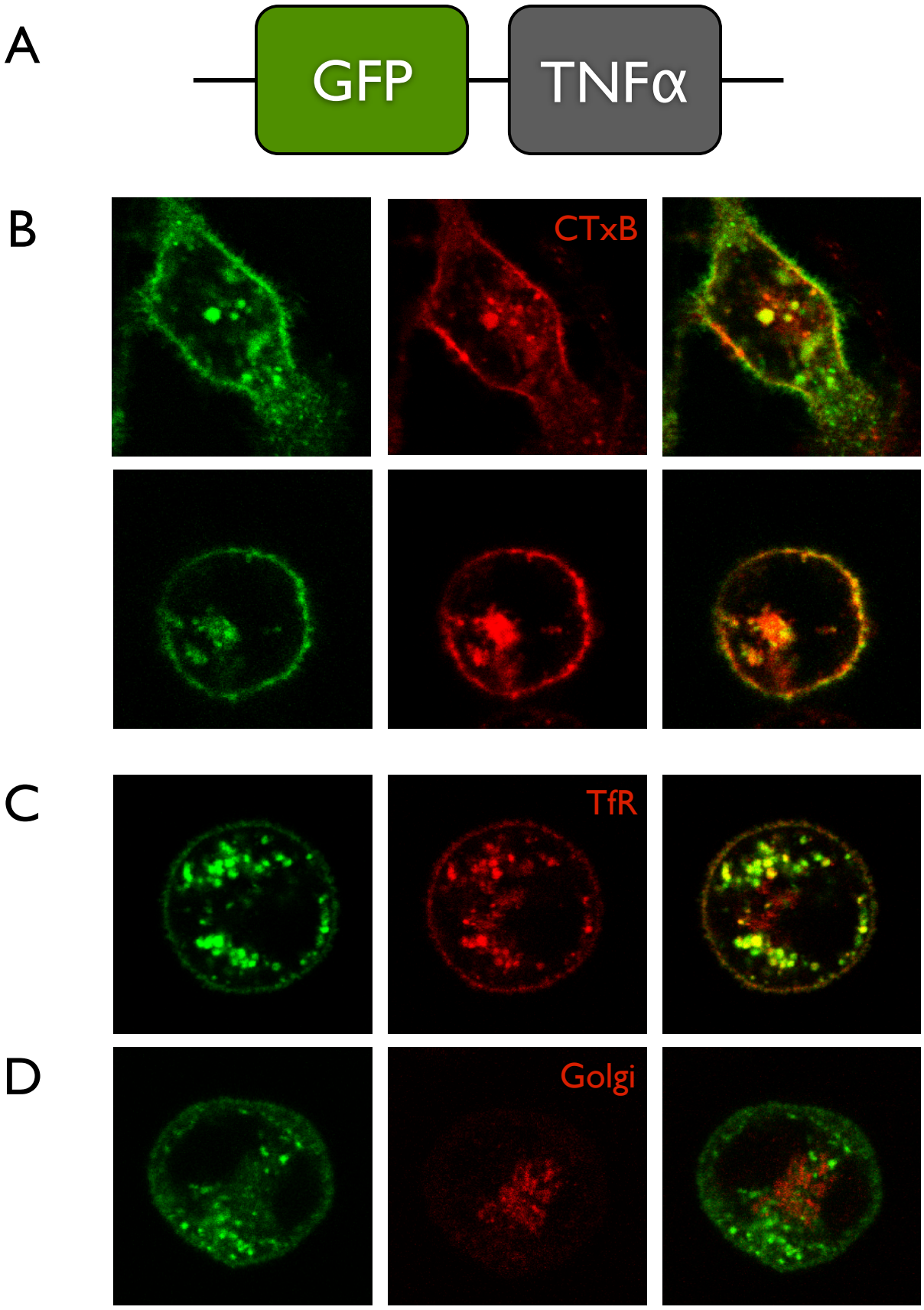
A
GFP
TNFα
B
CTxB
C
TfR
D
Golgi

I. Mellman [14] and subsequently used by Manderson et al. [7]. RE are specifically inactivated by targeting horseradish peroxidase (HRP)-conjugated transferrin to the RE, followed by an HRP-mediated oxidation process that renders the RE non-functional. Figure 4.7 demonstrates that this approach can be used to reduce antigen-stimulated outward trafficking of FITC-CTxB labeled RE. It will be interesting to see if this treatment reduces cytokine secretion in response to antigen signaling.

DISCUSSION

The versatile nature of mast cells is often underappreciated. While most common symptoms of allergies are caused by mast cell secretion of histamine, mast cells also secrete cytokines that attract multiple immune effector cells. In allergic responses, this can lead to additional inflammatory responses and extensive tissue remodeling. Furthermore, it is also established that mast cells can contribute to the initiation of important host defense to pathogens, primarily through the secretion of cytokines. Determining the intracellular mechanisms that regulate cytokine secretion in mast cells is important for both situations: Understanding how/if regulated cytokine secretion occurs has important implications for limiting allergic disease and for generating effective immune responses that may be mediated through mast cells.

Murray et al., demonstrated TNFα secretion via RE in macrophages [6]. This result prompted us to hypothesize that mast cells might use a similar mechanism to regulate secretion. Our studies confirmed that IgE/FcεRI signaling in RBL mast cells triggers the production and secretion of cytokines IL-4 and TNFα. Furthermore,

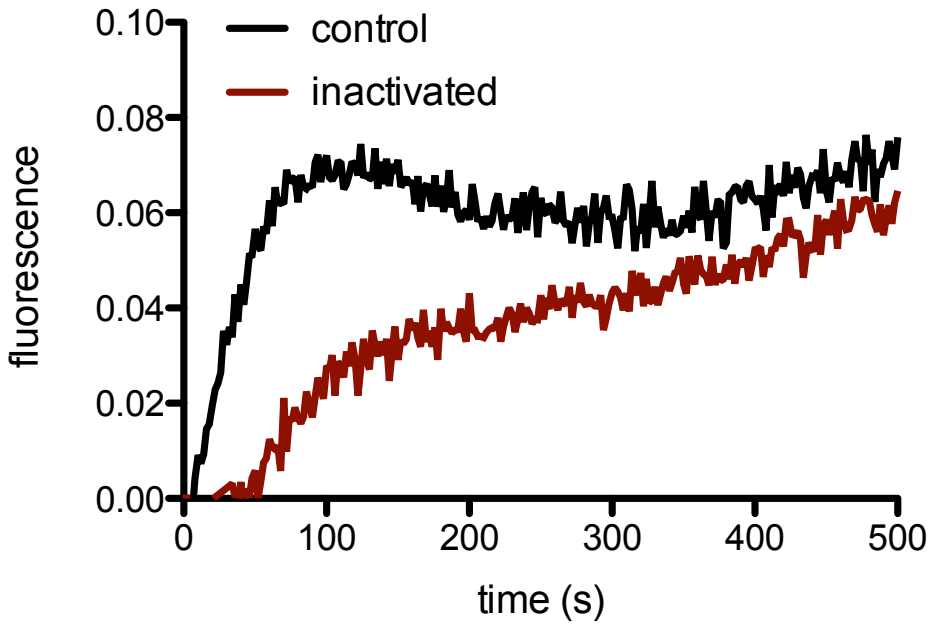

Figure 4.7. Antigen-stimulated RE trafficking is reduced by chemical inactivation of RE. Figure shows representative FITC-CTxB trafficking in response to antigen in control (black) or diaminobenzidine (DAB)-peroxidase inactivated (red) RBL cells.

secretion of IL-4 and TNFα is not synchronous, suggesting possible differences in the regulated secretion of these two cytokines. Similarly, in macrophages, IL-6 and TNFα reside in different subcompartments of the RE prior to secretion [7]. In RBL mast cells we detect colocalization of newly synthesized IL-4 with the RE marker CTxB, suggesting that RE contribute to intracellular cytokine trafficking.

To distinguish between factors necessary for activation of transcription and secretion, we added pharmacological inhibitors either prior to antigen stimulation or after one hour, at which time gene transcription should have been induced [20]. Our pharmacological studies with wortmannin and BIM demonstrate that IL-4 has similar requirements for PI3 kinase and PKC activity for gene transcription as has been previously demonstrated for TNFα [21, 22]. Interestingly, our experiments exploring the effects of cytochalasin D demonstrate that the secretion of IL-4 and TNFα are differentially sensitive to actin depolymerization. Our results support the hypothesis that the secretion of IL-4 is generally negatively regulated by the actin cytoskeleton, whereas TNFα secretion per se is not regulated by this mechanism.

Rab11 is a known regulator of RE trafficking, as overexpression of dominant negative Rab11 retards RE processes [19]. We hypothesized that siRNA-mediated knockdown of Rab11A would delay or reduce secretion of IL-4 and/or TNFα. To our surprise, Rab11A knockdown enhanced the secretion of both cytokines. A possible explanation for this is that the RE is composes of different subpopulations are known to be regulated by different GTPases, particularly Rab11 and Arf6. If, in fact, Arf6 regulates cytokine secretion, one would expect Rab11A knockdown to have either little or a

compensatory enhancing effect [23]. In the future, additional knockdown studies that systematically reduce expression of these regulatory GTPases, alone or in combination, may be instructive. Alternatively we could use dominant negative or constitutively active mutant forms of Rab11 and Arf6, known to alter RE trafficking [19, 24].

Visualizing TNFα by immunofluorescence proved to be technically challenging. To circumvent this issue we constructed a GPF-TNFα construct using rat cDNA for TNFα. Functionally we expect this construct to be similar to that used by Stowe and colleagues [6, 7, 25]. Initial characterizations show some RE localization during steady state expression. A fluorescently tagged TNFα construct opens the possibility of looking at live trafficking processes. In particular, utilizing this construct in conjunction with a patterned antigen surface [10, 26, 27] we could probe the possibility of directional TNFα trafficking in mast cells. Additionally, using cycloheximide to block new protein synthesis may help us more directly address issues of cytokine trafficking.

RE trafficking in RBL mast cells has proven to be relatively insensitive to inhibition of PKC or PI3 kinases [18], and future studies into cytokine secretion and RE trafficking in RBL cells would benefit from additional methods to interfere with theses processes. To this end we have begun to utilize a method to chemically inactivate the RE [14]. Preliminary experiments demonstrate that antigen-stimulated RE trafficking is at least partially sensitive to RE inactivation. This is in contrast to our results showing that Rab11A knockdown does not effect RE trafficking. Together these results support the hypothesis that the RE is, in fact, a heterogeneous organelle that has differential regulation [23]. Our initial research into the involvement of RE in mast cell cytokine

secretion has raised new questions, but these new tools should facilitate our ongoing investigation of these mechanisms.

CONTRIBUTIONS AND ACKNOWLEDGEMENTS

Research designed by N. L. Smith, D. A. Holowka and B. A. Baird; N. L. Smith performed and analyzed experiments; N. L. Smith and A. Wagenknecht-Wiesner generated GFP-TNFα construct. Research supported by National Institutes of Heath Grants R01 AI022449 (B. A. Baird and D. A. Holowka).

We thank Ms. Carol Bayles for maintaining the Cornell Microscopy and Imaging Facility.

REFERENCES

1. Metcalfe, D.D., D. Baram, and Y.A. Mekori, *Mast cells.* Physiol Rev, 1997. **77**(4): p. 1033-79.

2. Marshall, J.S., *Mast-cell responses to pathogens.* Nat Rev Immunol, 2004. **4**(10): p. 787-99.

3. McCurdy, J.D., T.J. Lin, and J.S. Marshall, *Toll-like receptor 4-mediated activation of murine mast cells.* J Leukoc Biol, 2001. **70**(6): p. 977-84.

4. Grimbaldeston, M.A., et al., *Mast cell-derived interleukin 10 limits skin pathology in contact dermatitis and chronic irradiation with ultraviolet B.* Nat Immunol, 2007. **8**(10): p. 1095-104.

5. Stow, J.L., et al., *Cytokine secretion in macrophages and other cells: pathways and mediators.* Immunobiology, 2009. **214**(7): p. 601-12.

6. Murray, R.Z., et al., *A role for the phagosome in cytokine secretion.* Science, 2005. **310**(5753): p. 1492-5.

7. Manderson, A.P., et al., *Subcompartments of the macrophage recycling endosome direct the differential secretion of IL-6 and TNFalpha.* J Cell Biol, 2007. **178**(1): p. 57-69.

8. Huse, M., et al., *T cells use two directionally distinct pathways for cytokine secretion.* Nat Immunol, 2006. **7**(3): p. 247-55.

9. Reefman, E., et al., *Cytokine secretion is distinct from secretion of cytotoxic granules in NK cells.* J Immunol, 2010. **184**(9): p. 4852-62.

10. Wu, M., et al., *Differential targeting of secretory lysosomes and recycling endosomes in mast cells revealed by patterned antigen arrays.* J Cell Sci, 2007. **120**(Pt 17): p. 3147-54.

11. Posner, R.G., et al., *Aggregation of IgE-receptor complexes on rat basophilic leukemia cells does not change the intrinsic affinity but can alter the kinetics of the ligand-IgE interaction.* Biochemistry, 1992. **31**(23): p. 5350-6.

12. Gidwani, A., et al., *Disruption of lipid order by short-chain ceramides correlates with inhibition of phospholipase D and downstream signaling by FcepsilonRI.* J Cell Sci, 2003. **116**(Pt 15): p. 3177-87.

13. Gosse, J.A., et al., *Transmembrane sequences are determinants of immunoreceptor signaling.* J Immunol, 2005. **175**(4): p. 2123-31.

14. Ang, A.L., et al., *Recycling endosomes can serve as intermediates during transport from the Golgi to the plasma membrane of MDCK cells.* J Cell Biol, 2004. **167**(3): p. 531-43.

15. Smith, N.L., et al., *Sphingosine derivatives inhibit cell signaling by electrostatically neutralizing polyphosphoinositides at the plasma membrane.* Self Nonself, 2010. **1**(2): p. 133-143.

16. Holowka, D., E.D. Sheets, and B. Baird, *Interactions between Fc(epsilon)RI and lipid raft components are regulated by the actin cytoskeleton.* J Cell Sci, 2000. **113 (Pt 6)**: p. 1009-19.

17. Frigeri, L. and J.R. Apgar, *The role of actin microfilaments in the down-regulation of the degranulation response in RBL-2H3 mast cells.* J Immunol, 1999. **162**(4): p. 2243-50.

18. Naal, R.M., et al., *Antigen-stimulated trafficking from the recycling compartment to the plasma membrane in RBL mast cells.* Traffic, 2003. **4**(3): p. 190-200.

19. Ullrich, O., et al., *Rab11 regulates recycling through the pericentriolar recycling endosome.* J Cell Biol, 1996. **135**(4): p. 913-24.

20. Hide, I., et al., *Suppression of TNF-alpha secretion by azelastine in a rat mast (RBL-2H3) cell line: evidence for differential regulation of TNF-alpha release, transcription, and degranulation.* J Immunol, 1997. **159**(6): p. 2932-40.

21. Baumgartner, R.A., et al., *Secretion of TNF from a rat mast cell line is a brefeldin A-sensitive and a calcium/protein kinase C-regulated process.* J Immunol, 1994. **153**(6): p. 2609-17.

22. Pelletier, C., et al., *Specific signaling pathways in the regulation of TNF-alpha mRNA synthesis and TNF-alpha secretion in RBL-2H3 mast cells stimulated through the high affinity IgE receptor.* Inflamm Res, 1998. **47**(12): p. 493-500.

23. Balasubramanian, N., et al., *Arf6 and microtubules in adhesion-dependent trafficking of lipid rafts.* Nat Cell Biol, 2007. **9**(12): p. 1381-91.

24. D'Souza-Schorey, C., et al., *ARF6 targets recycling vesicles to the plasma membrane: insights from an ultrastructural investigation.* J Cell Biol, 1998. **140**(3): p. 603-16.

25. Kay, J.G., et al., *Cytokine secretion via cholesterol-rich lipid raft-associated SNAREs at the phagocytic cup.* J Biol Chem, 2006. **281**(17): p. 11949-54.

26. Torres, A.J., D. Holowka, and B.A. Baird, *Micropatterned Ligand Arrays to Study Spatial Regulation in Fc Receptor Signaling.* Methods Mol Biol, 2011. **748**: p. 195-207.

27. Torres, A.J., et al., *Focal adhesion proteins connect IgE receptors to the cytoskeleton as revealed by micropatterned ligand arrays.* Proc Natl Acad Sci U S A, 2008. **105**(45): p. 17238-44.

CHAPTER FIVE

Recycling Endosomal Membranes Contribute to *Toxoplasma gondii* Parasitophorous Vacuole Formation in Mast Cells

SUMMARY

Toxoplasma gondii is an obligate intracellular parasite that resides within a specialized organelle known as the parasitophorous vacuole (PV) in the host cell. *T. gondii* is a ubiquitous pathogen, infecting most mammalian and avian species, and is the causative agent of Toxoplasmosis. Determining how *T. gondii* utilizes the host cell membranes in the formation and remodeling of the PV membrane (PVM) will provide important information in understanding how productive infections are established. Initially, *T. gondii* forms the PV from plasma membrane (PM) as the parasite invades a host cell. However, it is not completely clear how the PVM is maintained and/or remodeled following initial infection. The recycling endosome (RE) is now appreciated as a complex organelle that contributes to multiple trafficking processes in many cell types and, in particular, has been shown to play a role in cellular processes that require extensive membrane remodeling such as migration and cell division. In RBL mast cells, we previously established that cholera toxin B (CTxB) bound to the ganglioside GM_1 localizes to RE membranes upon internalization, and antigen stimulation via IgE/FcεRI receptor complexes results in stimulated outward trafficking of the RE [1]. We provide evidence that RE membranes contribute to the PVM of *T. gondii* using RBL mast cells as a model system. Compared to conditions in which GM_1 labeling by CTxB is restricted to the PM, labeling of the RE pool of GM_1 enhances the accumulation of CTxB label in the PVM during the first hour following invasion. Furthermore, this preferential

labeling at the PVM by RE-derived membranes is observed in several different cell types. Additionally, we provide evidence that other recycling endosomal markers localize at the PVM. Collectively, these results show for the first time that RE contribute to nascent PV of *T. gondii*.

INTRODUCTION

The success of intracellular pathogens is dependent on their capacity to interact with the host cell in such a way that minimizes or controls immune recognition and maximizes survival and proliferative capacity. *Toxoplasma gondii*, like most apicomplexan parasites, meets this requirement by residing within a parasitophorous vacuole (PV), a specialized organelle from which the parasite can gain nutrients from the host cell while generally evading host recognition and degradation [2]. The nascent PV is formed as the *T. gondii* tachyzoite invades the cell, through a highly coordinated mechanism involving the formation of a moving junction containing parasite-derived proteins that are secreted by two specialized organelles, micronemes and the roptries [3]. This moving junction anchors at the host plasma membrane (PM) [4], via an unknown receptor or recognition motif, and facilitates parasite entry in such way that most plasma membrane proteins are excluded from the PM that makes up the nascent PV [5]. The PV membrane (PVM) is largely devoid of integral plasma membrane proteins, but contains host-derived glycophosphatidylinositol (GPI)- linked proteins and gangliosides in addition to various lipid species [6].

As an obligate organism, *T. gondii* scavenges various materials essential to its survival. *T.gondii* is known to be auxotrophic for multiple metabolites, including the amino acids tryptophan [7] and arginine [8]. Additionally, It has been established that parasites acquire needed cholesterol by taking advantage of a host pathway that utilizes endocytosed low-density lipoprotein (LDL) to provide cholesterol [9]. Intracellular parasites have also been shown to form tight associations with both host mitochondria and endoplasmic reticulum (ER) [2], and it has been hypothesized that these associations provide access to the necessary lipids and membrane for maintenance of the PVM.

An organelle known to be a large reservoir of lipids is the recycling endosomal complex (RE). The RE is a mildy acidic, tubulovesicular membrane pool that is distinct from the traditional endo-lysosomal pathway that often has a peri-nuclear localization, although this is cell type-dependent. This organelle acts as a junction where cargo and membrane from both sorting endosomes and the Golgi apparatus traffic before continuing to the cell surface or undergoing retrograde transport back to the Golgi complex [10]. Traditional markers of the RE include the plasma membrane constituents such as the transferrin receptor (TfR) [11, 12] and the ganglioside GM_1 [1]. In recent years, a body of evidence has grown to suggest that the RE is a heterogenous pool with multiple trafficking routes under the regulatory control of various proteins including the small GTPases Rab 11 [13] and Arf 6 [14]and the SNARE proteins VAMP 3 [15]. Interestingly, increased and directional trafficking of recycling endosomes is often seen

in membrane intensive cellular processes such as cytokinesis [16], migration [17, 18] and phagocyotis [15].

The establishment of the PV and its subsequent growth during parasite replication necessitate the acquisition of large amounts host derived membrane. We sought to determine if the host RE contributes to the PVM during the early stages of PV development. RBL-2H3 mast cells are a useful model system for studying processes involving RE [1, 19]: they have a morphologically discrete peri-nuclear RE compartment and recycling rates that are useful for experimental observation and manipulation. Through live cell and fixed cell confocal microscopy, we found evidence that the RE does contributes significantly to the nascent PVM.

MATERIALS AND METHODS

Chemicals, Reagents and DNA Plasmids.

Alexa488-cholera toxin B (A488-CTxB) was purchased from Invitrogen and FITC-CTxB was purchased from Sigma/Aldrich. Unless otherwise noted, all other chemicals were purchase from Sigma/Aldrich, and all tissue culture reagents were purchased from Invitrogen. Anti-DNP IgE was purified as described previously [20] and conjugated with Alexa488 succinimydl ester (Invitrogen).

The following DNA plasmids were used in the course of our study: Lyn-EGFP [21], PM-EGFP [22], PH-PLCδ-EGFP [23], PH-Akt-EGFP [24], and TfR-pHlorin[25].

Cells and Parasites

RBL-2H3 Culture

RBL-2H3 mast cells were grown in monolayer culture and harvested as previously described [26].

Rat Bone Marrow-Derived Mast Cells (rBMMCs)

rBMMCs were isolated as previously described [27]. Briefly, bone marrow stem cells isolated from 6-10 wk Lewis rat femurs were washed in Hanks buffered saline and cultured in DMEM with horse serum (20%), gentamicin sulfate (50 μg/ml), penicillin (100 U/ml), streptomycin (100 μg/ml) and L-glutamine (4 mM). Additionally media was supplemented with the growth factors IL-3β (10 U/ml) and GM-CSF (50 ng/ml). The cell population becomes over 90% pure after 10-14 days in culture, as assayed by Alcian blue staining. All rBMMCS were used between days 14-28 of culture.

Mouse Bone Marrow-Derived Macrophages (BMMϕs) and Dendritic Cells (BMDCs)

C57BL/6 mice were purchased from either The Jackson Laboratory (Bar Harbor, ME) or Taconic Farms (Germantown, NY) and used between 6-8 weeks of age. All mice were maintained in the Transgenic Mouse Core Facility at the Cornell University College of Veterinary Medicine, accredited by American Association of Accrediation of Laboratory Animal Care. BMMϕs were isolated as described previously [28]. Briefly, bone marrow-isolated from femurs was cultured in macrophage media (DMEM containing fetal calf serum (10 %)(Hyclone), sodium pyruvate (1mM), nonessential

amino acids (0.1 mM), L929 cell supernatant (20%), pencillin (100 U/ml) and streptomycin (100 μg/ml)). Media was changed on day 3, and cells were used on day 5 after nonadherent cells were removed. BMDCs were isolated as described previously [29]. Briefly, bone marrow from femurs were cultured in dendritic cell media (RPMI containing fetal calf serum (10%), penicillin (100 U/ml), streptomycin (100 μl/ml) and GM-CSF (20 ng/ml). Media was changed on days 3 and 6 post bone marrow collection, and BMDCs were used on day 9.

Parasites

RH-tomato, which have been engineered to express the tomato fluorescent protein, (generated by Dr. B. Striepen (University of Georgia) and kindly provided by Dr. E. Robey (University of California, Berkeley)) and RH strain tachyziotes were used in this study. Tachyzoites were maintained in vitro via passage through human foreskin fibroblast cultures in DMEM with FCS (1%), penicillin (100 U/ml) and streptomycin (100 μg/ml). Prior to use, tachyzoites were passed through a 3 μm track-etched membrane filter (Whatman) to remove fibroblast debris. Infections in all cell types were synchronized by brief centrifugation (200xg for 4 minutes) at a multiplicity of infection of 10:1 unless otherwise indicated.

Transfections

Cells were sparsely plated (1-3x10^5/ml) on no. 1.5 coverslips or in 35 mm glass bottom dishes (MatTek). After overnight incubation, media was replaced by OPTIMEM and DNA constructs of interest were transfected using 2 μg DNA and 8 μl Fugene HD

(Roche Diagnostics) per ml media for 1 hour before addition of 1 ng/ml phorbol 12,13-dibutyrate for 3-5hr [30]. Samples were then washed into normal media and incubated 16-24 hours to allow for protein expression.

Confocal Fluorescence Microscopy

For live imaging, RBL-2H3 cells were plated at 2-3x10^5 cells per 35 mm glass bottom dish (MatTek). Following overnight culture, cells were washed into a buffered saline solution (BSS: 135 mM NaCl, 5 mM KCl, 1 mM $MgCl_2$, 1.8 mM $CaCl_2$, 5.6 mM glucose, 20 mM HEPES, pH 7.4, 1 mg/ml BSA). Cells were labeled with A488-CtxB as previously described [19]. RH-tomato tachyzoites were introduced as described above, and imaging was performed at 37°C on a SP5 confocal microscope (Leica).

Fixed cell imaging samples were prepared as follows. For experiments labeling GM_1, FITC-CTxB was added either 1.5-2 hrs prior to infection to label both plasma membrane and recycling endosomes or just prior to infection to label only the plasma membrane. Alexa-488 conjugated Anti-2,4-dinitrophenyl (DNP) IgE was used to label FcεRI receptors on RBL-2H3 cells. Following tachyzoite infection (less than 1 hour), coverslips were washed with BBS and fixed with 4% paraformaldehyde plus 0.1% glutaraldehyde in phosphate buffered saline (PBS; 10 minutes at room temperature). Excess fixative was quenched by 10 mg/ml BSA in PBS with 0.01% azide. For immuno-labeling, an anti-GRA7 antibody (gift from Dr. I. Coppens, John Hopkins University) was used followed by secondary labeling with Alexa-555 anti-rabbit IgG (Invitrogen). Coverslips were mounted on slides using Prolong Gold (Invitrogen) to minimize

photobleaching. Fixed samples were imaged on an SP2 confocal microscope (Leica). When scoring the PVM for host membrane accumulation, a parasite was considered positive if membrane label accumulation was observed around at least half of the parasite.

Live Cell Ca^{2+} Imaging

Single cells Ca^{2+} measurements in infected and control cells were conducted using Fluo-4 AM as described previously [31] on the Leica SP5 confocal system with an image acquisition rate of 1 Hz.

Statistical Analyses

Analyses were conducted using Prism Software (GraphPad). One-way ANOVA (Analysis of Variance) was performed followed by Tukey's post-test to assess statistical significance. P values less than 0.05 were considered significant.

RESULTS

Toxoplasma gondii rapidly sheds host GM_1 from the nascent parasitophorous vacuole in RBL-2H3 mast cells.

Although *T. gondii* displays a preference for certain cell types such as macrophages and dendritic cells *in vivo* [32, 33], they are capable of infecting a large variety of cells *in vitro,* and these are often used to probe parasite-host cell interactions [34]. We assessed the ability of tachyzoites to invade RBL mast cells by live confocal microscopy. As expected, due to their relative promiscuity in a variety of host cells, *T. gondii* actively invades RBL cells, and as early as 10 minutes after introduction of RH-

tomato tachyzoites to adherent cells by centrifugation, we readily see infection in large percentage of cells. After one hour, infection rates typically exceed 60%. Consistent with other cell types, invasion is rapid, the entire process taking tens of seconds (see below). Furthermore, the invasion and infection are productive as parasite replication and cell lysis are seen if infection is monitored for 24 hours (Figure 5.1B).

Residing within reside within the PV allows *Toxoplasma* to evade degradation by host cell lysosomes. The vacuolar membrane is largely devoid of plasma membrane proteins, and the formation of a parasite-mediated moving junction during invasion has been hypothesized to account for the controlled composition of the parasitophorous vacuolar membrane (PVM) [6, 35]. One host marker reported to populate the parasitophorous vacuole shortly after infection is the ganglioside GM_1 labeled by the B subunit of Cholera toxin (CTxB) [6]. At steady state, CTxB label in RBL cells populates both the plasma membrane and RE. As shown in Figure 5.1A and Movie M5.1, we find that during invasion in RBL cells plasma membrane-derived GM_1 is quickly lost from the parisitophorous vacuole shortly after parasite entry. This rapid disappearance of CTxB label suggests CTxB-labeled GM_1 seen previously in PVMs is not simply retained from the plasma membrane that surrounds the parasite as it invades.

Recycling endosomal membrane label surrounds intracellular tachyzoites.

In RBL cells, GM_1 populates both the plasma membrane and the peri-nuclear RE compartment [1, 19]. The RE serves as a reservoir of host membrane, and we hypothesized that membrane from this organelle might contribute to the forming

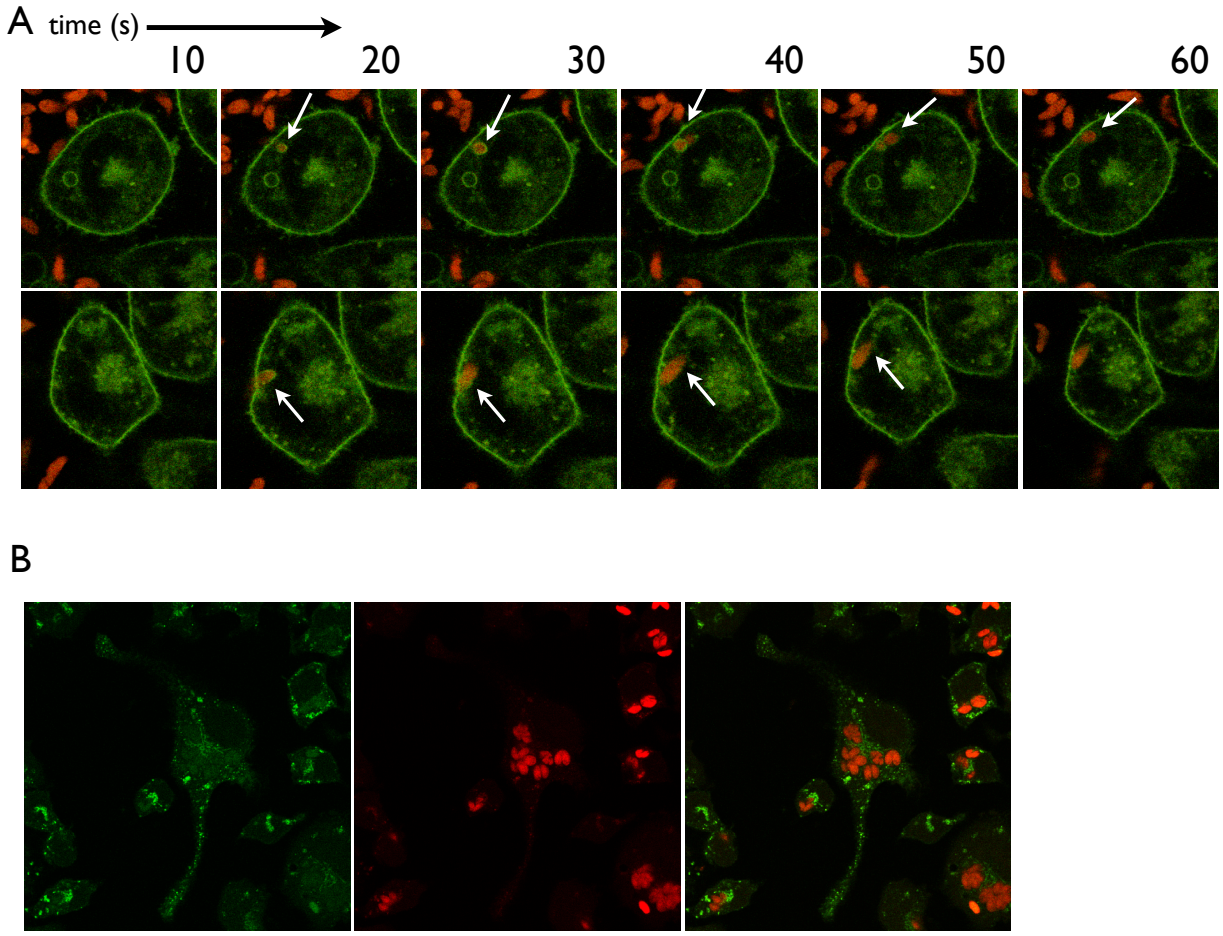

Figure 5.1. Upon invasion, *T. gondii* tachyzoites rapidly shed plasma membrane associated CTxB-GM_1. RBL-2H3 mast cells with plasma membrane and recycling endosomes labeled with Alexa488-CTxB (green) were incubated with RH-tomato (red) tachyzoites (MOI 10:1). (A) Live cell confocal microscopy of two cells during tachyzoite invasion. White arrows indicated invading parasite (Movie M5.1). (B) Parasite replication can be seen 24 hours post-infection.

parasitophorous vacuole at early times following infection. To test this hypothesis we took advantage our ability to differentially label the plasma membrane RE pool with CTxB in RBL cells. If cells are labeled for short times (less than 30 minutes at 37°C), the label stays primarily at the plasma membrane, although some trafficking to the RE can occur over that time. Under this labeling condition during infection CTxB-GM_1 is largely absent from the membrane surrounding the tachyzoite (Figure 5.2A, movie M5.2). Longer incubations at 37°C substantially increases trafficking of GM_1 to the recycling endosomal pool, such that both the plasma membrane and recycling endosomes are labeled with CTxB [1]. Under these conditions, robust labeling of PVM is observed (Figure 5.2B, movie M5.3). In other cell types, trans-membrane plasma membrane proteins such as CD44 are commonly excluded from the PVM [6]. In mast cells, FcεRI is the high affinity receptor for IgE that is a multi-subunit, transmembrane protein in the plasma membrane. We find that FcεRI labeled by Alexa488-IgE is excluded from the PVM (Figure 5.2C).

To quantify these observations, we scored internalized parasites in more than 80 cells for each condition to determine the percentage of parasites that have association with host membrane label under the conditions described above. As shown in Figure

5.2D, we find that cells with CTxB of recycling endosomes exhibit more than 60% of PVMs labeled, whereas cells with primarily plasma membrane label at the time of infection exhibit less than half this percentage of labeled PVMs. In comparison, IgE/FcεRI label is detected in less than 5% of the PVMs.

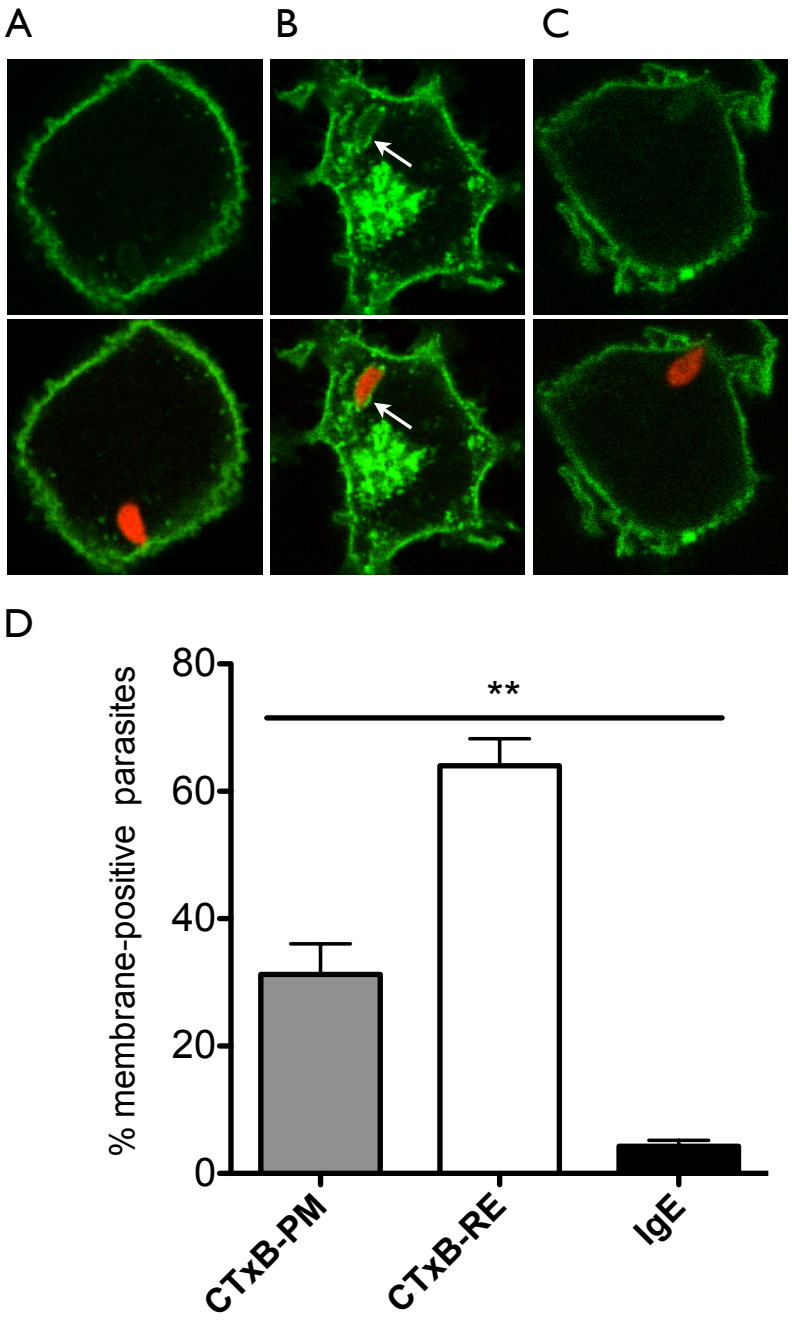

Figure 5.2. Recycling endosomal CTxB-GM_1 efficiently labels PV of *T. gondii*. Representative confocal Z-sections of RBL mast cells infected with RH-tomato tachyzoites (red) for ≤ 1hour. (A) Plasma membrane labeling with FITC-CTxB (green), (B) plasma membrane (PM) and recycling endosomal (RE) with FITC-CTxB (green) and (C) FcεRI labeling by Alexa488-IgE (green). (Movies M5.2-3)(D) Percentage positive vacuoles for conditions (A-C) (n=83,165,109 for conditions (A), (B) and (C), respectively). Error bars represent SEM.

Recycling endosomal GM_1 co-localizes with parasite derived GRA7 in the nascent PVM.

The appearance of CTxB-GM_1 around intracellular tachyzoites does not exclude the possibility that the host membrane is simply accumulating, not actually an integral part of the PV. To address this issue, we compared the distribution of a parasite-derived PV resident protein, GRA7 [36] with CTxB label. Samples were fixed after 20 minutes of infection and parasite GRA7 was immuno-fluorescently labeled following permeabilization. As shown in Figure 5.3A, GRA7 and CTxB show a high degree of co-localization at the PV when both the RE and PM are labeled by CTxB. As expected, when only the plasma membrane is CTxB-labeled there is very little CTxB label at the PV as delineated by GRA7 labeling (Figure 5.3B). This result shows that the CTxB-GM_1, derived from recycling endosomes, labels host-derived membrane in the PVM.

Markers from RE derived membranes also appear in PV in primary cell types.

We further investigated whether PV labeling by CTxB-GM_1 is a general feature of infected cells or particular to RBL mast cells. Using primary mast cells derived from rat bone marrow (rBMMCs), similar differential labeling of RE and PM with CTxB is observed. As in the RBL-2H3 cells, primarily plasma membrane labeling with CTxB-GM_1 results in little label in the PVM (Figure 5.4A). In contrast, when RE and PM are labeled by CTxB, CTxB label is apparent at the PVM (Figure 5.4B).

While mast cells are a good model for characterizing recycling endosomal trafficking, they are not a cell type that is frequently infected *in vivo*. Both dendritic cells and macrophages are known to be targets of *T. gondii in vivo*. We sought to determine if

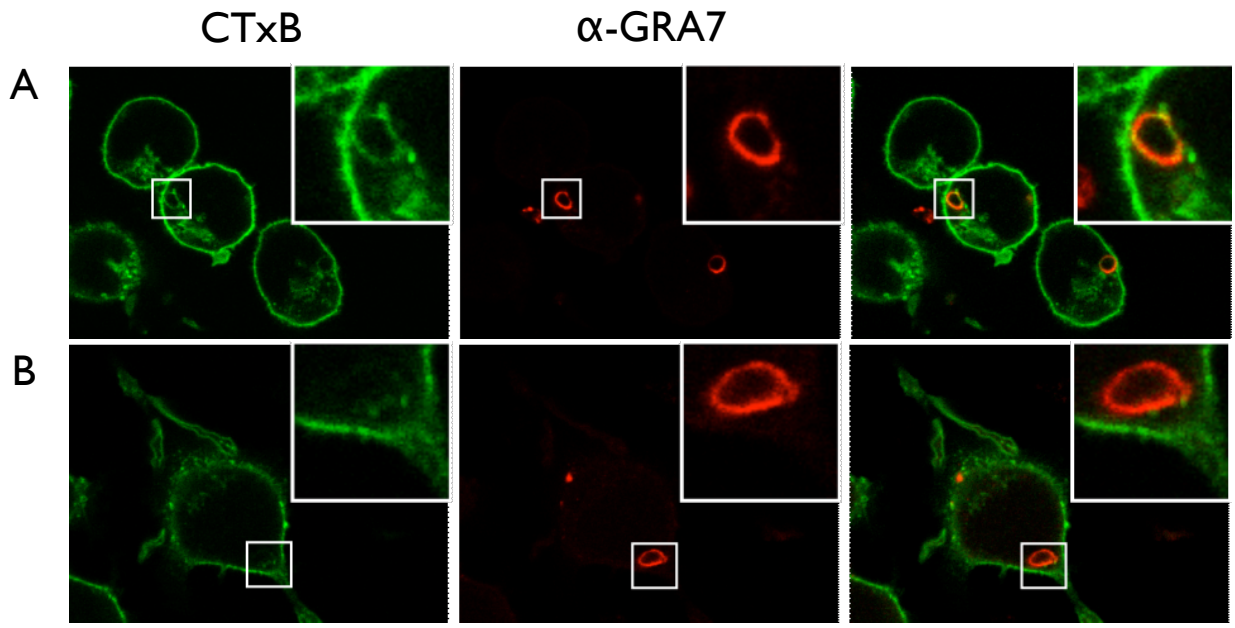

Figure 5.3. Parasite-derived GRA7 and host RE GM_1 colocalize to the PV within 20 minutes of invasion. Z-sections from confocal microscopy of RBL mast cells incubated with RH-tomato parasites for 20 minutes. (A) FITC-CTxB (green) labels both recycling endosomes and plasma membrane anti-GRA7 followed by Alexa555 secondary antibody (red) marks the parasitophorous vacuole of the tachyzoite. (B) FITC-CTxB primarily labels plasma membrane. Images are representative of two experiments.

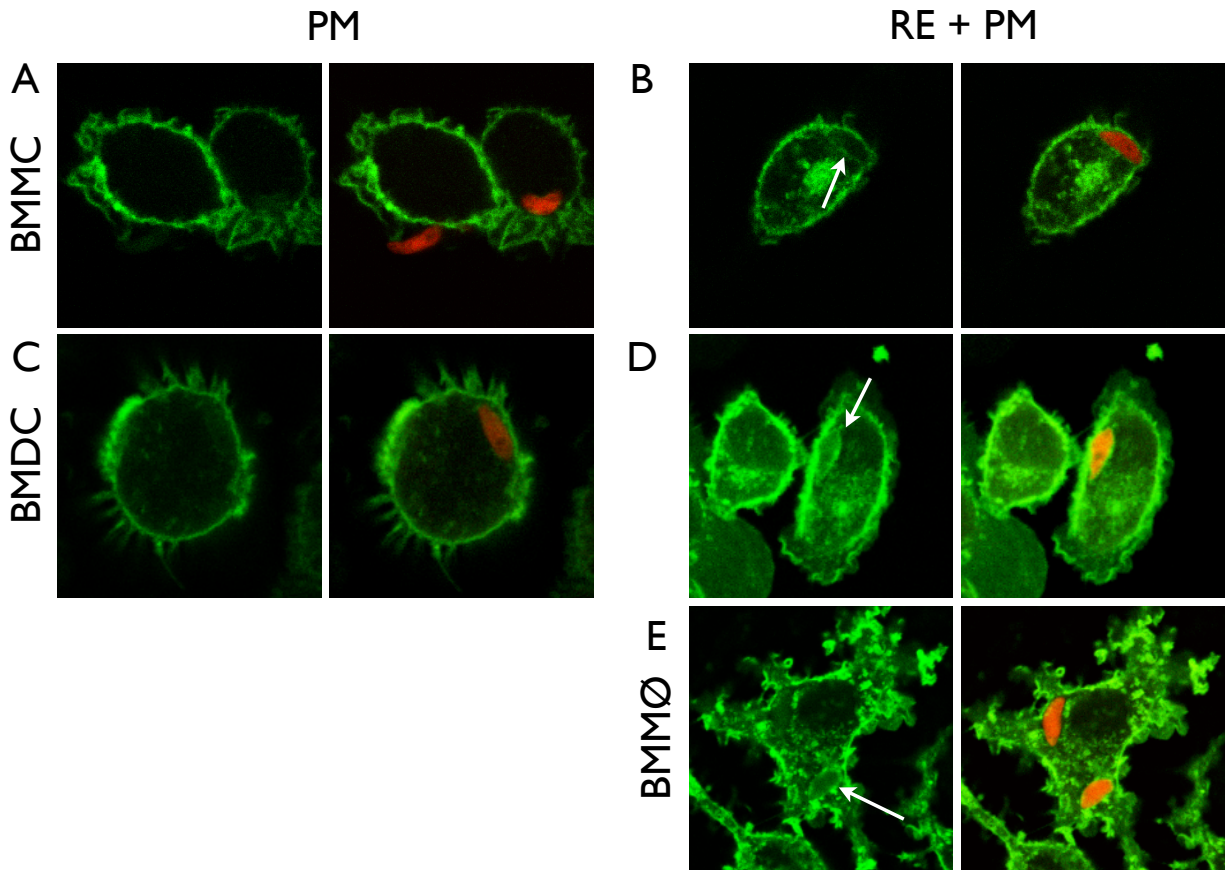

Figure 5.4. Recycling endosomes contribute to the parasitophorous vacuole in bone marrow-derived mast cells, dendritic cells and macrophages. Equatorial sections from confocal microscopy of fixed, RH-tomato (red) infected (≤ one hour) cells from various immune lineages. (A,B) Rat bone marrow-derived mast cells (BMMCs). (C,D) Mouse bone marrow-derived dendritic cells (BMDCs). (E) Mouse bone marrow-derived macrophages (BMMϕ). The left pairs of images represent conditions with minimal RE-derived CTxB (A,C) and the right pairs are conditions where both the RE and PM are labeled with CTxB (B,D,E) Images representative of 2-3 experiments.

the results seen in mast cells are also apparent in mouse bone marrow dendritic cells (BMDCs) and macrophages (BMMϕs). Initial experiments showed that BMDCs have similar CTxB-GM_1 internalization kinetics to mast cells, allowing us to employ the same CTxB-GM_1 labeling scheme described above. As with mast cells, if only the plasma membrane is labeled, CTxB labeling is largely absent from the PVM (Figure 5.4C). RE morphology in BMDCs is somewhat more disperse than in mast cells, but it still has a perinuclear concentration. In cells where both PM and RE contain CTxB-GM_1, some CTxB label appears at the parasite perimeter (Figure 5.4D).

BMMϕs have markedly different intracellular subcellular distributions CTxB-GM_1. Moreover, BMMϕs CTxB-GM_1 internalization is quite rapid. Within ten minutes of CTxB addition, significant internal CTxB-GM_1 label is located through out the cytoplasm in addition to uniform plasma membrane label. Due to this difference, the labeling scheme that we used for mast cells and BMDCs does not allow us to differentially compare plasma membrane versus recycling endosomal contribution to the PVM in BMMϕs. We reasoned that as recycling rates are some much faster in the BMMϕs we could add CTxB to pre-infected cells and ask if this CTxB appears at the PVM at later time points. Positive label around the parasite would indicate that there is trafficking of CTxB-GM_1 containing membrane to the PVM. Using this strategy we observe CTxB-GM_1 in the PVM around some parasites (Figure 5.4E). We do not see this labeling around all parasites, suggesting that GM_1 localization in the PVM is somewhat transient, perhaps indicating the parasite has some active mechanism for sorting some membrane components out of the host membrane it co-opts for the PVM. Collectively, these

results suggest that RE contribution to the PVM is not a unique feature of infection in RBL-2H3 mast cells but rather is a general phenomenon that occurs in multiple infected cell types.

Inner leaflet plasma membrane markers are excluded from the PVM.

Our results with FcεRI/IgE (Figure 5.2) and previous results [6] showed that host-derived transmembrane proteins at the plasma membrane are excluded from the nascent PV. To investigate whether inner leaflet-associated lipids or lipid-anchored proteins from the plasma membrane are localized to the PVM, we employed transient transfection of RBL-2H3 cells with two closely related, fluorescently labeled constructs, Lyn–EGFP and PM-EGFP. Lyn kinase associates with the inner leaflet of the plasma membrane through two N-terminal lipid modifications, a palmytolation and a myristolation. The PM-EGFP construct is the short protein sequence of Lyn that contains these two lipid modifications. Both constructs show good plasma membrane localization, but there is no accumulation of either marker around intracellular parasites (Figure 5.5A,B).

Phosphoinositide (PI) lipid species contribute to important signaling pathways as second messengers and help to designate organellar membrane identity. PH domains from different proteins have varying specificities for PI species. The PH domains from PLCδ and Akt have high specificity for PIP_2 and PIP_3, respectively. We used GPF constructs of these two PH domains to determine if the PV contains PIP_2 or PIP_3. Neither construct showed significant accumulation at the PV (Figure 5.5C,D).

Figure 5.5. RE markers localize to PV while markers of plasma membrane inner leaflet and phosphoinositides are excluded. (A-F) Representative confocal Z-sections of transiently transfected and fixed RBL-2H3 mast cells infected for ≤ one hour with RH-tomato tachyzoites. (A, B) Lyn-EGFP and PM-EGFP are inner leaflet plasma membrane markers. (C, D) $PH_{PLC}\delta$-GFP and PH_{Akt}-GFP bind to PIP_2 and PIP_3, respectively. (E, F) TfR-pHlorin and YFP-GPI are two markers known to associate with recycling endosomes. Arrowheads indicate lack of PV label and arrows highlight PV label by host RE markers. All images are representative of two or more experiments.

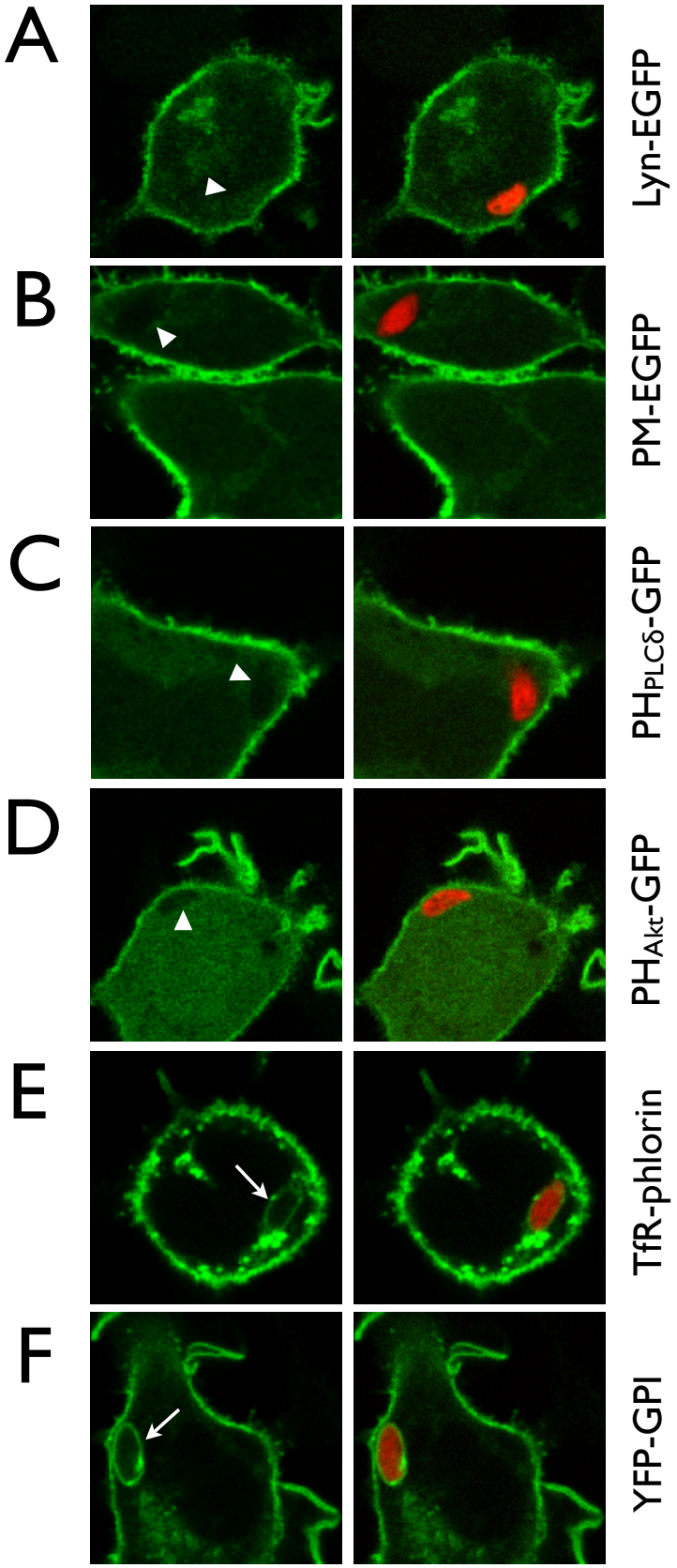
A
Lyn-EGFP
B
PM-EGFP
C
PHPLCδ-GFP
D
PHAkt-GFP
E
TfR-phlorin
F
YFP-GPI

In stark contrast to our results with inner leaflet plasma membrane and PH-domain affinity PI markers, known RE markers do localize to the PVM. Transferrin receptor (TfR) has long been known to concentrate in RE [12]. Figure 5.5E demonstrates that we can occasionally see TfR at that PVM. Our laboratory has recently determined that GPI-anchored proteins populate the RE (Wilson and Holowka, unpublished results), and these RE traffic in response to antigen much like CTxB/GM_1. The same glycosylphosphoinositol (GPI) anchored construct also shows remarkable localization with the PV (Figure 5.5F). This is consistent with observations by Mordue et al. [6], although they conclude that GPI-anchored proteins are from the plasma membrane. Accumulated data in our lab would suggest they, in fact, come from the RE. Collectively, our imaging studies show a strong correlation between recycling endosomal localization and appearance in the PVM (summarized in Table 5.1).

T. gondii invasion induces a Ca^{2+} wave.

In RBL cells, stimulated RE trafficking is a Ca^{2+} dependent process. One possible mechanism for *Toxoplasma*-stimulated RE trafficking to the PV is an invasion-induced Ca^{2+} response to parasite. To investigate this possibility, we monitored fluo-4 fluorescence as a measure of Ca^{2+} levels in RBL cells incubated with RH-tomato parasites. Figure 5.6 shows selected frames of a movie (M5.4) in which parasite entry results in the initiation of a global Ca^{2+} wave. In each of the two cases shown, the Ca^{2+} wave propagates from the site of parasite entry (white arrows) across the cell. We suggest that this host response might initiate RE trafficking to the PVM, and that this

Table 5.1

	Marker	Relative PV association*
Recycling Endosome		
	Cholera toxin B- GM_1 (PM + RE)	+++
	Transferrin Receptor-pHlorin	+
	YFP-GPI	+++
Plasma Membrane		
outer leaflet	Cholera toxin B- GM_1 (PM)	+
	IgE-FcεRI	-
inner leaflet	Lyn-EGFP	-
	PM-EGFP	-
Phosphoinositides		
	PIP_2 ($PH_{PLC}\delta$-GFP)	-
	PIP_3 (PH_{Akt}-GFP)	-

*Scoring: +++(> 50% association), + (30-50% association), - (< 10% association)

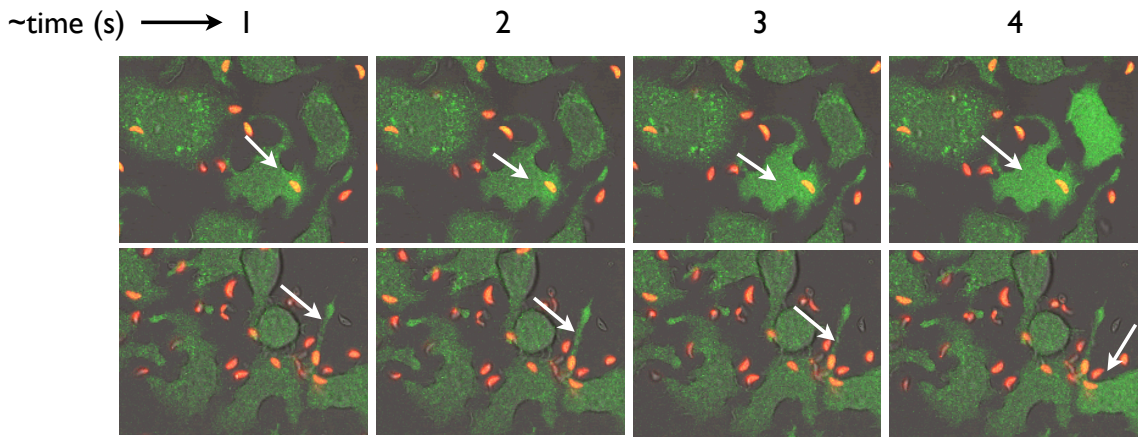

Figure 5.6. Parasite invasion triggers global Ca^{2+} wave. (A) Live confocal microscopy of fluo-4 loaded RBL-2H3 mast cells incubated with RH-tomato parasites (see movie M5.4). Arrows highlight time-dependent, transient fluorescence increase indicative of Ca^{2+} wave. Top and bottom panels show two individual cells and are representative examples from two experiments.

Ca^{2+} wave may also be responsible for a previously unidentified host Ca^{2+} response that is required for *T. gondii*-mediated MAPK signaling [37].

DISCUSSION

The moving junction that is formed at the site of *T. gondii* entry appears to selectively sort PM components from the membrane that initially forms the PV [6]. The PV is considered to be a non-fusogenic entity that avoids interactions with the endo-lysosomal system [2, 38]. The membrane systems of living cells are highly dynamic structures, and it has been estimated that the lipid population of the plasma membrane turns over hourly [39]. With that level of ongoing trafficking, it is difficult to envision how the PVM could maintain complete segregation from various membrane pools. Furthermore, it is clear that the PV must expand to accommodate the replicating parasites. To accommodate this requirement, the parasite may utilize membrane or lipid trafficking within the host cell. High-resolution electron microscopy has revealed that the PV is closely associated with host ER and mitochondria, and it has been hypothesized that these organelles may serve as a lipid sources for the PVM [2].

Most PM transmembrane proteins are excluded from the nascent PV, whereas host lipids, including gangliosides such as GM_1 as well as GPI-linked proteins, are readily found in PVM of intracellular parasites [6]. The assumption has been that these components are taken from the PM upon invasion. Our live microscopy experiments, in which we observe rapid loss of PM-derived CTxB/GM_1 label, suggest that the situation is not that simple. However, the RE compartment is also enriched in GM_1 and GPI-

linked proteins [1], (unpublished results). Our investigation of *T. gondii* invasion in RBL mast cells demonstrates, for the first time, that RE are contributors to the nascent PV.

Previously, Mordue et al. [38] dismissed the possibility of RE involvement in PV formation based on the absence of TfR labeling at the PV. While it is true that TfR is commonly used marker for RE, it is not a definitive test of RE contribution [40]. We argue that RBL cells are well-suited to the study of RE trafficking process for two reasons: (1) the concentrated perinuclear spatial localization of RE label and (2) the RE an PM compartments can be differentially labeled [1]. Using this system, we demonstrate that label of CTxB/GM_1 from the RE pool significantly contributes to membrane surrounding intracellular parasites. This system has the limitation that differential PM/RE labeling can only be achieved for rather short times at physiological temperature (< 30 minutes). Therefore alternative methods to maximize the difference between the labeled pools either with by stripping surface FITC-CTxB or replacing with unlabeled CTxB [19] may be useful in future studies. Alternatively, quenching surface FITC fluorescence with trypan blue [41] could aid in distinguishing between PM and RE contributions to the PVM. Despite the limitations of our differential labeling method our results clearly show that CTxB/GM_1 label is co-incident with parasite-derived GRA7 in the PVM only under conditions where RE are labeled. Consistent with previous studies [6], we also see strong localization of a GPI-anchored protein to the PV. We have substantial evidence that GPI-anchored proteins traffic via RE (Wilson and Holowka, unpublished results), so we posit that these components seen in the PVM are derived most directly from RE, rather than the PM.

To date, this is the first evidence that an intracellular host organelle contributes to the PVM. However, in a recent study, host-derived lipids were found to be the major source of lipids populating the intravacuolar network [42], an extensive network of tubules and vesicles that fills the luminal space of the PV [43, 44]. The authors hypothesize that these lipids may come from the host ER, but it is possible that other host membranes, such as the RE, contribute to these structures.

In attempting to better characterize the composition of the nascent PV, we also examined inner leaflet components. To our surprise, both lipid anchored proteins (Lyn-EGFP and PM-EGFP) and phosphoinositide lipid species (PIP_2 and PIP_3) also appear to be absent from the PVM. There is no precedent for this finding, and both the mechanism and the reason for such segregation are unclear at this time.

How RE might be triggered to traffic to PVM is still a mystery. Previously, we demonstrated that stimulated RE exocytosis is a Ca^{2+}-dependent process [1, 19]. Here we show that invasion can induce a single Ca^{2+} wave in host cells. It is tempting to speculate that this signal might, through unknown mechanisms, direct RE to the PVM. Previous studies have demonstrated that stimulated RE traffic is a robust process, refractory to many methods of inhibition [1]. Furthermore, the importance of this trafficking mechanism in *T. gondii* infection is still an unknown quantity. The most straightforward way to address this issue is to determine if modulation of RE trafficking effects the progression of *Toxoplasma* infection. RE trafficking is regulated by several GTPases including Rab11 and Arf6 [13, 14], and over expression of dominant negative, wild-type or constitutively active constructs are used to manipulate the efficiency of RE

trafficking. Alternatively, a chemically derived mutant version of RBL mast cells, B6A4C1 has multiple defects including a defect in lipid biosynthesis that results in a lack of ganglioside production [45]. This cell line does not bind CTxB and has a reduction in antigen stimulated RE trafficking (J. Wilson, unpublished results). Another option is the pharmacological inhibition of RE trafficking with phospholipase A_2 antagonists [46]. Asking any of these conditions effects parasite replication is one method to determine the importance of RE contribution to the PVM. That *T. gondii* can hijack the normal recycling might provide new insights concerning how RE trafficking is regulated; such findings would have important implications, not only for *Toxoplasma* infection but also for the basic understanding the regulation of host RE trafficking.

CONTRIBUTIONS AND ACKNOWLEDGEMENTS

Research designed by N. L. Smith, E.Y. Denkers and D. A. Holowka; N. L. Smith performed and analyzed experiments. Research supported by National Institutes of Heath Grants R01 AI022449 (B. A. Baird and D. A. Holowka).

We thank Carol Bayles for maintaining the Cornell Microscopy and Imaging Facility and Rodman Getchell for maintenance of the SP5 Leica Confocal system. We also thank Delbert S. Abi Abdallah and Barbara Butcher for helpful discussions.

REFERENCES

1. Naal, R.M., et al., *Antigen-stimulated trafficking from the recycling compartment to the plasma membrane in RBL mast cells.* Traffic, 2003. **4**(3): p. 190-200.

2. Sinai, A.P. and K.A. Joiner, *Safe haven: the cell biology of nonfusogenic pathogen vacuoles.* Annu Rev Microbiol, 1997. **51**: p. 415-62.

3. Carruthers, V. and J.C. Boothroyd, *Pulling together: an integrated model of Toxoplasma cell invasion.* Curr Opin Microbiol, 2007. **10**(1): p. 83-9.

4. Besteiro, S., J.F. Dubremetz, and M. Lebrun, *The moving junction of apicomplexan parasites: a key structure for invasion.* Cell Microbiol, 2011. **13**(6): p. 797-805.

5. Suss-Toby, E., J. Zimmerberg, and G.E. Ward, *Toxoplasma invasion: the parasitophorous vacuole is formed from host cell plasma membrane and pinches off via a fission pore.* Proc Natl Acad Sci U S A, 1996. **93**(16): p. 8413-8.

6. Mordue, D.G., et al., *Invasion by Toxoplasma gondii establishes a moving junction that selectively excludes host cell plasma membrane proteins on the basis of their membrane anchoring.* J Exp Med, 1999. **190**(12): p. 1783-92.

7. Pfefferkorn, E.R., M. Eckel, and S. Rebhun, *Interferon-gamma suppresses the growth of Toxoplasma gondii in human fibroblasts through starvation for tryptophan.* Mol Biochem Parasitol, 1986. **20**(3): p. 215-24.

8. Fox, B.A., J.P. Gigley, and D.J. Bzik, *Toxoplasma gondii lacks the enzymes required for de novo arginine biosynthesis and arginine starvation triggers cyst formation.* Int J Parasitol, 2004. **34**(3): p. 323-31.

9. Coppens, I., A.P. Sinai, and K.A. Joiner, *Toxoplasma gondii exploits host low-density lipoprotein receptor-mediated endocytosis for cholesterol acquisition.* J Cell Biol, 2000. **149**(1): p. 167-80.

10. Hsu, V.W. and R. Prekeris, *Transport at the recycling endosome.* Curr Opin Cell Biol, 2010. **22**(4): p. 528-34.

11. Hopkins, C.R. and I.S. Trowbridge, *Internalization and processing of transferrin and the transferrin receptor in human carcinoma A431 cells.* J Cell Biol, 1983. **97**(2): p. 508-21.

12. Yamashiro, D.J., et al., *Segregation of transferrin to a mildly acidic (pH 6.5) para-Golgi compartment in the recycling pathway.* Cell, 1984. **37**(3): p. 789-800.

13. Ullrich, O., et al., *Rab11 regulates recycling through the pericentriolar recycling endosome.* J Cell Biol, 1996. **135**(4): p. 913-24.

14. Balasubramanian, N., et al., *Arf6 and microtubules in adhesion-dependent trafficking of lipid rafts.* Nat Cell Biol, 2007. **9**(12): p. 1381-91.

15. Murray, R.Z., et al., *A role for the phagosome in cytokine secretion.* Science, 2005. **310**(5753): p. 1492-5.

16. Dyer, N., et al., *Spermatocyte cytokinesis requires rapid membrane addition mediated by ARF6 on central spindle recycling endosomes.* Development, 2007. **134**(24): p. 4437-47.

17. Veale, K.J., et al., *Recycling endosome membrane incorporation into the leading edge regulates lamellipodia formation and macrophage migration.* Traffic, 2010. **11**(10): p. 1370-9.

18. Prigozhina, N.L. and C.M. Waterman-Storer, *Decreased polarity and increased random motility in PtK1 epithelial cells correlate with inhibition of endosomal recycling.* J Cell Sci, 2006. **119**(Pt 17): p. 3571-82.

19. Smith, N.L., et al., *Sphingosine derivatives inhibit cell signaling by electrostatically neutralizing polyphosphoinositides at the plasma membrane.* Self Nonself, 2010. **1**(2): p. 133-143.

20. Posner, R.G., et al., *Aggregation of IgE-receptor complexes on rat basophilic leukemia cells does not change the intrinsic affinity but can alter the kinetics of the ligand-IgE interaction.* Biochemistry, 1992. **31**(23): p. 5350-6.

21. Hess, S.T., et al., *Quantitative analysis of the fluorescence properties of intrinsically fluorescent proteins in living cells.* Biophys J, 2003. **85**(4): p. 2566-80.

22. Pyenta, P.S., D. Holowka, and B. Baird, *Cross-correlation analysis of inner-leaflet-anchored green fluorescent protein co-redistributed with IgE receptors and outer leaflet lipid raft components.* Biophys J, 2001. **80**(5): p. 2120-32.

23. Varnai, P. and T. Balla, *Visualization of phosphoinositides that bind pleckstrin homology domains: calcium- and agonist-induced dynamic changes and relationship to myo-[3H]inositol-labeled phosphoinositide pools.* J Cell Biol, 1998. **143**(2): p. 501-10.

24. Srinivasan, S., et al., *Rac and Cdc42 play distinct roles in regulating PI(3,4,5)P3 and polarity during neutrophil chemotaxis.* J Cell Biol, 2003. **160**(3): p. 375-85.

25. Wu, M., et al., *Coupling between clathrin-dependent endocytic budding and F-BAR-dependent tubulation in a cell-free system.* Nat Cell Biol, 2010. **12**(9): p. 902-8.

26. Gidwani, A., et al., *Disruption of lipid order by short-chain ceramides correlates with inhibition of phospholipase D and downstream signaling by FcepsilonRI.* J Cell Sci, 2003. **116**(Pt 15): p. 3177-87.

27. Haig, D.M., et al., *Effects of stem cell factor (kit-ligand) and interleukin-3 on the growth and serine proteinase expression of rat bone-marrow-derived or serosal mast cells.* Blood, 1994. **83**(1): p. 72-83.

28. Leng, J., et al., *Toxoplasma gondii prevents chromatin remodeling initiated by TLR-triggered macrophage activation.* J Immunol, 2009. **182**(1): p. 489-97.

29. Abi Abdallah, D.S., et al., *Mouse neutrophils are professional antigen-presenting cells programmed to instruct Th1 and Th17 T-cell differentiation.* Int Immunol, 2011. **23**(5): p. 317-26.

30. Gosse, J.A., et al., *Transmembrane sequences are determinants of immunoreceptor signaling.* J Immunol, 2005. **175**(4): p. 2123-31.

31. Cohen, R., et al., *Ca2+ waves initiate antigen-stimulated Ca2+ responses in mast cells.* J Immunol, 2009. **183**(10): p. 6478-88.

32. Bierly, A.L., et al., *Dendritic cells expressing plasmacytoid marker PDCA-1 are Trojan horses during Toxoplasma gondii infection.* J Immunol, 2008. **181**(12): p. 8485-91.

33. Denkers, E.Y. and B.A. Butcher, *Sabotage and exploitation in macrophages parasitized by intracellular protozoans.* Trends Parasitol, 2005. **21**(1): p. 35-41.

34. Boyle, J.P. and J.R. Radke, *A history of studies that examine the interactions of Toxoplasma with its host cell: Emphasis on in vitro models.* Int J Parasitol, 2009.

35. Charron, A.J. and L.D. Sibley, *Molecular partitioning during host cell penetration by Toxoplasma gondii.* Traffic, 2004. **5**(11): p. 855-67.

36. Coppens, I., et al., *Toxoplasma gondii sequesters lysosomes from mammalian hosts in the vacuolar space.* Cell, 2006. **125**(2): p. 261-74.

37. Masek, K.S., et al., *Host cell Ca2+ and protein kinase C regulate innate recognition of Toxoplasma gondii.* J Cell Sci, 2006. **119**(Pt 21): p. 4565-73.

38. Mordue, D.G., et al., *Toxoplasma gondii resides in a vacuole that avoids fusion with host cell endocytic and exocytic vesicular trafficking pathways.* Exp Parasitol, 1999. **92**(2): p. 87-99.

39. Maxfield, F.R. and M. Mondal, *Sterol and lipid trafficking in mammalian cells.* Biochem Soc Trans, 2006. **34**(Pt 3): p. 335-9.

40. Maxfield, F.R. and T.E. McGraw, *Endocytic recycling.* Nat Rev Mol Cell Biol, 2004. **5**(2): p. 121-32.

41. Sahlin, S., J. Hed, and I. Rundquist, *Differentiation between attached and ingested immune complexes by a fluorescence quenching cytofluorometric assay.* J Immunol Methods, 1983. **60**(1-2): p. 115-24.

42. Caffaro, C.E. and J.C. Boothroyd, *Evidence for Host as the Major Contributor to Lipid in the Intravacuolar Network of Toxoplasma-Infected Cells.* Eukaryot Cell, 2011.

43. Magno, R.C., et al., *Intravacuolar network may act as a mechanical support for Toxoplasma gondii inside the parasitophorous vacuole.* Microsc Res Tech, 2005. **67**(1): p. 45-52.

44. Sibley, L.D., et al., *Regulated secretion of multi-lamellar vesicles leads to formation of a tubulo-vesicular network in host-cell vacuoles occupied by Toxoplasma gondii.* J Cell Sci, 1995. **108 (Pt 4)**: p. 1669-77.

45. Field, K.A., et al., *Mutant RBL mast cells defective in Fc epsilon RI signaling and lipid raft biosynthesis are reconstituted by activated Rho-family GTPases.* Mol Biol Cell, 2000. **11**(10): p. 3661-73.

46. de Figueiredo, P., et al., *Inhibition of transferrin recycling and endosome tubulation by phospholipase A2 antagonists.* J Biol Chem, 2001. **276**(50): p. 47361-70.

CHAPTER SIX

Toxoplasma gondii Inhibits Mast Cell Degranulation by Inhibiting PLCγ_1-mediated Ca^{2+} Mobilization

SUMMARY

T. gondii infects a wide variety of cell types, including many of the hematopoietic lineage. To better understand its capacity to subvert normal immune responses, we investigated the effects of *Toxoplasma* on specific pathways that are mobilized during IgE/FcεRI signaling that leads to granule exocytosis in mast cells. In the current study we used the well-studied RBL mast cell model to probe the capacity of *T. gondii* to modulate immune signaling within the first hour of infection. We find that *T. gondii* inhibits antigen-stimulated degranulation in infected cells in a strain-independent manner. Under these conditions, we find that, whereas antigen-triggered FcεRI tyrosine phosphorylation is unchanged by parasite infection, stimulated cytoplasmic Ca^{2+} mobilization is reduced. In particular, antigen-mediated Ca^{2+} release from stores is reduced in infected cells. Furthermore, stimulation-dependent PLCγ_1 tyrosine phosphorylation is also inhibited by infection. Therefore, we postulate that the inhibitory effects are likely due to parasite-mediated inhibition of PLCγ activation resulting in reduced cleaveage of PIP_2. Interestingly, inhibition of IgE/FcεRI signaling is retained when tachyzoite invasion is arrested via cytochalasin D treatment, suggesting inhibition of PLCγ may be mediated by a parasite-derived factor that is secreted during the

invasion process. Our study provides direct evidence, for the first time, that initiation of immune subversion by *T. gondii* occurs concurrently with invasion.

INTRODUCTION

The apicomplexan *Toxoplasma gondii* has evolved to be an extremely successful obligate intracellular parasite. It uses a multitude of mammalian and avian species as intermediate hosts. The Center for Disease Control and Prevention estimates 22.5% of U.S. population is latently infected with *T. gondii*. In most hosts, infection is asymptomatic and continues throughout their lifetimes. Nevertheless, under certain conditions, such as immuno-compromised individuals, acute Toxoplasmosis poses serious health risks [1].

T. gondii invades host cells through a process of active invasion that is markedly different from phagocytosis, and through this process is able to avoid fusion with the phagolysosomal system [2]. One of the reasons for the success of *Toxoplasma* as an intracellular pathogen is its development of immuno-modulatory mechanisms to evade and control the host response to infection [3, 4]. *In vivo* infection results in a strong protective immune response that is necessary for the host and, as a result, for parasite survival [5]. At the same time, it is established that infection actively suppresses production of many proinflammatory cytokines [4]. Virulence factors such as ROP 16 and ROP 18 are secreted from parasite rhoptries and may act to directly modulate host cell signaling [6, 7]. Despite this breadth of knowledge, much remains unknown. For example, it has been unclear how rapidly *Toxoplasma* effects immuno-modulation, and

the molecular mechanisms that mediate this immuno-modulation are largely unknown. Studies of *T. gondii* invasion in the context of an immune model where signaling is completed rapidly, on the order of tens of minutes, could provide key insights into mechanisms of *Toxoplasma* immune subversion.

Mast cells are of hematopoietic lineage, express the high affinity receptor for IgE, FcεRI, and are primary mediators of the allergic response [8]. They are also appreciated as key players in innate immunity and defense against helminths [9]. Multivalent antigen crosslinking of IgE-FcεRI complexes on the cell surface is the first step in the cascade of signaling events that results in the exocytosis of preformed mediators, such as histamine and serine proteases with a time course of minutes [8]. FcεRI belongs to the family of multichain immune recognition receptors (MIRRs) that also include B-cell and T-cell receptors [10]. Signal transduction through FcεRI has been extensively studied and involves PLCγ activation leading to calcium mobilization and PKC activation that are both necessary for stimulated granule exocytosis. These common signaling pathways are also shared by other immunoreceptors [11].

In the present study we use RBL mast cells to investigate the capacity of *Toxoplasma* to rapidly modulate immune signaling. We find that within an hour of the initiation of infection, parasites significantly inhibit antigen-mediated degranulation. Furthermore, whereas stimulated Ca^{2+} mobilization initiated by IP_3 production is inhibited, stimulated FcεRI receptor phosphorylation remains uninhibited. Additional experiments reveal that $PLC\gamma_1$ activation is inhibited by *Toxoplasma* infection, and this inhibition prevails in the presence of cytochalasin D to prevent parasite invasion.

Collectively, these results support a model in which *T. gondii* inhibits FcεRI receptor signaling by an unidentified product, likely secreted as invasion occurs, which acts by blocking the functional activation of PLCγ_1 that normally results in hydrolysis of phosphatidylinositol 4,5-bisphphosphate (PIP_2) to produce the second messengers IP_3 and DAG.

MATERIALS AND METHODS

Chemicals and Reagents

Indo-1-AM and Fluo-4-AM were purchased from Invitrogen Corp. 4-methylumbelliferyl-N-acetyl-β-D-glucosaminide, cytochalasin D, FITC-dextran, and thapsigargin were purchase from Sigma-Aldrich. Unless otherwise noted all other tissue culture reagents were purchased from Invitrogen and all other chemicals were purchased from Sigma-Aldrich. Anti-DNP IgE was purified as described previously [12].

Cells and Parasites

RBL-2H3 Mast Cells

RBL-2H3 mast cells were maintained in monolayer culture through weekly passage as described previously [13]. For stimulation, cells were sensitized with 1 μg/ml anti-DNP IgE for 4-24 hours

Parasites

RH, PTG, CTG, Veg and RH-tomato strains of parasites were used in this study. The RH-tomato strain of parasite, stably expressing tomato fluorescent protein, was

generated by Dr. B. Striepen (University of Georgia; kindly provided by Dr. E. Robey (University of California, Berkeley)). All tachyzoites were maintained in vitro via passage through human foreskin fibroblast cultures in DMEM with FCS (1%), penicillin (100 U/ml) and streptomycin (100 μg/ml) (Fibroblast media). For experiments, tachyzoites were harvested and passed through a 3 μm track-etched membrane filter (Whatman) to remove fibroblast debris. Infections were performed at a multiplicity of infection (MOI) of 10:1 unless otherwise indicated and were synchronized by brief centrifugation (200xg for 4 minutes).

Degranulation

β-Hexosaminidase Release

Cells were sensitized and plated in triplicate at a density of $5x10^5$/well and incubated overnight. The next day, cells were washed with fibroblast media and parasites were introduced as described above. For some experiments, 1 μM cytochalasin D was added during infection to prevent invasion. Following infection, cells were washed three times with buffered saline solution (BSS:135 mM NaCl, 5 mM KCl, 1 mM $MgCl_2$, 1.8 mM $CaCl_2$, 5.6 mM glucose, 20 mM HEPES, pH 7.4, 1 mg/ml BSA) and β-hexosaminidase was assessed as described previously [14].

Live Cell Degranulation Imaging

Sensitized cells were plated overnight in 35 mm glass bottom dishes (MatTek) in the presence of FITC-dextran (1 mg/ml) and 5-HT serotonin (0.2 mM). The next day, cells were washed with fibroblast media and infected with RH-tomato tachyzoites as

described above. Following one hour of infection, cells were washed three times with BSS. Imaging was conducted at 37°C on a SP5 confocal microscope (Leica) at an image acquisition rate of 1.7 Hz. Cells were monitored for 1 minute prior to addition of antigen (10 ng/ml), then monitored for an additional 9 minutes.

Western Blotting

Sensitized, adherent cells were infected as described above. Following infection, cells were stimulated for 0 to 10 minutes and whole cell western blotting samples were prepared and blotted as described previously [15]. Samples were run on Tris-glycine gels under non-reducing conditions. For assessment of receptor phosphorylation, anti-phosphotyrosine (clone 4G10) (Millipore) was used and the β subunit was identified based on molecular weight. To assess sample loading, a stimulation insensitive phosphotyrosine band from the original blot, or α-tubulin reprobing with anti-tubulin (clone N.593, U.S. Biologicals) was used. To determine relative intensity, first a ratio of band intensity for β to loading control was taken. Samples were then compared to the control sample at 10 minutes post-stimulation. PLCγ_1 and PLCγ_1-Y783 were probed with antibodies from Santa Cruz Biotechnology and Cell Signaling Technology, respectively.

Intracellular Ca^{2+} Measurements

Fluorimetry

Measurement of intracellular Ca^{2+} mobilization in response to 10 ng/ml DNP-BSA or 200 nM thapsigargin was carried out in tachyzoite infected cells using indo-1 as a Ca^{2+} indicator dye as described previously [16]. Time-integrated responses were

determined as the area under the stimulated timecourse minus the baseline over 400 sec, normalized to the maximal response in Triton X-100 lysed cells [17].

Live Cell Ca^{2+} Imaging

Single cells Ca^{2+} measurements in infected and control cells were conducted using Fluo-4 AM as described previously [18] on the Leica SP5 confocal system with an image acquisition rate of 0.5 Hz.

Analysis of Ca^{2+} oscillations in individual cells was performed using Matlab software (Mathworks). Briefly, code was written to track the location and average fluorescence intensity of the green channel (Fluor-4) within a circular region of interest (ROI) in the cytoplasm of each cell. These measurements were plotted with respect to time, and the number of oscillations for each ROI, reflected by increases in fluorescence intensity, was enumerated.

Measurements of Polyphosphoinositide (PIP_2 and PIP_3) Localization

Cells were sparsely plated (1-3x10^5/ml) on no. 1.5 coverslips or in 35 mm glass bottom dishes (MatTek). After overnight culture, cells were transfected with either PH-PLCδ-EGFP [19] and PH-Akt-EGFP [20] using 2 μg DNA and 8 μl Fugene HD (Roche Diagnostics) in 1 ml OptiMEM for 1 hour before addition of 1 ng/ml phorbol 12,13-dibutyrate for 3-5hr [21]. Samples were then washed into full media and cultured for 16-24 hours to allow for protein expression.

Transfected cells were infected for 1-2 hours with RH-tomato parasites followed by fixation with 4% paraformaldehyde and 0.1% glutaraldehyde in phosphate buffered saline (PBS; 10 minutes at room temperature). Excess fixative was quenched by 10 mg/ml BSA in PBS with 0.01% azide. Fixed cells were imaged on a SP2 confocal system (Leica). Line scan analysis of equatorial cross sections using ImageJ (NIH) was performed using average fluorescence values to determine the ratio of PH domain plasma membrane to cytoplasmic concentrations [16].

Statistical Analyses

Statistical analysis was performed with Prism software (Graphpad). All bar graphs display mean ± SEM unless otherwise noted. Statistical significance was determined by 1-way ANOVA (Analysis of Variance) followed by Tukey's post test. Level of significance is denoted as follows: * $P<0.05$, ** $P<0.01$, *** $P<0.001$ and **** $P<0.0001$.

RESULTS

Toxoplasma gondii infection rapidly inhibits antigen-mediated mast cell degranulation.

T. gondii is well know to actively modulate normal signaling in the immune cells it infects. However, most studies have focused on the immuno-modulatory effects that occur on longer timescales. We sought to determine if *T. gondii* acutely affects signal transduction at very early time points following infection. Mast cell signaling through the IgE receptor FcεRI is a well-studied immune signaling pathway that occurs on the time

scale of minutes. The end result of this signaling is granule fusion and release of histamine, serine proteases and proteoglycans in a process termed degranulation [22].

We infected RBL-2H3 mast cells with type I (RH), II (PTG) or type III (CTG or Veg) tachyzoites for one hour and assessed the capacity of the infected cells to degranulate in response to multivalent antigen. Under theses conditions, infection rates are between 50-70%. We find in a bulk assay that acute *T. gondii* infection reduces degranulation by approximately 50%, irrespective of the genotype of parasite used (Figure 6.1A). This inhibition directly correlates with multiplicity of infection (MOI), suggesting that inhibition is dependent on infection (Figure 6.1B). Furthermore, we used RH-tomato parasites in live imaging experiments to assess degranulation by FITC-dextran release (Figure 6.1C, movie M6.1). FITC-dextran is loaded in to the granules, and remains quenched until the acidic contents of the lysosome are neutralized upon fusion. It is apparent from these experiments that infected cells do not respond efficiently and show more delayed exocytosis. Neighboring uninfected cells respond robustly to antigen as seen by release of FITC-dextran from granules (black arrows) and apparent flattening and ruffling (Movie M6.1). Taken together, these results indicate that *T. gondii* inhibits mast cell degranulation, and this inhibition correlates with infection and is not merely a bystander effect.

FcεRI receptor phosphorylation is not altered by T. gondii infection.

Following the crosslinking of IgE-receptor complexes by multivalent antigen, phosphorylation of tyrosine residues within ITAMs in the cytoplasmic segments of the β

Figure 6.1. Acute *T. gondii* infection inhibits antigen-mediated mast cell degranulation. (A) RBL mast cells infected were with type I (RH, red), type II (PTG, blue) or type III (CTG or Veg, green) tachyzoites for 1 hr at an MOI of 10:1 (resulting in 50-70% infection), and antigen-stimulated (1ng/ml) degranulation assessed by β-hexosaminindase release. Results summarize an average of 5 to 7 experiments, and error bars represent SEM (*, $P<0.05$; ***, $P<0.001$ compared to control uninfected cells). (B) Inhibition of degranulation increases with increasing MOI. (C) Live fluorescent confocal microscopy of degranulation events monitored by FITC-dextran bursts (green) in RBL cells infected with RH-tomato tachyzoites (red) and uninfected RBL cells in the same field. White arrows (0 s frame) indicate infected cells. Black arrows highlight degranulation events in uninfected cells (see supplemental movie M6.1).

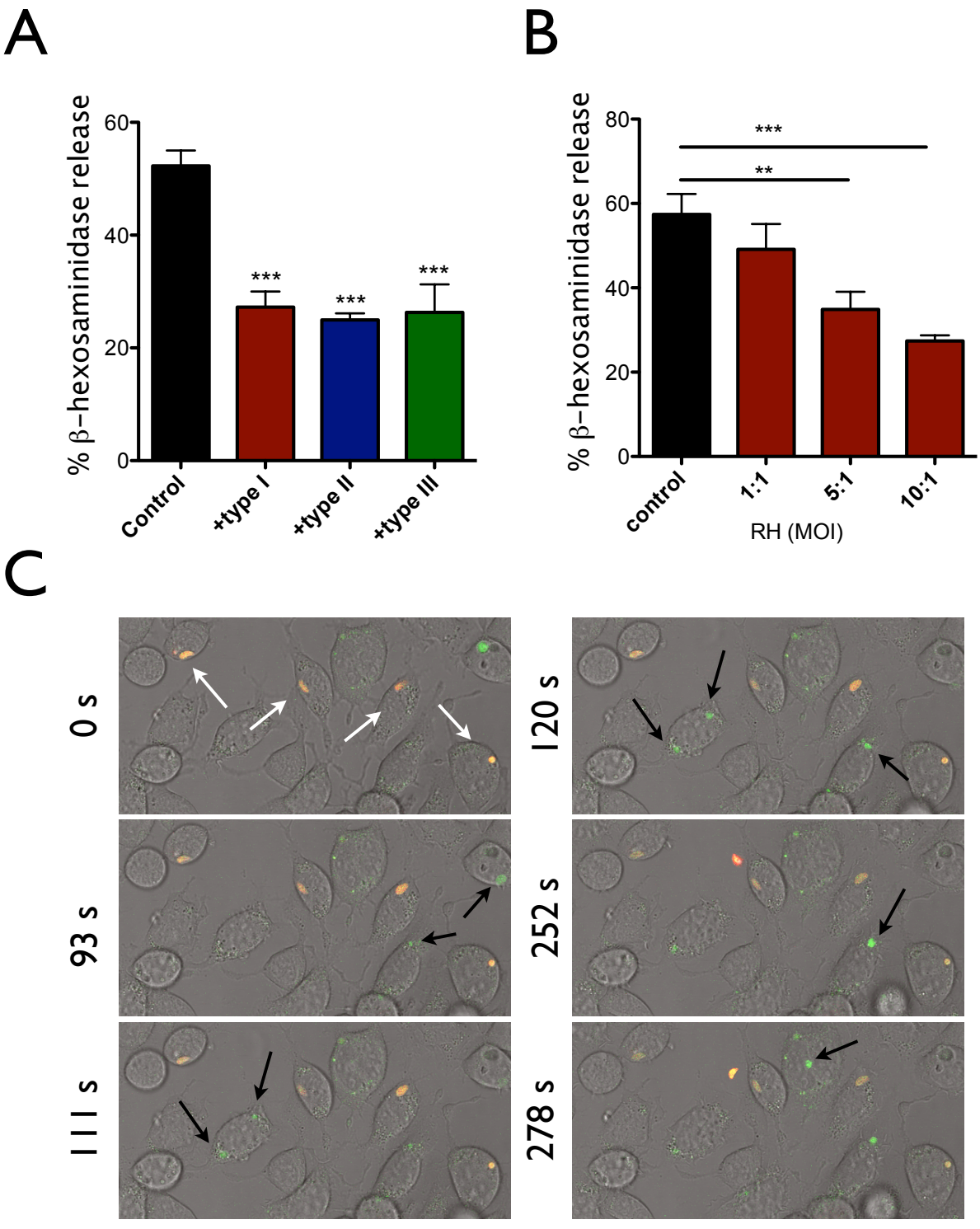
A
% β–hexosaminidase release
60
40
20
0
***
***
***
Control
+type I
+type II
+type III
B
% β–hexosaminidase release
80
60
40
20
0
***
**
control
1:1
5:1
10:1
RH (MOI)
C
0 s
93 s
111 s
120 s
252 s
278 s

and γ subunits of FcεRI is the initial step in signaling that leads to degranulation. To determine the mechanism by which *T. gondii* inhibits mast cell degranulation, we first asked if receptor phosphorylation in response to antigen is normal in infected cells. In contrast to the significant inhibition of degranulation responses, FcεRI-β phosphorylation following stimulation, assayed by anti-phosphotyrosine western blotting, is largely unchanged by *Toxoplasma* infection (Figure 6.2A). For confirmation, we quantified the relative level of β subunit phosphorylation and detected no significant change in the parasite-infected samples, regardless of parasite type (Figure 6.2B). Given this result, we conclude that parasite inhibition is acting downstream of receptor phosphorylation in the degranulation signaling cascade.

Ca^{2+} mobilization in response to antigen is reduced in Toxoplasma-infected RBL-2H3 mast cells.

Ca^{2+} release from ER stores, followed by store operated Ca^{2+} entry (SOCE) are important downstream process in the sequellae that lead to degranulation in mast cells [23]. Measurement of intracellular Ca^{2+} in suspended RBL cells reveals that infection by *T. gondii* significantly reduces the Ca^{2+} response to antigen (Figure 6.3A). Integration of Ca^{2+} responses over 10 minutes shows on average a 39% reduction in Ca^{2+} mobilizaton (Figure 6.3B). While all three types of parasites significantly inihibit Ca^{2+} influx, it is interesting to note that the type II strain, PTG, is the most consistent and dramatic in its inhbition, reducing the net Ca^{2+} response by half. In these bulk population measurements, it is difficult to evaluate what percentage of infected cells is inhibited. To better address this question, we conducted live cell imaging experiments to evalulate

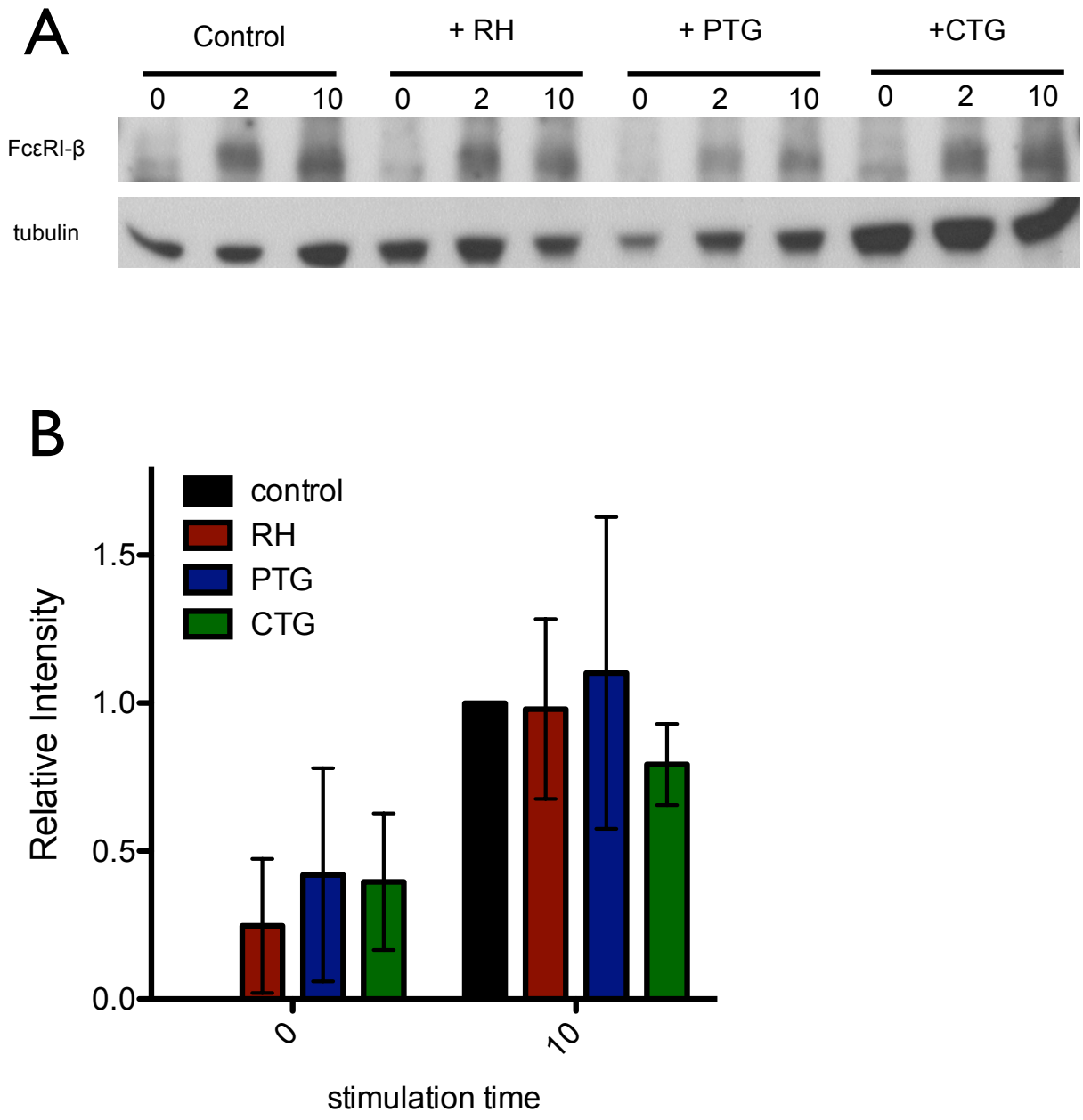

Figure 6.2. FcεRI receptor tyrosine phosphorylation is not altered in *T. gondii* infected cells. IgE-sensitized RBL cells were infected for 1 hr with RH, PTG or CTG tachyzoites as indicated. Antigen-stimulated cells were lysed at 0, 2 or 10 minutes after addition of DNP-BSA (10 ng/ml). (A) Representative blot. Top panel shows phosphorylation of β subunit of the FcεRI receptor. Bottom panel shows loading control (α-tubulin) (B) Quantification of β subunit band intensity (see material and methods for details). Error bars represent SEM of 2-4 independent experiments.

Figure 6.3. *T. gondii* infection reduces antigen-mediated calcium responses in RBL mast cells. (A) Representative Indo-1 fluorescence measurements of Ca^{2+} responses to 10 ng/ml antigen in control uninfected (black), RH-infected (red), PTG-infected (blue) or CTG-infected (green) infected cells (MOI 10:1). (B) Integrated calcium responses over 300 seconds of stimulation as a percentage of control Ca^{2+} response. Histogram shows averages for 3-5 independent experiments. (C) Live Fluo-4 (green) Ca^{2+} imaging in uninfected or RH-tomato (red) infected RBL-cells. (see supplemental movies M6.2 and M6.3). Quantification of the percentage of responding cells (D) or average number of calcium oscillations per cell in 10 minutes (E) in these live calcium imaging experiments (n=174 cells over 3 experiments). Error bars represent SEM (* is $P<0.05$, *** is $P<0.001$, and **** is $P<0.0001$ relative to uninfected cells).

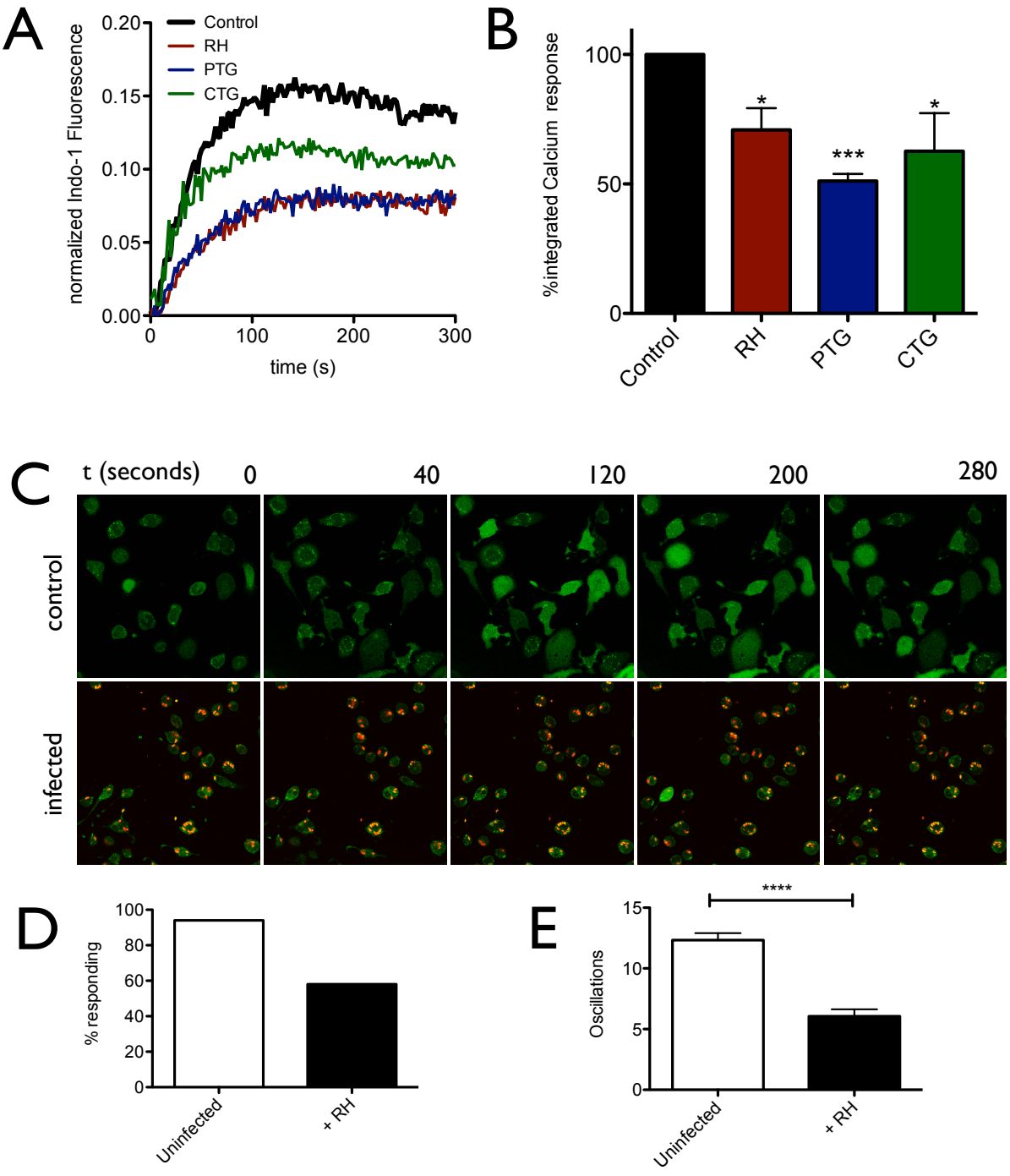
A
normalized Indo-1 Fluorescence
0.20
0.15
0.10
0.05
0.00
0
100
200
300
time (s)
Control
RH
PTG
CTG
B
%integrated Calcium response
100
50
0
*
***
*
Control
RH
PTG
CTG
C
t (seconds)
0
40
120
200
280
control
infected
D
% responding
100
80
60
40
20
0
Uninfected
+ RH
E
Oscillations
15
10
5
0
****
Uninfected
+ RH

Ca^{2+} responses in individual cells. Figure 6.3C, top panel, and movie M6.2 show that control uninfected cells show robust Ca^{2+} signaling in response to antigen, with 94% of the cells responding with an average of 12 oscillations during a 10-minute period. In contrast, as shown in Fig. 6.3C, bottom, and movie M6.3, the RH-tomato infected cells are much less responsive, such that only 58% of cells with one or more parasites inside respond, typically with a slower onset, and with an average of 6 oscillations over the same time period. These parameters are compared in Figures 6.3D and E.

It is known that intracellular parasites interact extensively with the ER [24], and one possibility is that these interactions somehow block the exit of Ca^{2+} from the ER during antigen-stimulated, IP_3-dependent depletion of ER Ca^{2+}. Receptor-mediated, IP_3-dependent release of Ca^{2+} from ER stores can be bypassed by treating cells with thapsigargin, a SERCA pump inhibitor, resulting in passive leakage of Ca^{2+} from the ER that activates SOCE. Under this treatment, cells infected with any type of parasite have comparable Ca^{2+} responses to uninfected cells (Figure 6.4 A,B), showing that *T. gondii* is not directly blocking SOCE. Collectively, these results indicate that a common factor, shared by the three genotypes of parasite, inhibits granule exocytosis via a mechanism that inhibits Ca^{2+} mobilization upstream of SOCE.

T. gondii does not markedly change the abundance of phosphoinositides at the plasma membrane of infected cells.

Antigen stimulation of FcεRI activates phospholipase Cγ (PLCγ), resulting in cleavage of phosphatidylinositol 4,5-bisphphosphate (PIP_2) to diacylglycerol (DAG) and

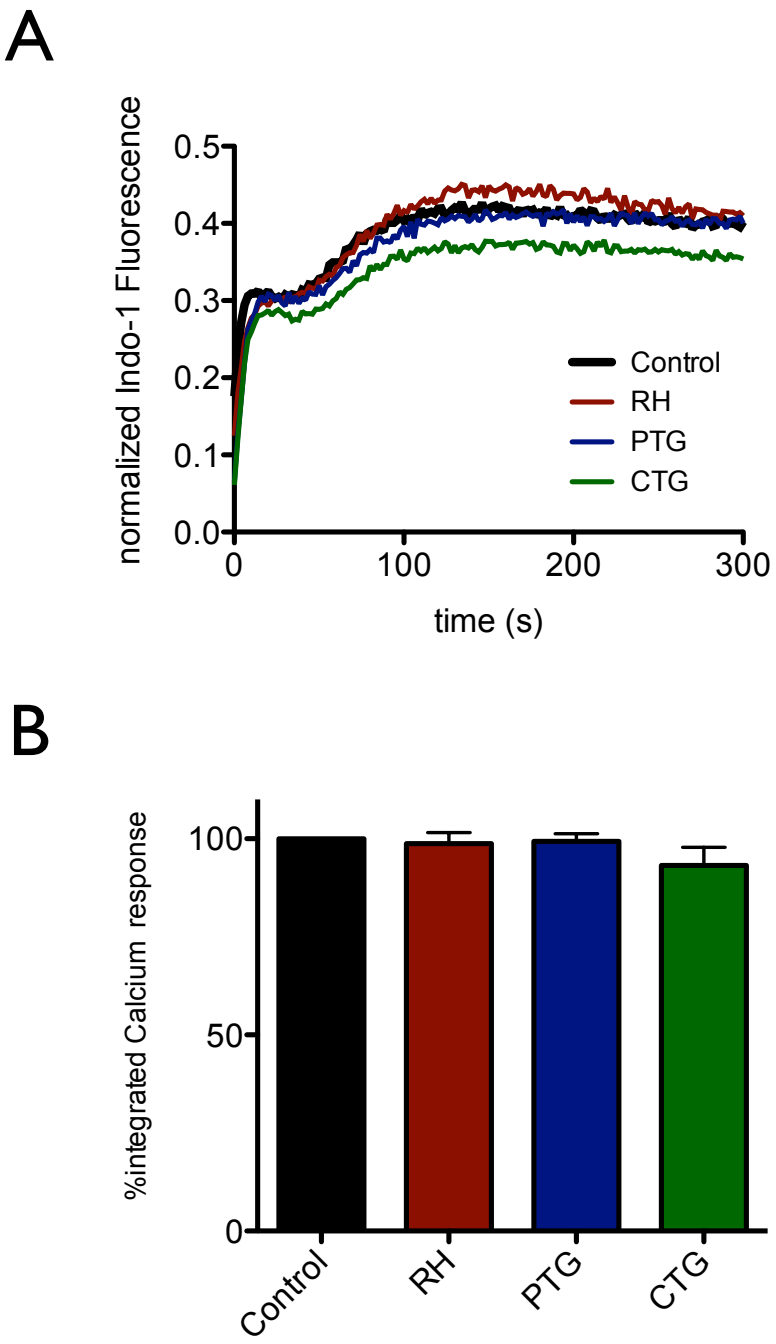

Figure 6.4. Infection does not affect calcium responses to ER store release by thapsigargin. (A) Representative Indo-1 fluorescence measurements of calcium responses to 200 nM thapsigargin in control (black), RH (red), PTG (blue) or CTG (green) infected cells (MOI 10:1). (B) Integrated calcium responses over 300 seconds of stimulation as a percentage of control calcium response. Bars represent average of 3-5 independent experiments. Error bars represent SEM.

inositol 1,4,5-trisphosphate (IP_3). This, in turn, triggers Ca^{2+} release from ER stores via IP_3 receptors at the ER. One possible mechanism of inhibition of this process is that intracellular parasites might sequester PIP_2, such that it is no longer available for cleavage by PLCγ. To address this possibility, we assessed whether infection by *Toxoplasma* alters the plasma membrane association of GFP-tagged PH-PLCδ that is highly specific for PIP_2 [25]. The relative concentration of PIP_2 at the plasma membrane was assessed by determining the ratio GFP-PH-PLCδ at this membrane to its concentration in the cytoplasm as illustrated in Figure 6.5A. As summarized in Figure 6.5B, we find that infection does not change the ratio of plasma membrane to cytoplasmic fluorescence, indicating that *T. gondii* does not reduce PIP_2 levels at the plasma membrane, and thus does not apparently inhibit antigen-stimulated Ca^{2+} mobilization by this mechanism. In Chapter 5 we also documented that PIP_2 is not sequestered in the PVM.

Previously, it was shown that phosphorylation of PLCγ_1 is dependent on PI3 kinase (PI3K) [26]. We reasoned if *T. gondii* infection alters PI3K activity, we should see a change in the amount of phosphatidylinositol 3,4,5-trisphosphate (PIP_3) at the plasma membrane. Similar to detection of PIP_2 with GFP-PLCδ PH domain, we could use a GFP-tagged PH domain (PH-Akt) that specifically binds PI 3,4-P_2 and PIP_3 as an affinity tag to assess the relative amount of these species at the plasma membrane.

We found that, like PIP_2, there does not appear to be a gross change in the amount of PIP_3 at the plasma membrane (Figure 6.5C, D). These results make it

Figure 6.5. PIP_2 and PIP_3 levels at the plasma membrane are not altered by *T. gondii* infection. (A) Representative images showing uninfected (top) or RH-tomato infected (bottom) RBL cells transiently transfected with EGFP-PH-PLCδ. Accompanying fluorescence intensity profiles are taken along the white lines indicated in each image. (B) Ratio of plasma membrane to cytoplasmic EGFP-PH-PLCδ fluorescence (given by intensity profiles as shown in (A)) as a relative measure of PIP_2 at the plasma membrane. (C) Representative images showing uninfected (top) or RH-tomato infected (bottom) RBL cells transiently transfected with EGFP-PH-Akt. Accompanying fluorescence intensity profiles are taken along the white lines indicated in each image. (D) Ratio of plasma membrane to cytoplasmic EGFP-PH-Akt fluorescence as a relative measure of PIP_3 at the plasma membrane. Data in (B) and (D) represent at least 30 cells for each condition collected over 3 experiments. Error bars indicate SEM.

A

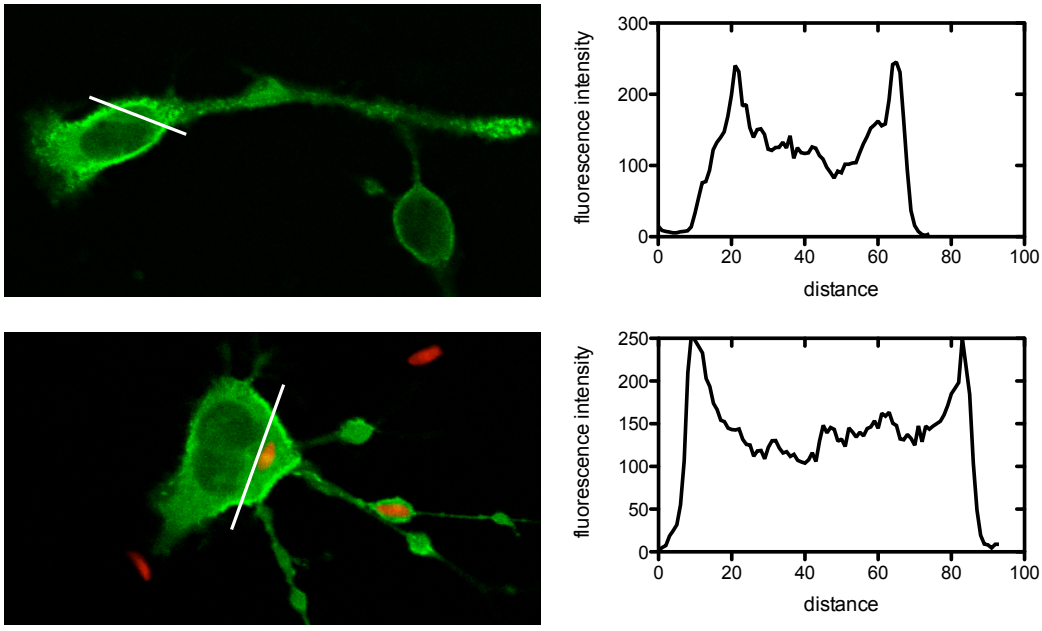
fluorescence intensity
300
200
100
0
0
20
40
60
80
100
distance
fluorescence intensity
250
200
150
100
50
0
0
20
40
60
80
100
distance

B

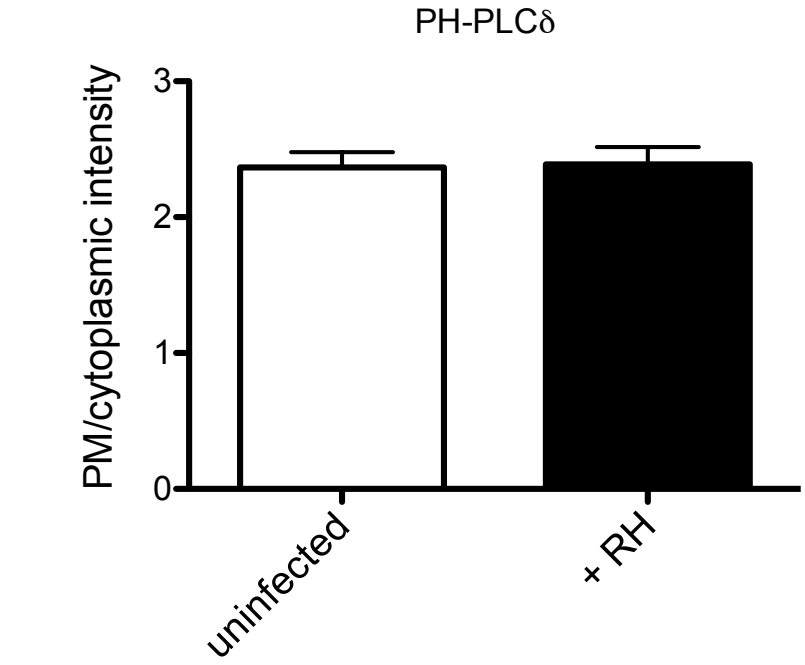
PH-PLCδ
PM/cytoplasmic intensity
3
2
1
0
uninfected
+ RH

Figure 6.5. (continued)

C

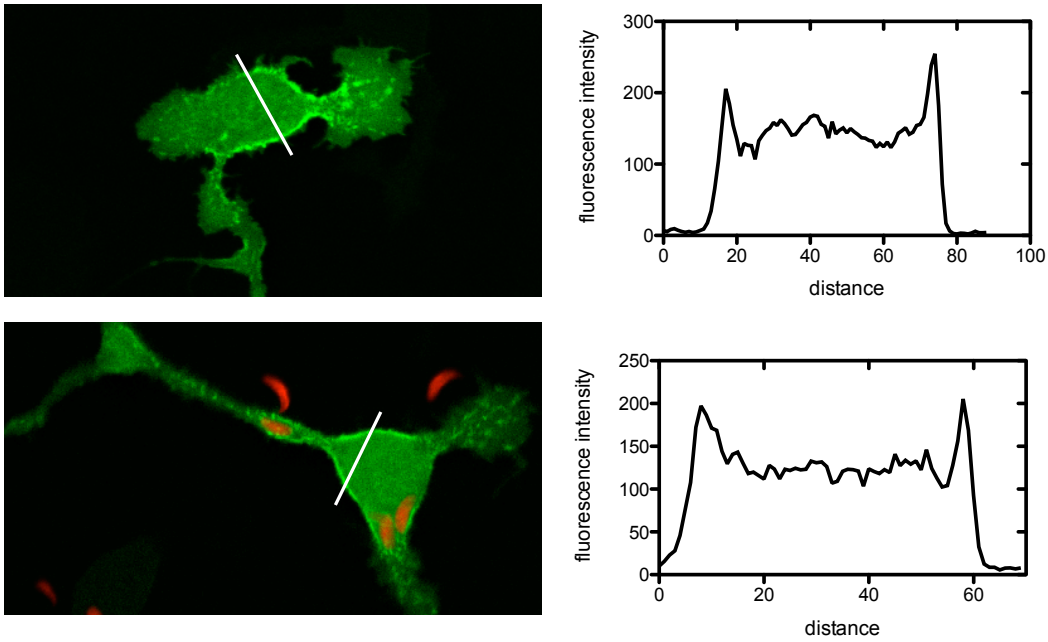

D

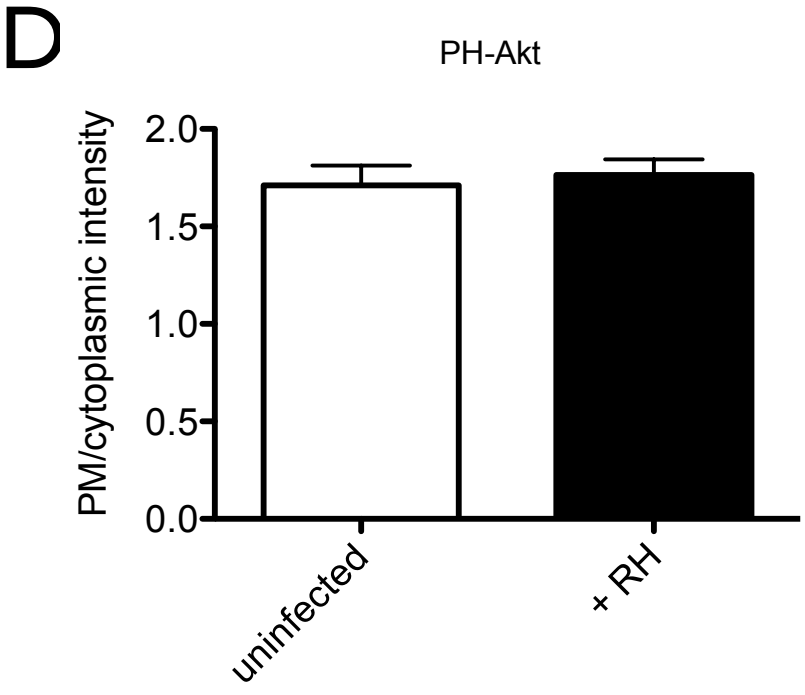

unlikely that changes in PIP_3 levels are the cause of reduced Ca^{2+} mobilization caused by *Toxoplasma* infection.

PLCγ activation is reduced in Toxoplasma-infected RBL-2H3 cells.

Since phosphoinositide availability at the plasma membrane does not appear to be significantly changed in infected RBL cells, we next asked whether the parasite-mediated inhibition is due to a defect in $PLC\gamma_1$ activitation. In order for $PLC\gamma_1$ to enzymatically cleave PIP_2, it must be recruited to the plasma membrane and phosphorylated at tyrosine 783 (Y783). Western blotting with anti-pY783-$PLC\gamma_1$ shows that this antigen-stimulated phosphorylation is reduced in infected samples following antigen stimulation (Figure 6.6A). At 10 minutes post-stimulation in the presence of RH parasite, pY783-$PLC\gamma_1$ is reduced by ~50% (figure 6.6B).

To further assess the activity of PLCγ, we asked if antigen-mediated IP_3 generation was reduced in *T. gondii* infected RBL cells. Specifically, we looked at calcium mobilization in the absence of extracellular calcium as a measurement of PLCγ functionality. Figure 6.6C is a representative experiment that shows all parasite types significantly reduce the amount of calcium released from stores in response to antigen. Over multiple experiments, parasite infection reduces the peak calcium release by 37, 50 and 49% for RH, PTG and CTG, respectively (Figure 6.6D). Together, these results support a mechanism in which *T. gondii* acts to inhibit PLCγ activation through blocking the tyrosine phosphorylation of this lipase.

Figure 6.6. PLCγ_1 activity is reduced in T. gondii-infected RBL-2H3 cells. (A) Representative Indo-1 fluorescence measurements of Ca^{2+} responses to 10 ng/ml DNP-BSA in the absence of extracellular Ca^{2+} in control uninfected (black), RH-infected (red), PTG-infected (blue) or CTG-infected (green) cells (MOI 10:1). (B) Peak calcium responses as a percentage of control Ca^{2+} response. Histogram shows averages of 3 independent experiments. Error bars represent SEM (* is $P<0.05$ and ** is $P<0.01$ relative to control cells). (C) Western blot of phospho-PLCγ_1 (pY-783) (top) or total PLCγ_1 (bottom) in control or RH infected (MOI 10:1, 1 hr) cells lysed at 0, 2, 5, or 10 minutes after addition of DNP-BSA (10 ng/ml). (D) Ratio of phospho-PLCγ_1 (pY-783) to total PLCγ_1 shown in (C).

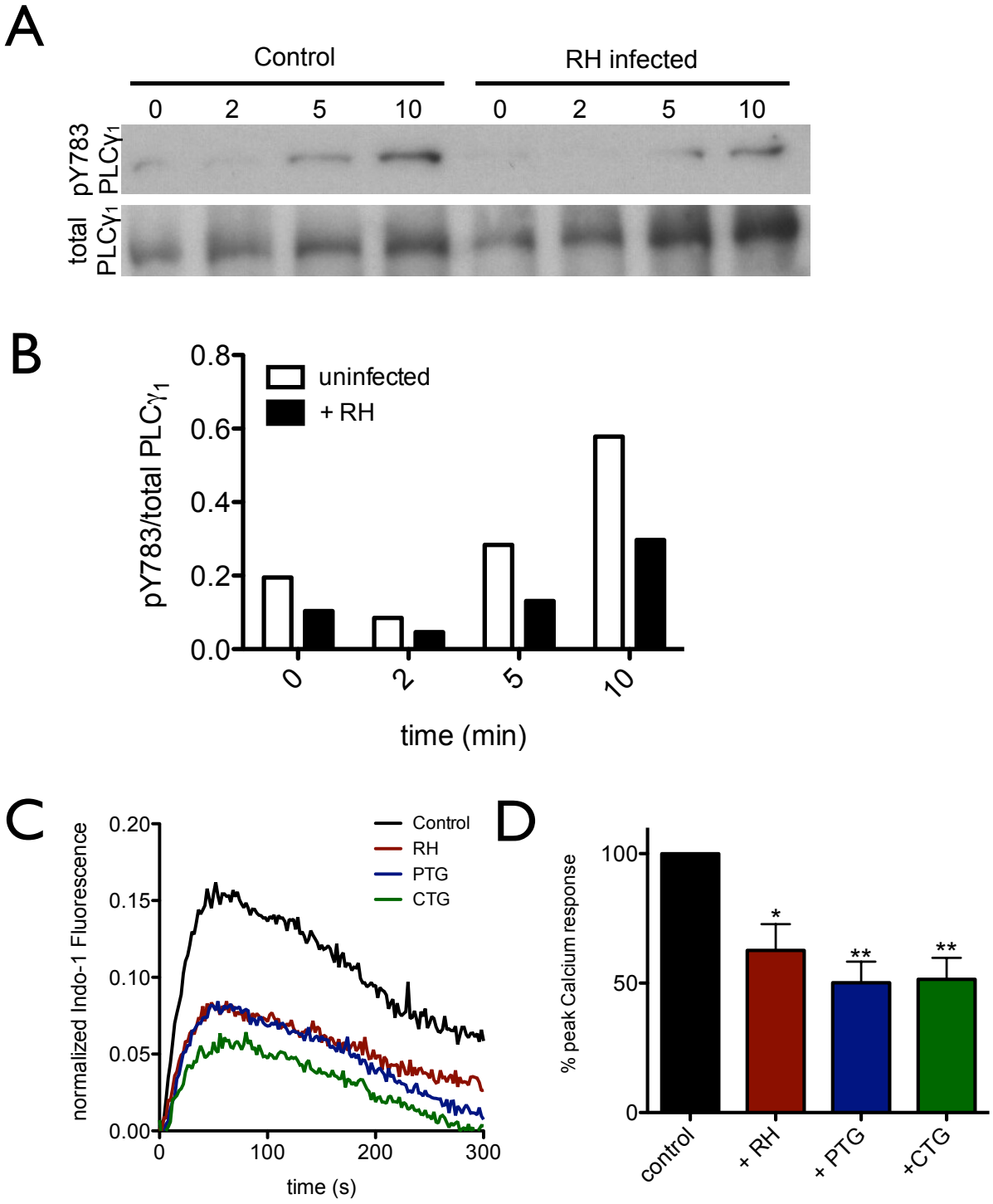
A
Control
RH infected
0
2
5
10
0
2
5
10
pY783 PLCγ1
total PLCγ1
B
pY783/total PLCγ1
0.8
0.6
0.4
0.2
0.0
uninfected
+ RH
0
2
5
10
time (min)
C
normalized Indo-1 Fluorescence
0.20
0.15
0.10
0.05
0.00
Control
RH
PTG
CTG
0
100
200
300
time (s)
D
% peak Calcium response
100
50
0
*
**
**
control
+ RH
+ PTG
+CTG

Inhibition of mast cell signling by T. gondii requires parasite attachment, but not complete invasion.

Our single cell Ca^{2+} and degranulation measurements indicate that the inhibitory action of *T. gondii* requires direct contact between the host cell and parasite, and possibly parasite entry. To more directly address these issues, we initially compared the effect of infecting RBL cells with the RH parasite strain to incubation with the supernatant from an equivalent number of parasites on antigen-stimulated degranulation. As shown in Figure 6.7A, neither the RH supernatant nor the supernatant from RH-infected fibroblasts were capable of inhibition antigen-stimulated degranulation under conditions in which infection by intact parasites was effective. In fact, the supernatant from the RH parasites caused a modest potentiation of the degranulation response to antigen. Additionally, degranulation cannot be inhibited by heat-killed or fixed parasites (data not shown).

Invasion is dependent on the parasite cytoskeleton [27]. Therefore, infections carried out in the presence of the actin inhibitor cytochalasin D result in a frustrated state where parasites can attach and secrete proteins into the host cell but cannot complete invasion [27]. Cytochalasin D is known to enhance degranulation responses of RBL cells to antigen [28], and, as expected, we see robust stimulated degranulation under these conditions (Figure 7.7B). However, degranulation in the presence of cytochalasin D and RH parasites is reduced by 50% compared to that in the absence of the parasites (Figure 7.7B). Microscopic observations under these conditions show, as expected, that infection rates in the presence of cytochalasin D are quite low (Figure

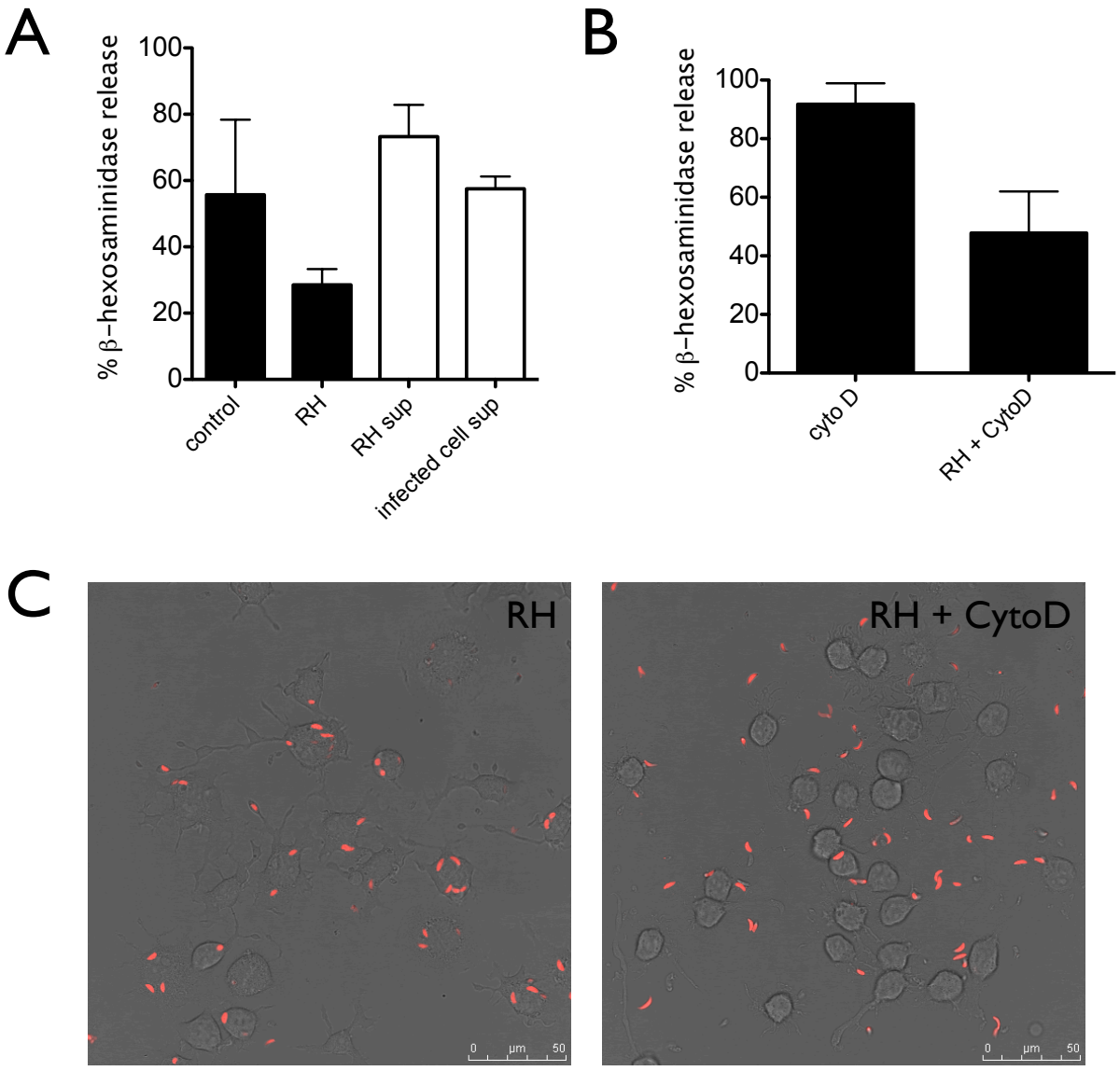

Figure 6.7. Tachyzoite attachment, but not invasion, is necessary for inhibition of degranulation. (A) RBL-2H3 cells were incubated with parasites (RH) or with supernatants from parasites (RH sup) or infected fibroblast supernatant (infected cell sup). Degranulation assessed by β-hexosaminindase release after 1 hour of infection as described in Materials and Methods. (B) *T. gondii* infections (MOI 10:1) were carried out in the presence of cytochalasin D (1 μM) to prevent invasion. Histogram shows averages from triplicate samples and error bars represent SD. (C) Confocal microscopy of RBL cells infected with RH tomato parasites in the presence or absence of cytochalasin D. Data are representative of 2-3 independent experiments.

7.7C), consistent with the conclusion that inhibition under these conditions is due to attached, not intracellular parasites. This result indicates that the agent responsible for mediating inhibition of degranulation, likely by acting on PLCγ activation, is secreted very early during the invasion process.

DISCUSSION

Based on its global prevalence and ability to infect a multitude of hosts, *T. gondii* is seen as one of the world's most successful parasites. Its success is due, in part, to the arsenal of immune-modulatory mechanisms it employs. Recent evidence demonstrates *T. gondii* disrupts normal chromatin remodeling resulting in the downregulation of cytokine expression [29]. These parasites also secrete proteins that act on signaling steps upstream of cytokine gene transcription, dramatically altering the type of immune response generated [3]. These examples suggest that a major strategy of *T. gondii* immune subversion is one of efficiency. That is, the parasite precisely targets cell signaling mechanisms that results in broad changes that overall benefit parasite survival and replication. Our current study uncovers another central target of parasite interference.

In vivo, *T. gondii* is known to preferentially infect immune effector cells, including macrophages and dendritic cells [30, 31]. For many immune cells, effector function is measured by cytokine production, a process that can often take several hours or even days to occur. We set out to determine if *T. gondii* has the capacity to interfere with signaling steps that happen more immediately. FcεRI-triggered degranulation in mast

cells occurs within minutes of stimulation and continues for at least an hour. As a result, this is an appropriate model to investigate how infection may acutely modulate immune signaling. Intracellular Ca^{2+} levels are tightly regulated and elevation of intracellular Ca^{2+} is critical in immune responses in multiple cell types and contexts [11, 32, 33]. Intracellular parasites are sensitive to host Ca^{2+} responses, in fact, exogenously stimulating Ca^{2+} influx by treatment with calcium ionophore triggers tachzioyte egress [34].

Ca^{2+} mobilization is an important and well-studied aspect of IgE/FcεRI-mediated signaling in mast cells. When our initial experiments revealed that parasite infection suppresses degranulation responses in RBL cells, it immediately suggested that parasites might act at the level of Ca^{2+} mobilization. We showed that parasite infection can block antigen-mediated, but not thapsigargin-triggered, Ca^{2+} elevation, indicating that infection acts upstream of Ca^{2+} release from stores. Inhibition of Ca^{2+} mobilization in the absence of extracellular Ca^{2+} further supports this explanation. Hydrolysis of PIP_2 mediated by PLCγ to produce IP_3 and DAG is a critically important in Ca^{2+} mobilization by antigen. One possible mechanism to account for decreased Ca^{2+} store release in response to antigen is that the parasite alters the amount or availability of PLCγ's substrate, PIP_2, at the plasma membrane. Our results make this unlikely, as we detect no significant change in the association of PH-PLCδ with PIP_2 at the plasma membrane due to infection by T. gondii. We do, however, see a reduction the level of activating tyrosine phosphorylation of $PLC\gamma_1$ during infection, suggesting that *Toxoplasma* is not actively reducing the amount of PIP_2 but rather the host's capacity hydrolyze that PIP_2.

PLCγ_1 activity in mast cells is regulated by PI3 kinase-mediated production of PIP_3 [26], but our results indicate that the parasite doe not significantly changes the level of PIP_3, in infected cells. Our data collectively suggest a model in which a *T. gondii* derived protein acts directly to reduce the activity of PLCγ_1, thereby reducing the levels of IP_3 and inhibiting subsequent signaling steps.

Additionally, our work suggests that the factor is a secreted product released by the parasite at very early steps during the invasion process. Previous work determined that invasion is a multi-step process. In early steps, parasites attach to the host plasma membrane and release the contents of the rhoptries [27]. Genomic sequencing revealed that rhoptry proteins of the ROP family, including ROP16 and ROP18, which are secreted during invasion, are key virulence factors in *T. gondii* infection [6, 7]. Recently, ROP16 has been shown to directly phosphorylate host proteins [35, 36]. Their temporal release, relation to virulence and immunomodulatory capabilites [35, 37] make ROP proteins attractive candidates for the *Toxplasma* secreted factor responsible for the reduction of PLCγ_1 activity. Future work should aim to determine which parasite-derived protein(s) are responsible for the inhibition we observe.

Furthermore, it will be important to assess whether downregulation of PLCγ signaling is manifest in other immune cells that are targeted by *T. gondii*. To this end, there is initial evidence that *T. gondii* infection reduces fMLP-triggered Ca^{2+} signaling in mouse neutrophils (Abi Abdallah and Denkers, unpublished results). Collectively, these results suggest that *T. gondii* targets PLC activation as a mechanism to globally down regulate immune signaling that occurs via Ca^{2+} mobilization.

CONTRIBUTIONS AND ACKNOWLEDGEMENTS

Research designed by N. L. Smith, E.Y. Denkers and D. A. Holowka; N. L. Smith performed and analyzed experiments. Research supported by National Institutes of Heath Grants R01 AI022449 (B. A. Baird and D. A. Holowka).

We thank Carol Bayles for maintaining the Cornell Microscopy and Imaging Facility and Rodman Getchell for maintenance of the SP5 Leica Confocal system. We also thank Delbert S. Abi-Abdallah and Barbara Butcher for helpful discussions.

REFERENCES

1. Dubey, J.P., *Advances in the life cycle of Toxoplasma gondii.* Int J Parasitol, 1998. **28**(7): p. 1019-24.

2. Sibley, L.D., *Intracellular parasite invasion strategies.* Science, 2004. **304**(5668): p. 248-53.

3. Laliberte, J. and V.B. Carruthers, *Host cell manipulation by the human pathogen Toxoplasma gondii.* Cell Mol Life Sci, 2008. **65**(12): p. 1900-15.

4. Leng, J., B.A. Butcher, and E.Y. Denkers, *Dysregulation of macrophage signal transduction by Toxoplasma gondii: past progress and recent advances.* Parasite Immunol, 2009. **31**(12): p. 717-28.

5. Lambert, H. and A. Barragan, *Modelling parasite dissemination: host cell subversion and immune evasion by Toxoplasma gondii.* Cell Microbiol, 2010. **12**(3): p. 292-300.

6. Saeij, J.P., et al., *Polymorphic secreted kinases are key virulence factors in toxoplasmosis.* Science, 2006. **314**(5806): p. 1780-3.

7. Taylor, S., et al., *A secreted serine-threonine kinase determines virulence in the eukaryotic pathogen Toxoplasma gondii.* Science, 2006. **314**(5806): p. 1776-80.

8. Metcalfe, D.D., D. Baram, and Y.A. Mekori, *Mast cells.* Physiol Rev, 1997. **77**(4): p. 1033-79.

9. Marshall, J.S., *Mast-cell responses to pathogens.* Nat Rev Immunol, 2004. **4**(10): p. 787-99.

10. Cambier, J.C., *Antigen and Fc receptor signaling. The awesome power of the immunoreceptor tyrosine-based activation motif (ITAM).* J Immunol, 1995. **155**(7): p. 3281-5.

11. Putney, J.W., *Capacitative calcium entry: from concept to molecules.* Immunol Rev, 2009. **231**(1): p. 10-22.

12. Posner, R.G., et al., *Aggregation of IgE-receptor complexes on rat basophilic leukemia cells does not change the intrinsic affinity but can alter the kinetics of the ligand-IgE interaction.* Biochemistry, 1992. **31**(23): p. 5350-6.

13. Gidwani, A., et al., *Disruption of lipid order by short-chain ceramides correlates with inhibition of phospholipase D and downstream signaling by FcepsilonRI.* J Cell Sci, 2003. **116**(Pt 15): p. 3177-87.

14. Naal, R.M., et al., *In situ measurement of degranulation as a biosensor based on RBL-2H3 mast cells.* Biosens Bioelectron, 2004. **20**(4): p. 791-6.

15. Young, R.M., et al., *Reconstitution of regulated phosphorylation of FcepsilonRI by a lipid raft-excluded protein-tyrosine phosphatase.* J Biol Chem, 2005. **280**(2): p. 1230-5.

16. Smith, N.L., et al., *Sphingosine derivatives inhibit cell signaling by electrostatically neutralizing polyphosphoinositides at the plasma membrane.* Self Nonself, 2010. **1**(2): p. 133-143.

17. Field, K.A., et al., *Mutant RBL mast cells defective in Fc epsilon RI signaling and lipid raft biosynthesis are reconstituted by activated Rho-family GTPases.* Mol Biol Cell, 2000. **11**(10): p. 3661-73.

18. Cohen, R., et al., *Ca2+ waves initiate antigen-stimulated Ca2+ responses in mast cells.* J Immunol, 2009. **183**(10): p. 6478-88.

19. Varnai, P. and T. Balla, *Visualization of phosphoinositides that bind pleckstrin homology domains: calcium- and agonist-induced dynamic changes and relationship to myo-[3H]inositol-labeled phosphoinositide pools.* J Cell Biol, 1998. **143**(2): p. 501-10.

20. Srinivasan, S., et al., *Rac and Cdc42 play distinct roles in regulating PI(3,4,5)P3 and polarity during neutrophil chemotaxis.* J Cell Biol, 2003. **160**(3): p. 375-85.

21. Gosse, J.A., et al., *Transmembrane sequences are determinants of immunoreceptor signaling.* J Immunol, 2005. **175**(4): p. 2123-31.

22. Blank, U. and J. Rivera, *The ins and outs of IgE-dependent mast-cell exocytosis.* Trends Immunol, 2004. **25**(5): p. 266-73.

23. Di Capite, J. and A.B. Parekh, *CRAC channels and Ca2+ signaling in mast cells.* Immunol Rev, 2009. **231**(1): p. 45-58.

24. Sinai, A.P. and K.A. Joiner, *Safe haven: the cell biology of nonfusogenic pathogen vacuoles.* Annu Rev Microbiol, 1997. **51**: p. 415-62.

25. Ferguson, K.M., et al., *Scratching the surface with the PH domain.* Nat Struct Biol, 1995. **2**(9): p. 715-8.

26. Barker, S.A., et al., *Wortmannin-sensitive phosphorylation, translocation, and activation of PLCgamma1, but not PLCgamma2, in antigen-stimulated RBL-2H3 mast cells.* Mol Biol Cell, 1998. **9**(2): p. 483-96.

27. Hakansson, S., A.J. Charron, and L.D. Sibley, *Toxoplasma evacuoles: a two-step process of secretion and fusion forms the parasitophorous vacuole.* EMBO J, 2001. **20**(12): p. 3132-44.

28. Frigeri, L. and J.R. Apgar, *The role of actin microfilaments in the down-regulation of the degranulation response in RBL-2H3 mast cells.* J Immunol, 1999. **162**(4): p. 2243-50.

29. Leng, J. and E.Y. Denkers, *Toxoplasma gondii inhibits covalent modification of histone H3 at the IL-10 promoter in infected macrophages.* PLoS One, 2009. **4**(10): p. e7589.

30. Bierly, A.L., et al., *Dendritic cells expressing plasmacytoid marker PDCA-1 are Trojan horses during Toxoplasma gondii infection.* J Immunol, 2008. **181**(12): p. 8485-91.

31. Denkers, E.Y. and B.A. Butcher, *Sabotage and exploitation in macrophages parasitized by intracellular protozoans.* Trends Parasitol, 2005. **21**(1): p. 35-41.

32. Andersson, T., et al., *Characterization of fMet-Leu-Phe receptor-mediated Ca2+ influx across the plasma membrane of human neutrophils.* Mol Pharmacol, 1986. **30**(5): p. 437-43.

33. Penner, R. and E. Neher, *Secretory responses of rat peritoneal mast cells to high intracellular calcium.* FEBS Lett, 1988. **226**(2): p. 307-13.

34. Caldas, L.A., W. de Souza, and M. Attias, *Calcium ionophore-induced egress of Toxoplasma gondii shortly after host cell invasion.* Vet Parasitol, 2007. **147**(3-4): p. 210-20.

35. Ong, Y.C., M.L. Reese, and J.C. Boothroyd, *Toxoplasma rhoptry protein 16 (ROP16) subverts host function by direct tyrosine phosphorylation of STAT6.* J Biol Chem, 2010. **285**(37): p. 28731-40.

36. Yamamoto, M., et al., *A single polymorphic amino acid on Toxoplasma gondii kinase ROP16 determines the direct and strain-specific activation of Stat3.* J Exp Med, 2009. **206**(12): p. 2747-60.

37. Butcher, B.A., et al., *Toxoplasma gondii Rhoptry Kinase ROP16 Activates STAT3 and STAT6 Resulting in Cytokine Inhibition and Arginase-1-Dependent Growth Control.* PLoS Pathog, 2011. **7**(9).

CHAPTER SEVEN

Summary and Future Directions

While mast cells are best known for the detrimental effects of allergies and asthma, which alone make them an important subject of investigation, they can also play more diverse effector roles in the immune system. Furthermore, the well-studied FcεRI signaling pathway serves as a useful model for related, and sometimes more complicated, signaling pathways in other immune cells types. The breadth of this thesis demonstrates how studying the cellular responses of mast cells under various conditions can reveal a tremendous amount of information in subjects as diverse as membrane heterogeneity and the molecular mechanisms of parasitic immunomodulation.

For many years, it was thought that the precise nature of the lipid environment surrounding signaling proteins was not important for the signaling outcome, but rather simply an environment through which the proteins could freely diffuse. Research in our lab and others has demonstrated the important regulatory contributions that ordered lipid microenvironments make to immune signaling [1]. The relevance of these so-called lipid rafts has not been without controversy, in part because of the non-physiological methods used for examination as well as the transient and nanoscale features of these membrane domains [2, 3].

While using non-physiological methods requires some caution, they are still useful correlative tools. One such method is detergent resistant fractionation of cellular

membranes, and this provided the foundation for the mass spectrometric analysis described in Chapter 2. We established that stimulation-induced changes in the lipid composition of DRMs are mimicked by destabilizing the actin cytoskeleton and prevented by stabilizing the actin cytoskeleton. These results imply that regulation of the actin cytoskeleton plays a large role in regulating the lipid composition of the DRMs. By extension, our results suggest an important interplay between cytoskeletal proteins and the lipids involved in the membrane heterogeneity surrounding signaling proteins in mast cells.

Non-destructive methods for visualizing and understanding the nature of membrane heterogeneity are being developed [4, 5]. In particular, recent advances in sub-optical resolution light microscopy [6], will prove useful for the visualization of membrane heterogeneities, which are estimated to exist on sub-micron length scales under physiological conditions. Nearly all methods suffer from experimental or interpretational limitations, so a combination of methods will be necessary to fully reveal the mechanisms that regulate membrane heterogeneity as it relates to immunoreceptor signaling.

The signaling that emanates from IgE-FcεRI crosslinking has been extensively studied for many years, but it is only recently appreciated that this signaling alters RE trafficking. Naal et al. first established that IgE-mediated signaling results in the stimulated outward trafficking of RE [7]. Furthermore, this trafficking is extremely robust and refractory to many modes of inhibition, but it is sensitive to inhibition of Ca^{2+} moblization [7]. Chapter 3 demonstrated that sphingosine derivatives, D-sphingosine

and DMS, are potent inhibitors of antigen and ionophore-stimulated RE trafficking. These derivatives also inhibit degranulation. Ca^{2+} mobilization is a shared signal for both RE trafficking and granule exocytosis, and is also inhibited by sphingosine derivatives. The use of a genetically encoded PM-associated phosphoinositide sensor, mRFP-MARCKS ED^{SA3}, indicated that these derivatives function by neutralizing negatively charged phosphoinositides at the plasma membrane and thereby causing inhibition of Ca^{2+} mobilization, a central player in multiple signaling pathways.

Revealing the mechanism by which sphingosine derivatives inhibit mast cell signaling has several important ramifications. It demonstrates a role for plasma membrane phosphoinositdes in Ca^{2+} signaling. It provides a likely mechanism for earlier work showing that sphingosine derivatives inhibit SOCE [8] and the more recent finding that sphingosine derivatives reduce coupling of Orai1 and Stim1 necessary for SOCE [9]. Additionally, D-sphingosine and DMS also block Ca^{2+} signaling upstream of store release, indicating that these derivatives act at multiple steps of Ca^{2+} mobilization. At the same time, it makes less likely that the inhibitory effects of DMS are a result of blocking sphingosine-1-kinase production of sphingosine-1-phosphate as previously proposed [10, 11].

In part, the initial motivation for our study of sphingosine-mediated inhibition was to develop tools to probe the function and regulation of RE trafficking in mast cells. The initial work by Naal et al. suggested that the rapid outward trafficking of RE in stimulated RBL cells provided membrane necessary for processes such as plasma membrane remodeling and ruffling [7]. Interestingly, when antigen was restricted to specific regions

of a patterned surface, RE trafficked to the site of antigen ligation [12]. Such directed trafficking is an extremely interesting phenomenon, and suggests a specific function. In other immune cells types, RE are known to transport cytokines [13, 14], and even more interestingly they are involved in directed trafficking of certain cytokines [15]. Collectively, these results were the motivation for assessing the involvement of RE in the trafficking of cytokines in mast cells.

Preliminary experiments demonstrated partial colocalization of newly synthesized IL-4 with RE. Surprisingly, siRNA knockdown of Rab11A, which is known to regulate RE trafficking, does not inhibit cytokine release. Further studies reveal that Rab11A knockdown does not negatively impact antigen-mediated outward trafficking of CTxB-labeled RE. These results suggest, in agreement with Balasubramanian et al., that RE do not exist as a homogeneous organelle, but instead are comprised of differentially regulated pools of membrane [16]. The inability to precisely target and inhibit RE trafficking in RBL cells continues to be a limitation, and, as a result, this limits the conclusions that can be made concerning the involvement of RE in cytokine trafficking. Future studies will need new methods to more directly address this problem. Making use of chemical inactivation [17] or genetically encoded markers (e.g. TNFα) in conjunction with dominant negative or constitutively active GTPases, such as Rab11A and Arf6, may prove useful.

RE have diverse functions in multiple cell types, often in processes that require directional trafficking of large quantities of membrane [18]. One such example is the demonstration that RE traffic to the site of phagocytosis [13]. Additionally, RE are

implicated in interactions with several bacterial vacuoles [19, 20]. The obligate intracellular parasite *Toxoplasma gondii* enters host cells through a process of active invasion distinct from phagocytosis [21], but, similar to phagocytosis, the parasite resides inside a host-derived membrane following invasion. The precise sources of this membrane have been unclear. Utilizing a differential CTxB labeling protocol to distinguish between RE and PM membrane pools in RBL mast cells, the results in Chapter 5 strongly suggest that RE of host cells contribute to the nascent PV of *Toxoplasma*. Evidence from experiments using additional RE markers support this result.

The importance of RE trafficking to the *T. gondii* vacuole is currently being addressed. One hypothesis is that RE contributions to the PV provide membrane necessary for PV expansion during parasite replication. The use of mutant RBL cells with defects in RE trafficking (J. Wilson, unpublished results) will be useful for these studies. Additionally, over-expression or siRNA-mediated knockdown of RE regulators may be illuminating. Uncovering the details of RE-*Toxoplasma* interactions will provide important information concerning both the unique intracellular environment of *Toxoplasma* and, more generally, the regulation of RE trafficking.

Like many pathogens, *T. gondii* has developed multiple mechanisms to subvert the immune function of its host [22]. Chapter 6 documents a previously unknown mechanism of immunomodulation, *Toxoplasma*-mediated inhibition of PLCγ_1 that results in the reduction of antigen-stimulated Ca^{2+} mobilization and degranulation in RBL mast cells. Future work should aim to determine the parasite-derived factor

necessary for PLCγ_1 inhibition. The demonstration that inhibition can occur in the presence of cytochalasin D, suggests that proteins secreted at the time of invasion are promising candidates. A good example of possible effectors is the ROP family of proteins secreted by parasite rhoptries concurrently with invasion. PLCγ-mediated cleavage of PIP_2 into DAG and IP_3 plays an essential role in FcεRI receptor signaling, but is also extremely important in other immune signaling pathways. As such, these results may extend to modulation of PLCγ-mediated signaling in macrophages and dendritic cells, as both are preferentially infected by *T. gondii*. Furthermore, it will be important to investigate how this inhibitory mechanism interacts with other known mechanisms of immunomodulation to affect the course of infection.

Additionally, there is the possibility that down regulation of immune responses in mast cells is important in *in vivo* infections, particularly co-infection situations. Laboratory conditions are tightly controlled to ensure that experimental hosts only encounter a single pathogen. However, in nature that probably not the case, in fact, it is more likely hosts are routinely dealing with concurrent exposure to multiple pathogens. Thus, while infection of mast cells by *T. gondii* is not thought to be common, there are situations in which mast cell infection could be highly relevant. For example, individuals infected with the parasitic worm *Trichinella spiralis* experience mastocytosis in the gut that is accompanied by increased intestinal permeability and parasite-induced intestinal damage [23]. If a *Trichinella*-infected host was concurrently infected with *T. gondii*, this altered intestinal environment might contribute to dramatic increases in the number of

Toxoplasma-infected mast cells. In this situation, *Toxoplasma* could very well need a mechanism to control normal mast cell function.

Collectively, this body of work demonstrates how detailed research on the well-documented IgE-FcεRI signaling pathways continues to reveal important discoveries on aspects of mast cell biology and function. Furthermore, these efforts do much more than just further our understanding of the allergic response; this work contributes to our understanding of many topics important in immune function, including the basis of membrane heterogeneity, regulation and function of membrane trafficking, and how pathogens and their hosts interact.

REFERENCES

1. Holowka, D., et al., *Lipid segregation and IgE receptor signaling: a decade of progress.* Biochim Biophys Acta, 2005. **1746**(3): p. 252-9.

2. Edidin, M., *The state of lipid rafts: from model membranes to cells.* Annu Rev Biophys Biomol Struct, 2003. **32**: p. 257-83.

3. Munro, S., *Lipid rafts: elusive or illusive?* Cell, 2003. **115**(4): p. 377-88.

4. Brown, D.A., *Lipid rafts, detergent-resistant membranes, and raft targeting signals.* Physiology (Bethesda), 2006. **21**: p. 430-9.

5. Sengupta, P., B. Baird, and D. Holowka, *Lipid rafts, fluid/fluid phase separation, and their relevance to plasma membrane structure and function.* Semin Cell Dev Biol, 2007. **18**(5): p. 583-90.

6. Toomre, D. and J. Bewersdorf, *A new wave of cellular imaging.* Annu Rev Cell Dev Biol, 2010. **26**: p. 285-314.

7. Naal, R.M., et al., *Antigen-stimulated trafficking from the recycling compartment to the plasma membrane in RBL mast cells.* Traffic, 2003. **4**(3): p. 190-200.

8. Mathes, C., A. Fleig, and R. Penner, *Calcium release-activated calcium current (ICRAC) is a direct target for sphingosine.* J Biol Chem, 1998. **273**(39): p. 25020-30.

9. Calloway, N., et al., *Molecular clustering of STIM1 with Orai1/CRACM1 at the plasma membrane depends dynamically on depletion of Ca2+ stores and on electrostatic interactions.* Mol Biol Cell, 2009. **20**(1): p. 389-99.

10. Itagaki, K. and C.J. Hauser, *Sphingosine 1-phosphate, a diffusible calcium influx factor mediating store-operated calcium entry.* J Biol Chem, 2003. **278**(30): p. 27540-7.

11. Jolly, P.S., et al., *Transactivation of sphingosine-1-phosphate receptors by FcepsilonRI triggering is required for normal mast cell degranulation and chemotaxis.* J Exp Med, 2004. **199**(7): p. 959-70.

12. Wu, M., et al., *Differential targeting of secretory lysosomes and recycling endosomes in mast cells revealed by patterned antigen arrays.* J Cell Sci, 2007. **120**(Pt 17): p. 3147-54.

13. Murray, R.Z., et al., *A role for the phagosome in cytokine secretion.* Science, 2005. **310**(5753): p. 1492-5.

14. Reefman, E., et al., *Cytokine secretion is distinct from secretion of cytotoxic granules in NK cells.* J Immunol, 2010. **184**(9): p. 4852-62.

15. Manderson, A.P., et al., *Subcompartments of the macrophage recycling endosome direct the differential secretion of IL-6 and TNFalpha.* J Cell Biol, 2007. **178**(1): p. 57-69.

16. Balasubramanian, N., et al., *Arf6 and microtubules in adhesion-dependent trafficking of lipid rafts.* Nat Cell Biol, 2007. **9**(12): p. 1381-91.

17. Ang, A.L., et al., *Recycling endosomes can serve as intermediates during transport from the Golgi to the plasma membrane of MDCK cells.* J Cell Biol, 2004. **167**(3): p. 531-43.

18. van Ijzendoorn, S.C., *Recycling endosomes.* J Cell Sci, 2006. **119**(Pt 9): p. 1679-81.

19. Huang, B., et al., *The Anaplasma phagocytophilum-occupied vacuole selectively recruits Rab-GTPases that are predominantly associated with recycling endosomes.* Cell Microbiol, 2010. **12**(9): p. 1292-307.

20. Smith, A.C., et al., *Interaction of the Salmonella-containing vacuole with the endocytic recycling system.* J Biol Chem, 2005. **280**(26): p. 24634-41.

21. Sibley, L.D., *Intracellular parasite invasion strategies.* Science, 2004. **304**(5668): p. 248-53.

22. Laliberte, J. and V.B. Carruthers, *Host cell manipulation by the human pathogen Toxoplasma gondii.* Cell Mol Life Sci, 2008. **65**(12): p. 1900-15.

23. Else, K.J. and F.D. Finkelman, *Intestinal nematode parasites, cytokines and effector mechanisms.* Int J Parasitol, 1998. **28**(8): p. 1145-58.